GENERATION OF Q-SWITCHED AND SOLITON MODE-LOCKED PULSES WITH 8-HYDROXYQUINOLINO CADMIUM CHLORIDE HYDRATE AND CHROMIUM ALUMINUM CARBIDE SATURABLE ABSORBER

MUSTAFA MOHAMMED NAJM

FACULTY OF ENGINEERING
UNIVERSITY OF MALAYA
KUALA LUMPUR

2022

GENERATION OF Q-SWITCHED AND SOLITON MODE-LOCKED PULSES WITH 8-HYDROXYQUINOLINO CADMIUM CHLORIDE HYDRATE AND CHROMIUM ALUMINUM CARBIDE SATURABLE ABSORBER

MUSTAFA MOHAMMED NAJM

THESIS SUBMITTED IN FULFILMENT OF THE REQUIREMENTS FOR THE DEGREE OF DOCTOR OF PHILOSOPHY

FACULTY OF ENGINEERING
UNIVERSITY OF MALAYA
KUALA LUMPUR

2022

UNIVERSITY OF MALAYA

ORIGINAL LITERARY WORK DECLARATION

Name of Candidate: MUSTAFA MOHAMMED NAJM

Matric No: 17198607/1 & KVA180069

Name of Degree: DOCTOR OF PHILOSOPHY

Title of Project Paper/Research Report/Dissertation/Thesis ("this Work"):

GENERATION OF Q-SWITCHED AND SOLITON MODE-LOCKED PULSES WITH 8-HYDROXYQUINOLINO CADMIUM CHLORIDE HYDRATE AND CHROMIUM ALUMINUM CARBIDE SATURABLE ABSORBER

Field of Study: Photonic (Electronics & Automation)

I do solemnly and sincerely declare that:

(1) I am the sole author/writer of this Work;
(2) This Work is original;
(3) Any use of any work in which copyright exists was done by way of fair dealing and for permitted purposes and any excerpt or extract from, or reference to or reproduction of any copyright work has been disclosed expressly and sufficiently and the title of the Work and its authorship have been acknowledged in this Work;
(4) I do not have any actual knowledge nor do I ought reasonably to know that the making of this work constitutes an infringement of any copyright work;
(5) I hereby assign all and every rights in the copyright to this Work to the University of Malaya ("UM"), who henceforth shall be owner of the copyright in this Work and that any reproduction or use in any form or by any means whatsoever is prohibited without the written consent of UM having been first had and obtained;
(6) I am fully aware that if in the course of making this Work I have infringed any copyright whether intentionally or otherwise, I may be subject to legal action or any other action as may be determined by UM.

Candidate's Signature Date: 28/3/2022

Subscribed and solemnly declared before,

Witness's Signature Date: 28 Mar 2022

Name:

Designation:

GENERATION OF Q-SWITCHED AND SOLITON MODE-LOCKED PULSES WITH 8-HYDROXYQUINOLINO CADMIUM CHLORIDE HYDRATE AND CHROMIUM ALUMINUM CARBIDE SATURABLE ABSORBER

ABSTRACT

This thesis describes the fabrication of new saturable absorber (SA) devices based on 8-Hydroxyquinolino cadmium chloride hydrate (8-HQCdCl_2H_2O) and chromium aluminum carbide (Cr_2AlC) materials and test them in a ring-cavity Erbium-doped fiber laser (EDFL) for Q-switching and mode-locking applications. This study aims to develop an efficient and low-cost Q-switched and mode-locked fiber lasers operating in the nanosecond and picosecond regime, respectively using the newly developed SAs. The SAs are fabricated first using mechanical exfoliation and thin film methods, their physical, chemical, and optical characteristics are then investigated. The modulation depth of the exfoliated 8-HQCdCl_2H_2O on scotch tape, 8-HQCdCl_2H_2O thin film and Cr_2AlC thin film are obtained at 11 %, 18 % and 3.2 %, respectively, indicating their suitability for Q-switching and mode-locking applications. Subsequently, the ring cavity is constructed using an Erbium-doped fiber as the gain medium, and the prepared SA is integrated and optimized into the laser cavity for Q-switched nanosecond and soliton pulse generations. Much time is then spent trying to optimize the cavity and utilize the 8-HQCdCl_2H_2O and Cr_2AlC SAs successfully. The nanosecond pulse generation was successfully realized using the 8-HQCdCl_2H_2O or Cr_2AlC film as SA. The Q-switched laser produced 726 ns pulses with a repetition rate of 150 kHz at pump power of 167 mW with 8-HQCdCl_2H_2O thin film. By optimizing EDFL cavity, mode-locked pulse train operating in 1.5 μm region with a pulse width within picosecond to femtosecond regime was successfully realized using the newly developed 8-HQCdCl_2H_2O and Cr_2AlC SAs. These SAs successfully used to demonstrate different mode locked pulses in different EDFL cavities. For instance, femtosecond soliton pulses were obtained in the 33 m EDFL

cavity. The laser produced a soliton pulse with the full width at half-maximum (FWHM) of 950 fs at a repetition rate of 5.6 MHz. These fiber lasers have many potential applications in various fields including biomedical imaging, material processing, and optical communication.

Keywords: Q-switching, mode-locking, organic saturable absorber, MAX phases

PENJANAAN DENYUT SUIS-Q DAN SELAKAN-MOD SOLITON DENGAN PENYERAP BOLEH TEPU 8-HYDROXYQUINOLINO CADMIUM CHLORIDE HYDRATE AND CHROMIUM ALUMINUM CARBIDE

ABSTRAK

Tesis ini menerangkan fabrikasi peranti penyerap boleh tepu baru (SA) berdasarkan bahan 8-Hydroxyquinolino Cadmium Chloride Hydrate (8-HQCdCl_2H_2O) dan Chromium Aluminum Carbide (Cr_2AlC) dan mengujinya dalam kaviti cincin laser gentian Erbium-doped (EDFL) untuk aplikasi suis-Q dan selakan-mod. Kajian ini bertujuan untuk membangunkan laser gentian suis-Q dan selakan-mod yang cekap dan kos rendah yang beroperasi dalam rejim nanodetic dan picosecond, masing-masing menggunakan SA yang baru dibangunkan. SA dibuat terlebih dahulu menggunakan kaedah pengelupasan mekanikal dan saput nipis, ciri fizikal, kimia, dan sifat optik kemudian disiasat. Kedalaman modulasi 8-HQCdCl_2H_2O yang terkelupas pada pita scotch, saput nipis 8-HQCdCl_2H_2O dan saput nipis Cr_2AlC diperoleh masing-masing pada 11%, 18% dan 3.2%, menunjukkan kesesuaian mereka untuk aplikasi suis-Q dan selakan-mod. Seterusnya, kaviti cincin dibina menggunakan gentian Erbium-doped sebagai medium penguatan, dan SA yang disiapkan disatukan dan dioptimumkan ke dalam kaviti laser untuk penjanaan denyutan nanosecond dan suis-Q soliton. Banyak masa kemudian dihabiskan untuk mengoptimumkan kaviti dan memanfaatkan 8-HQCdCl_2H_2O dan Cr_2AlC SA dengan jayanya. Penjanaan denyut nanodetic berjaya direalisasikan menggunakan saput 8-HQCdCl_2H_2O atau Cr_2AlC sebagai SA. Laser suis-Q menghasilkan denyutan 726 ns dengan kadar pengulangan 150 kHz pada kuasa pam 167 mW dengan saput nipis 8-HQCdCl_2H_2O. Dengan mengoptimumkan kaviti EDFL, denyut tren selakan-mod yang beroperasi di kawasan 1.5 μm dengan lebar denyut dalam rejim picosecond hingga femtosecond berjaya direalisasikan menggunakan 8-HQCdCl_2H_2O dan Cr_2AlC SA yang baru dibangunkan. SA ini berjaya digunakan untuk

menunjukkan perbezaan denyut selakan-mod dalam kaviti EDFL yang berbeza. Sebagai contoh, denyutan soliton femtosecond diperoleh dalam kaviti EDFL 33 m. Laser menghasilkan denyut soliton dengan full width at half-maximum (FWHM) 950 fs pada kadar pengulangan 5.6 MHz. Laser gentian ini mempunyai banyak aplikasi yang berpotensi dalam berbagai bidang termasuk pengimejan bioperubatan, pemprosesan bahan, dan komunikasi optik.

Kata Kunci: Suis-Q, Selakan-mod, Penyerap boleh tepu organik, Fasa MAX

ACKNOWLEDGEMENTS

First of all, we praise is to ALLAH for giving me this opportunity to write this thesis. First and foremost, I am extremely grateful to my supervisors, Prof. Dr. Sulaiman Wadi Harun and Prof. Dr. Hamzah Arof, for their valuable advice, continuous support, excellent guidance, and patience during my Ph.D. study. Their immense knowledge, companionship, and plentiful experience have encouraged me in all the times to produce this thesis. I would like to thank colleagues Bilal Nizamani, Ahmed Shakir Al-Hiti, and Abbas A. Al-Azzawi for their help and support during my Ph.D. study.

I would like to thank all my colleagues and friends at Photonic Engineering Lab for companionship, discussions, and suggestions. It is their kind help and support that has made my study and life in Malaysia wonderful. Finally, I would like to express my gratitude and thanks to my parents, brother, and sister. Without their tremendous support and encouragement in the past few years, it would be impossible for me to complete my studies. In addition, I appreciate all my friends who wished me the best.

To all and everything, thank you.

TABLE OF CONTENTS

LIST OF FIGURES

LIST OF TABLES

LIST OF SYMBOLS AND ABBREVIATIONS

I_{sat}	:	Saturation Intensity
α_s	:	Modulation Depth
α_{ns}	:	Non-saturable Absorption
f_{rep}	:	Pulse Repetition Rate
λ	:	Wavelength
τ_p	:	Pulse Duration
μs	:	Microsecond
ps	:	Picosecond
fs	:	Femtosecond
dB	:	Decibel
2D	:	Two-dimensional
8-HQ	:	8-Hydroxyquinolino
ASE	:	Amplified Spontaneous Emission
BP	:	Black Phosphorus
CNTs	:	Carbon Nanotubes
CW	:	Continuous Wave
$CdCl_2H_2O$	:	Cadmium Chloride Hydrate
Cr_2AlC	:	Chromium Aluminum Carbide
CARS	:	Coherent Anti-stokes Raman Scattering
DI	:	Deionized Water
ESA	:	Excited State Absorption
EDF	:	Erbium-Doped Fiber
EDFA	:	Erbium-Doped Fiber Amplifier
EDFL	:	Erbium-Doped Fiber Laser

EDX	:	Energy Dispersive X-Ray
Er^{3+}	:	Erbium
FESEM	:	Field Emission Scanning Microscopy
FTIR	:	Fourier Transform Infrared Spectroscopy
FWHM	:	Full-Width at Half Maximum
FET	:	Field-Effect Transistor
GVD	:	Group Velocity Dispersion
GDD	:	Group Delay Dispersion
ISO	:	Isolator
LASER	:	Light Amplification by Stimulated Emission of Radiation
LD	:	Laser Diode
MoS_2	:	Molybdenum Disulfide
MWCNTs	:	Multi-Walled Carbon Nanotubes
MoS_2	:	Molybdenum Disulfide
NPR	:	Nonlinear Polarization Rotation
NPE	:	Nonlinear Polarization Evolution
NA	:	Numerical Aperture
Nd^{3+}	:	Neodymium
OC	:	Output Coupler
OC	:	Optical Coupler
OSA	:	Optical Spectrum Analyzer
OSC	:	Oscilloscope
OPM	:	Optical Power Meter
OLED	:	Organic Light-Emitting Diode
PVA	:	Polyvinyl Alcohol
PCF	:	Photonic Crystal Fiber

PC	:	Polarization Controller
RFSA	:	Radio Frequency Spectrum Analyzer
RBW	:	Resolution Bandwidth
SA	:	Saturable Absorber
SEM	:	Scanning Electron Microscope
SESAMs	:	Semiconductor Saturable Absorption Mirrors
SMF	:	Single-Mode Fiber
SNR	:	Signal to Noise Ratio
SWCNT	:	Single-Walled Carbon Nanotubes
$Sech^2$	:	Secant Hyperbolic
SPM	:	Self-Phase Modulation
TBP	:	Time-Bandwidth Product
TMD	:	Transition Metal Dichalcogenide
TI	:	Topological Insulators
Ti_2AlC	:	Titanium Aluminum Carbide
VBW	:	Video Bandwidth
WLS	:	White Light Source
WDM	:	Wavelength Division Multiplexing
WTe_2	:	Tungsten Ditelluride

CHAPTER 1: INTRODUCTION

1.1 Background and Motivation

Over the years, countless efforts have been made by scientists around the world to produce a reliable and powerful laser for a multitude of industrial applications (Addanki et al., 2018; Dubey et al., 2008). In the past few decades, the laser-produced is in the form of a bulk solid-state laser (Keller, 2003). However, the limitations of this laser bring the research on another type of laser, which uses an optical fiber doped with rare-earth material as a gain medium. This type of laser is referred to fiber laser. The progress of optical communication has arisen a series of research works in fiber lasers and amplifiers (Al-Azzawi et al., 2019; Giles et al., 1991; Saglamyurek et al., 2015). The communication bandwidth ranging from 1.3 to 1.6-μm can be accomplished by implementing several rare-earth ions as the active medium in silica glasses as host materials (Desurvire et al., 1991). For instance, an erbium (Er^{3+})-doped fiber operates in 1.55-μm region. To date, fiber laser has been widely used in a variety of disciplines, including biomedical imaging, material processing, and optical communication (Keller, 2003; Okhotnikov et al., 2004; Wise et al., 2008) due to their advantages of good beam quality, short-pulses, and high peak power. They may be accomplished by utilizing a neodymium-, erbium-, and thulium-doped fiber as such gain medium to operate in a wavelength region of 1000 nm, 1550 nm, and 2000 nm, respectively (Mary et al., 2014; Shi et al., 2014). The widely investigated fiber laser is erbium-doped fiber laser (EDFL) as it produces pulses at a 1.55 μm regime. This type of laser is suitable for various applications including telecommunication systems.

Pulsed lasers are required in certain applications including telecommunications and medicine (Clowes, 2008; Nishizawa, 2014; O'Mahony et al., 2001). For instance, Q-switched pulses got much attention in medicine and material processing due to its potential for generating a pulse within microsecond to nanosecond width (Al-Hiti et al.,

2021). Besides, Q-switching is capable to produce pulses that have high energy (Salam et al., 2019). The mode-locking technique had a role in the generation of pulses with picosecond to femtosecond width (Keller, 2003). Also, mode-locked pulses are useful to the optical communications for transmitting the pulses over long distances. Q-switched and mode-locked pulses can be generated from fiber lasers using either active or passive techniques. The active techniques have many limitations such as bulky, requiring alignment-dependent set up, and expensive maintenance operation. These limitations can be overcoming by the deployment of passive techniques based on saturable absorber (SA). The passive techniques have several advantages like cost-effective, simplicity in the design, flexible configuration, and compactness (Guoyu et al., 2015).

In the past years, several types of SA have been reported for generating Q-switched and mode-locked pulses inside the fiber laser cavity, such as, semiconductor saturable absorber mirrors (SESAM) (Zhang et al., 2010), graphene (Zhang et al., 2009), carbon nanotube (CNT) (Set et al., 2004), and black phosphorus (BP) (Ismail et al., 2016). SESAMs have precise control of the wavelength and a fast recovery time, which are vital for producing ultra-short pulses (Keller et al., 1996). However, SESAMs require complicated fabrication procedure, which is costly. Graphene and CNTs have also been well-known as SAs because of their outstanding physical and chemical features. They have advantages in terms of broad operating bandwidth and low fabrication cost (Li et al., 2014; Wang et al., 2015; Zhang et al., 2009). But these SAs also exhibit some drawbacks which limits their applications. Graphene has a low modulation depth per layer, while CNT has a spectral range response that is impacted by its nanotubes diameter (Al-Hiti et al., 2020). BP-based SA has a wide range of the spectrum but it has a relatively lower damage threshold and its pulsing performance also degrades with time, as this material reacts with oxygen present in the environment (Chen et al., 2015). In recent years, another 2D nanomaterial, including transition metal dichalcogenide (TMD) and

topological insulators (TI) have also been reported as SA to generate lasers in various regions. TMD such as WS_2 (Mao et al., 2015; Yang et al., 2019), SnS_2 (Niu et al., 2018), and $MoSe_2$ (Liu et al., 2018) has excellent absorption properties. However, it is suffering from low optical damage tolerance and difficult process manufacture. Topological Insulators (TI) such as Bismuth telluride (Bi_2Te_3) (Lee et al., 2014), Bismuth selenide (Bi_2Se_3) (Yu et al., 2014) and Antimony telluride (Sb_2Te_3) (Al-Masoodi et al., 2018) based SAs are difficult to fabricate as they require high temperatures for fabrication (Ali et al., 2013).

On the other hand, organic materials have also attracted much interest in recent years for various electronic and photonics applications since they have ultrafast nonlinear response and wide spectral tunability (Al-Hiti et al., 2020; Li et al., 2019). Moreover, they are advantageous in terms of low fabrication cost (Ji et al., 2020), good electrical conductivity (Sheberla et al., 2014), mechanical flexibility (Park et al., 2015) and thermal stability (Zhao et al., 2006). The organic materials have good electrical properties which make them suitable for the applications in various electronic devices such as photovoltaic in the solar panel (Spalatu et al., 2017), organic light-emitting diode (OLED) (Meftah et al., 2020; Puniredd et al., 2013), and field-effect transistor (FET) (Sun et al., 2017). For instance, 8-Hydroxyquinolino cadmium chloride hydrate (8-$HQCdCl_2H_2O$) is widely used in electronic devices (Shahedi et al., 2017). Also, the 8-$HQCdCl_2H_2O$ has excellent properties that make it useful for different applications, these characteristics include good conductivity (Salyulev et al., 2016), thermal stability (Baraker et al., 2018), reliability (Gurnani et al., 2003) and simple fabrication (Fung et al., 2012). Nowadays, various research studies have also been reported on MAX phases material due to their excellent optical capabilities such as a large effective nonlinear absorption coefficient (Ahmad et al., 2019), a fast optical-switching capability (Lee et al., 2019) and a high optical damage

tolerance (Jafry et al., 2020). This makes the MAX phases to be a preferable material for SA application, in comparison to other 2D-based materials.

This research work aims to investigate the potential of 8-HQCdCl_2H_2O as organic thin-film SA and chromium aluminum carbide (Cr_2AlC) as a MAX phases thin-film SA to generate nanosecond Q-switched and soliton ultrashort pulses in EDFL cavity.

1.2 Research Objectives

The aim of this work is to develop efficient and low-cost Q-switched and mode-locked fiber lasers operating in the nanosecond and picosecond regime, respectively using two types of SA materials: 8-HQCdCl_2H_2O and Cr_2AlC. Several objectives have been outlined to guide the research direction toward achieving the aim:

1. To fabricate and characterize new passive SAs based on two different materials: 8-HQCdCl_2H_2O and Cr_2AlC.
2. To design and optimize EDFL cavity to generate Q-switched pulse train in 1.5 μm region with a pulse width in nanosecond regime using the newly developed 8-HQCdCl_2H_2O and Cr_2AlC SAs.
3. To design and optimize EDFL cavity to generate mode-locked pulse train in 1.5 μm region with a pulse width within picosecond to femtosecond regime using the newly developed 8-HQCdCl_2H_2O and Cr_2AlC SAs.

1.3 Thesis Organization and Structure

This thesis is structured in 6 main chapters, in which a comprehensive study on Q-switched and mode-locked pulse generations by using the newly developed SAs is presented. This introductory chapter presents a background, motivation, and objectives of this study. Chapter 2 is intended to present the overview of fiber laser technologies and provides detail explanation on erbium-doped fiber laser (EDFL) technology, theory of

laser oscillation, laser configuration and pulse generations via Q-switching and mode-locking approaches. This chapter also presents a brief literature review on saturable absorber (SA) development and highlights the important parameters for output pulses.

In chapter 3, three types of SAs are successfully developed based on two different materials: 8-HQCdCl_2H_2O and Cr_2AlC, which belong to the organic and MAX Phases family, respectively as a based material. The 8-HQCdCl_2H_2O SA is prepared based on mechanical exfoliation and drop-casting technique (thin film) while Cr_2AlC is only prepared in form of thin film. PVA is used as a host polymer in the fabrication of thin film. The physical and optical characterizations of these SAs are also described in this chapter.

Chapter 4 aims to demonstrate the generation of nanosecond Q-switched pulses in EDFL cavity using the newly developed SAs. The Q-switched pulses with a duration of 726 ns and 780 ns are achieved with the use of 8-HQCdCl_2H_2O and Cr_2AlC thin film, respectively. Chapter 5 demonstrates the generation of soliton mode-locked pulses in an EDFL cavity using the newly developed passive SAs. The effect of cavity length on the pulse generation is also investigated in this chapter. Chapter 6 concludes the thesis and summarizes the findings of the research investigation. The future direction of this research work is also discussed in this chapter.

CHAPTER 2: LITERATURE REVIEW

2.1 Fiber Laser Overview

Lasers have become widely used in a variety of disciplines, including materials processing, telecommunications, metrology, medicine, and fundamental science. Pulsed lasers are critical for variety of medical applications including nonlinear confocal microscopy (Cutruneo et al., 2012). The confocal microscopy is realized by using various nonlinear optical processes, such as two-photon absorption, coherent anti-Stokes Raman scattering (CARS), second harmonic generation, etc (Prasad et al., 2007). These nonlinear processes only occur in high intensity focal points, which can only be realized by making use of short pulses to generate high peak powers with low average power to prevent damaging the samples (Prasad et al., 2007). This allows for precise localization of nonlinear signals produced in the sample, ideal for confocal microscopy. Pulsed lasers can also be used to replace surgical knives in medical application (Clowes, 2008).

Conventionally, the solid-state lasers were used to generate short and ultrashort pulses based on Q-switching and Kerr-lens mode-locking, respectively. However, these lasers are limited in real-world applications due to their cooling requirements, size, cost and need for precise alignment of bulk optical components (Sennaroglu, 2017). As an alternative route, various fiber lasers have been proposed and demonstrated in recent years to generate high energy Q-switched and ultra-short pulses. The fiber laser uses doped-optical fiber as a laser medium and thus has many benefits over solid-state lasers counterparts. For instance, the waveguide feature of optical fiber allows for perfect overlap of the pump and signal in the gain medium, allowing entirely alignment-free lasers with no free space components to be built. In addition, the large ratio of the surface area to the volume of the fiber eliminates the need for water cooling of the laser medium. Finally, the properties of single-mode fiber provide exceptional beam quality (Shi et al.,

2014). Practically, fiber lasers aim to be less costly than solid-state lasers, allowing laser technology to be used more extensively, particularly outside of specialized laboratories.

Despite the various benefits of optical fiber, the performance of pulsed fiber lasers has fallen behind that of solid-state lasers due to the tight confinement of powerful pulses in the fiber's core. Various schemes have been proposed and demonstrated to increase the performance of fiber lasers through Q-switching or mode-locking techniques. The pulse generations can be realized by two different schemes: passive and active. The active scheme uses a complicated acoustic-optic modulator to regulate the loss inside the laser cavity (Chen et al., 2015). Otherwise, the passive scheme generally includes a thin-film saturable absorber (SA) made from functional materials. It also has basic features such as simplicity, flexibility, and compactness (Keller, 2003). This thesis intends to improve high-performance Q-switched and mode-locked fiber lasers utilizing novel SA devices.

2.2 Theory of Erbium-Doped Fiber laser

The rare-earth doped fibers were initially employed as a gain medium in optical amplifiers and lasers in the early 1960s when Snitzer et al. created and demonstrated the first glass laser using neodymium (Nd^{3+}) doped glass (Snitzer, 1966). Snitzer realized that the waveguiding structure of the glass can be used to generate laser with high power density where the light is constrained to a narrow core zone. Since then, several advancements in optical fiber manufacturing have been accomplished, including the reduction of transmission loss at the region of 1550 nm and the development of single-mode fibers. Payne et al. has capitalized this work to report for the first time the potential for trivalent erbium (Er^{3+}) as a dopant for optical amplification and lasing in silica fibers in 1987 (Mears et al., 1987). Many issues related to the silica of erbium-doped fiber (EDF) fabrication, such as the distribution and solubility of rare-earth ions inside the silica fiber core, were also resolved in the 1990s. For instance, the incorporation of chemicals

compounds such as Al_2O_3, Si-O-, GeO_2, and P_2O_5 to the core fiber can enhance the solubility of Erbium ions in silica. This leads to the development of highly doped EDF without any clustering effects. Today, EDFs have been widely used as gain medium in both optical amplifier for optical communications and fiber lasers for industrial applications (Desurvire, 1994).

In 1917, Albert Einstein proposed the theory of light amplification for the first time. He mentioned the amplification process can be realized by stimulated emission (Gould, 1959). Figure 2.1 explains the laser principle, which involves three main processes: absorption, spontaneous and stimulated emission. The laser is generated due to the interaction between the light and the atom. The absorption process transports the ions from a low energy level (i.e., ground state) into a high energy level (i.e., excited state) by absorbing the incident photons. The excited state level has a short lifetime and thus these ions only stay briefly in the high energy level. They fall into the lower energy level to emit the photon, and this process is referred to spontaneous emission. The emitted photons have the same energy with the difference between two energy level. These ions in the excited state can also be stimulated to drop into the lower energy level by the incident photons, providing the incident photon energy is equivalent to the energy difference between the two levels. This process is referred to a stimulated emission (Siegman, 1986). The process of duplicating photons will increase the number of photons between the ground state and excited state. This process can be translated to the increase the intensity of light or amplification.

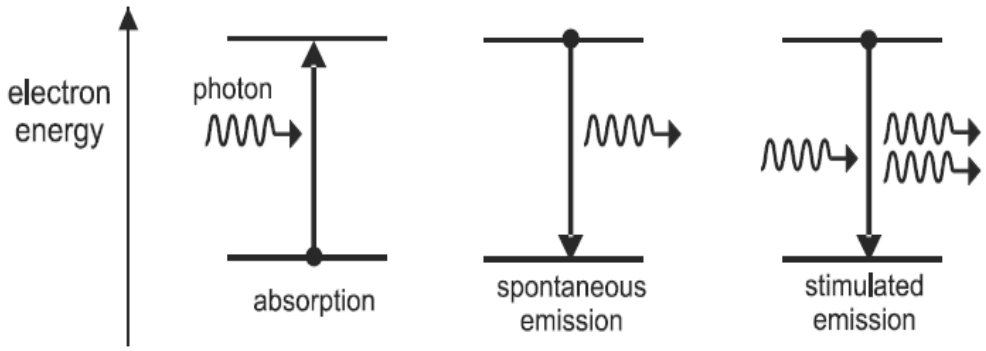

Figure 2.1: The absorption, spontaneous emission, and stimulated emission processes inside the active material (Siegman, 1986)

Figure 2.2 depicts the atomic energy band structure of erbium, especially the energy levels important for optical amplification utilizing the Er^{3+}. The energy levels are broadening due to the Stark splitting effect (Zulkipli et al., 2020), which leads to a relatively broad emission bandwidth. Atomic vibrations produce this energy variation. When 974 nm pump photons are fed into an EDF, Er^{3+} will be excited from the ground state to the excited state level. The excited ions on excited state will rapidly decay to metastable level through nonradioactive emission. These ions on the metastable level eventually return to ground state through spontaneous emission, which produces photons in the wavelength band of 1520 nm – 1570 nm .As the spontaneous emission propagates through the EDF, it will be amplified, especially when the pump laser intensity is increased to generate an amplified spontaneous emission (ASE). The ASE operates in a wide wavelength range from 1520 to 1570nm. The diagram simply depicts the most important transitions in this thesis. The transitions that are non-shown include pump photon absorption at 1480 nm, excited-state absorption (ESA), and the absorption of the multi-photon; the latter two happen naturally and are a source of noise in the laser cavity.

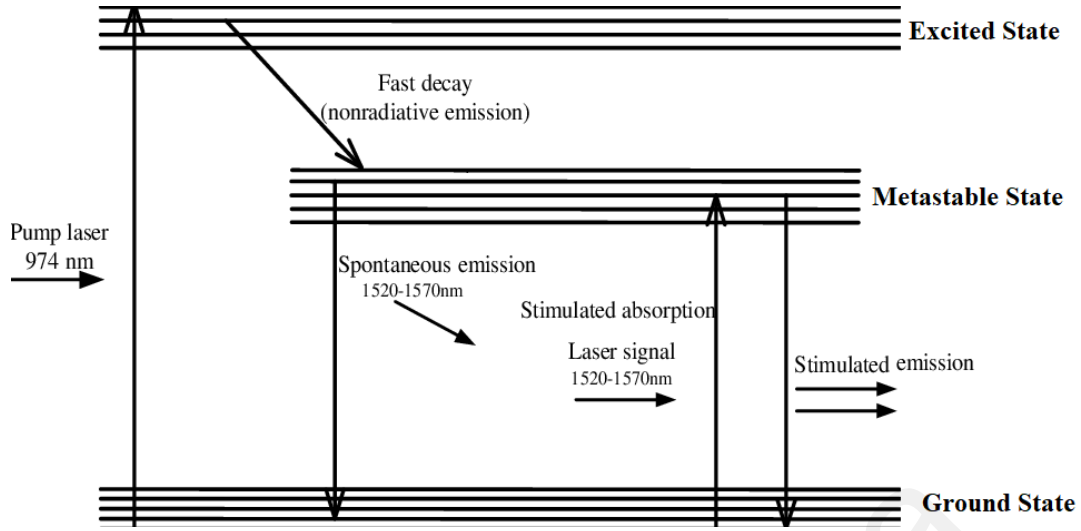

Figure 2.2: Energy level diagram of Er^{3+} ions in EDF (Ngo, 2010)

When pump laser power is high enough that the population inversion is achieved between the excited state and metastable level of EDF, the input laser signal (within a wavelength region between 1520 and 1570 nm) passing through the fiber is then be amplified. Thus, optical amplifier can be constructed using the EDF and 974 nm pump laser. This amplifier is referred to erbium-doped fiber amplifier (EDFA), which is extensively diffused in optical communication system. If the EDF and pump laser are integrated into a closed ring or linear cavity, erbium-doped fiber laser (EDFL) can be realized.

2.3 Theory of Laser Oscillation

As the pump radiation is absorbed along the length of the EDF in a laser cavity, spontaneous emission in 1550 nm region begins to happen, which then causes stimulated emission in the same wavelength region. The stimulated emission process creates coherent signal photons to increase the amount of light (or gain) in the 1550 nm band. Similarly, the amount of coherent light also reduces (or loss) in the 1550 nm band through various processes including scattering, absorption, etc. The general requirement for the lasing to happen when the gain saturation higher than cavity losses. It is worthy to

mention that the amount of gain is depended on the population inversion of the Er^{3+} ions in the gain medium. The level of population inversion is determined by the amount of pump power.

Here, a simple mathematical analysis of the laser oscillation is presented. At first, we consider the case of the unpumped laser cavity. The population inversion is not possible without the pump radiation since the majority of the Er^{3+} ions are populated in the ground state. Without the population inversion, no stimulated emission or gain will take place, the laser cavity only exhibits optical loss (via absorption and scattering). As the input light intensity I_o is launched into a fiber or laser cavity, the light intensity inside the fiber, I will decrease along the fiber length according to the following equation:

$$I = I_0 e^{-\alpha x} \tag{2.1}$$

where α is the fiber loss, x is the distance along the fiber. This indicates that the light intensity decays exponentially as it travels along the unpumped fiber.

If the EDF is pumped by 974 nm laser diode, the population inversion is achieved to provide gain. As with the loss, the gain generated by the stimulated emission is defined by β. The net change of signal or net gain can then be calculated by taking the difference between the gain and loss or β - α. With pumping, the light intensity inside the fiber, I_p is given by:

$$I_p = I_0 e^{(\beta-\alpha)x} \tag{2.2}$$

Assuming that the length of EDF is similar to cavity length, a singular value for x can be used. This assumption is not always true, and it leads to the creation of two new variables, ℓ_t and ℓ_p, representing the total cavity and pumped EDF lengths, respectively.

Assuming that β is constant and α remains unsaturated throughout the EDF length, the above equation for I_p can be simplified as:

$$I_p = I_0 e^{\beta \ell_p - \alpha \ell_t} \tag{2.3}$$

The net gain is defined as the ratio of I_p to I_o and is given as:

$$G = \frac{I_p}{I_0} = e^{\beta \ell_p - \alpha \ell_t} \tag{2.4}$$

In practise, measuring this gain value is complicated due to the difficulty to obtaining I_o (the intensity of light coupled into the EDF). The laser's output light intensity can be measured significantly more easily. It is easier to compare the light intensity that exiting the unpumped EDF, I_u with the intensity of light exiting the pumped EDF, I_p. I_u is given by the following equation:

$$I_u = I_0 e^{-\alpha \ell_t} \tag{2.5}$$

and the gross gain, g is given by the following equation:

$$g = \frac{I_p}{I_u} = e^{\beta \ell_p} \tag{2.6}$$

Equation 2.6 indicates the level of the gain that a single pass of signal light through the EDF component may achieve. For lasing to occur, a feedback mechanism is required in the cavity.

2.4 Laser Configuration

One of the main laser elements is a feedback mechanism or laser resonator. It functions to return part of the photons which was created inside the gain medium, back for further amplification. The laser resonator can be formed based on either linear or ring cavity. The linear cavity employs two reflectors on the both ends of the active gain medium to provide

the feedback mechanism and allows each photon to pass many times through the gain medium, so enough amplification will result. One of the reflectors only partially reflects the radiations while allowing the other part to be transmitted out as a laser output. Figure 2.3 shows the typical configuration of a ring cavity of erbium-doped fiber laser (EDFL), where the EDF's output is linked back to the EDF's input to form a continuous fiber loop. It uses a wavelength division multiplexer (WDM) to launch the pump radiation to the EDF by using a laser diode placed outside the laser cavity. The fiber coupler is an optical component that divides the light beam from one arm into two distinct arms. In a ring EDFL, it is used as a feed mechanism while tapping out the laser from the cavity. Some of the more common splitting ratios are 90/10, 80/20 and 50/50. For instance the 90/10 coupler utilized as the feedback technique, 90% of the pulsating light within the EDFL cavity is sent back into the cavity's beginning, passing via the WDM, and then back into the EDF. However, for laser output assessment, 10% of the laser output from the ring resonator will be directed outside of the cavity. An optical isolator ensures unidirectional operation of the cavity. In this thesis, all the laser setups are designed based on the ring configuration.

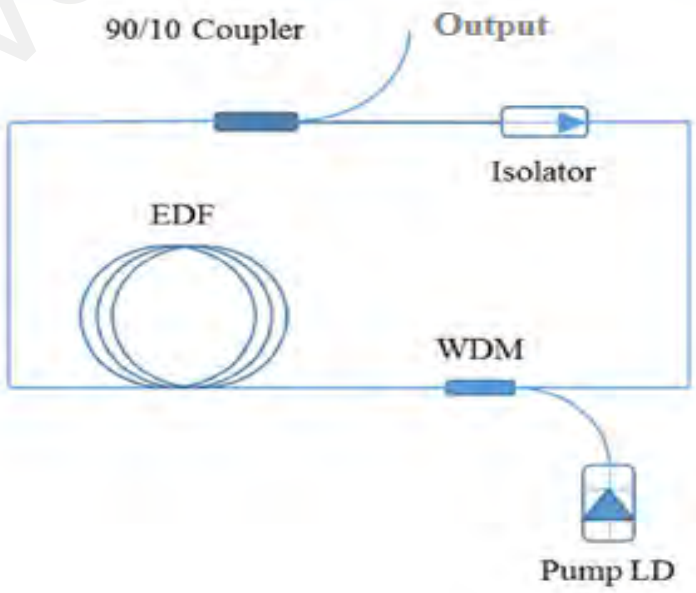

Figure 2.3: A typical EDFL setup with a ring configuration (Bao et al., 2009)

2.5 Pulse Generation in Fiber Laser

Fiber laser generates continuous wave (CW) output in which the intensity of light constants in time, in a normal setup. However, in some applications such as medical requires a pulse type of laser which has a higher peak power. The first pulse laser operation was generated in 1966 by Nd:glass laser (Stetser et al., 1966). The Q-switching and mode-locking techniques are being used to produce the pulsed laser. The mechanism of both techniques will be explained in this section.

2.5.1 Q-switching

Q-switching refers to one of the pulsing laser techniques used to produce short-pulse in the range between microseconds to nanoseconds. It generates the pulses by modulating the Q factor inside the laser cavity. The Q factor has important role in the laser cavity, it is defined as the ratio of stored energy to the dissipated energy for each oscillation cycle. It is given in the following equation:

$$Q = 2\pi \times \frac{energy\ stored\ in\ resonator}{energy\ loss\ per\ resonator\ cycle} \tag{2.7}$$

Consequently, the higher Q-factor, the greater the potential energy produced by the resonator. Typical Q-factor values are highly positive; however, not all the stored energy gets converted into laser output during each resonator cycle, and of the percentage that does, a certain amount is lost before it can escape the cavity as useable light. By varying the Q-factor, the energy output of the laser can also be varied. In Q-switching, the Q-factor is varied via modulating the cavity loss, and thus the energy output cavity (Bollig et al., 1995; Spühler et al., 1999; Wang, 1963). Q-switching can be realized by either active or passive techniques.

In the case active Q-switching, an active Q-switch is inserted into the laser cavity to modulate the cavity losses by the externally controlled variable attenuator. An acousto-

optic switch or fast shutter is normally used as active Q-switcher device (Catella, 2009; Cole et al., 2017). A passive Q-switching is realized by modulating the loss of the cavity without utilize an external controller devices. In both cases, the cavity losses are modulated such that the overall loss is changed between values greater than and less than the cavity gain. The gain inside the laser cavity is provided by a gain medium such as EDF, which is pumped by a laser diode. If the loss inside the cavity is higher than the gain, lasing cannot occur, and the laser is effectively 'off'. However, as the loss is reduced to be less than the gain, the lasing occurs and the laser is 'turns on', So, the Q-switcher effectively acts as an 'on/off' switch for the laser cavity by modulating the Q-factor or cavity losses appropriately.

Figure 2.4 explains the passively Q-switched laser's pulse formation. Initially, the cavity loss is higher than the cavity gain, due to the incorporation of SA device. The cavity gain is provided by the energy from the pump source and the SA creates the high-loss state. At this state, the energy from the pump source is stored in the gain medium as the pump power increases. The maximum potential amount of stored energy is generally limited by the available pump energy. Then, the cavity is switched to a low-loss state due to the saturation of the SA, causing the energy stored in the gain medium to be released. When the loss is suddenly dropped, spontaneous emission noise from the gain medium is allowed to oscillate and amplify in the cavity. This amplification of the noise increases the intra-cavity light power and saturates the gain. Once gain saturation is reached, the intra-cavity power decreases as the remaining energy stored in the gain medium is extracted. The process is then repeated as the cavity is switched back to high-loss state and the energy stored in the gain medium is allowed to refill to high level. In summary, the high-loss state allows more energy to be stored in the gain medium than during CW operation, the sudden drop to a low-loss state rapidly depletes the stored energy faster

than the pump can replenish it, and this rapid depletion of stored energy generates a large spike in light output, or a pulse.

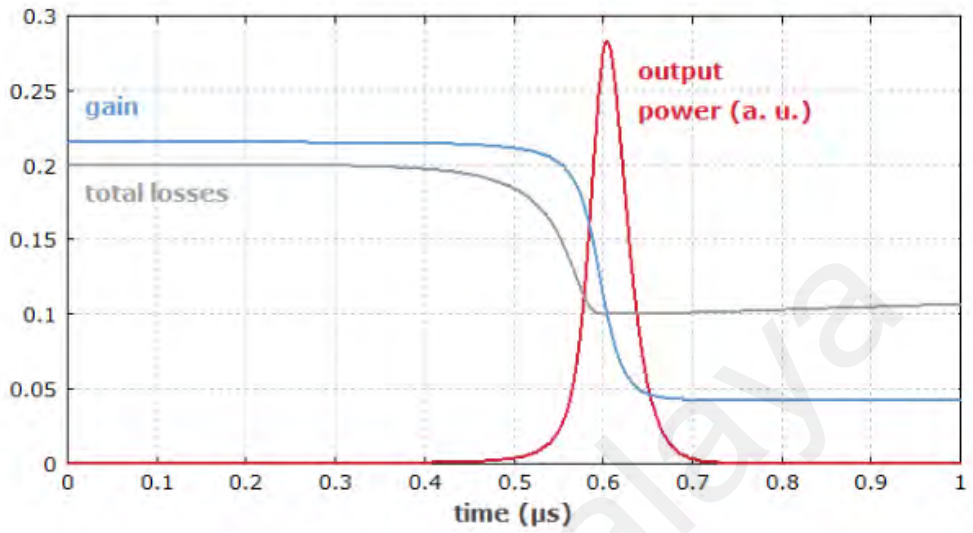

Figure 2.4: Temporal relationship of gain and loss in the laser cavity and resultant pulse in a passively Q-switched laser (Quimby, 2006)

The passive modulation of the cavity losses required for pulse generation is normally obtained using the SA device. The two qualities needed for a material to be a good SA is a large absorption cross section overlapping the laser wavelength and a bleaching effect under higher optical powers. Saturable absorbers are generally easier to integrate into a laser cavity than any active means of Q-switching and require no controlling electronics. Many materials have been used for Q-switching operation in the past, including carbon nanotubes and graphene thin films. The thin film's saturation rises before the active gain medium's saturation when the active medium's energy reaches the sufficient degree of saturation to form an emitted pulse, as well as the cavity losses modulated by thin-film (Degiorgio et al., 1967; Degnan, 1995; Li et al., 2005). Hence, it is possible to control the generation of pulse repetition rate and pulse width that is dependent entirely on the changing of laser pump power (Pirzio et al., 2020). The Q-switching will produce pulse width in the range between microseconds and nanoseconds and repetition rate in kHz (Al-Hiti et al., 2021).

2.5.2 Mode-locking

Mode-locking is one of the laser pulsing techniques used in fiber lasers to produce an ultra-short pulse in the picosecond and femtosecond range (Fermann et al., 1990; Mayer et al., 2017; Tang et al., 2008). It refers to the generation of pulses by constructive interference when many longitudinal modes oscillate in the phase in a laser resonator. Figure 2.5 shows the ultra-short pulse formation via the mode-locking mechanism. Without mode-locking, the phase of longitudinal modes is random. This results in a random intensity distribution and no pulse is formed as shown in Figure 2.5 (a). If these modes are locked in phase and added up, the intensity gets localized at positions where all the modes have a maximum and destructively interfere elsewhere as shown in Figure 2.5 (b). All the longitudinal modes satisfy the standing wave condition $m\lambda = 2L$, where m is a positive integer and L the length of the cavity. The frequency spacing is determined by adding half a wavelength ($m \rightarrow m + 1$) and is given by:

$$\Delta\upsilon = \frac{c}{2L} \tag{2.8}$$

Every round-trip time, the coherent interruption of many longitudinal modes scattered over a broad-spectrum and this results in an ultra-short pulse creation. The number of longitudinal modes that can be locked is proportional to the bandwidth gain of the active laser medium, $\Delta\upsilon_g$. The number of modes oscillating in the cavity increases with pumping power (Weiner, 2011). At sufficiently strong pumping, the total number of longitudinal modes are given by:

$$N_{tot} = \frac{\Delta\upsilon_g}{c/2L} \tag{2.9}$$

and the shortest pulse width is estimated to be:

$$\tau_{min} \approx \frac{1}{\Delta\upsilon_g} \tag{2.10}$$

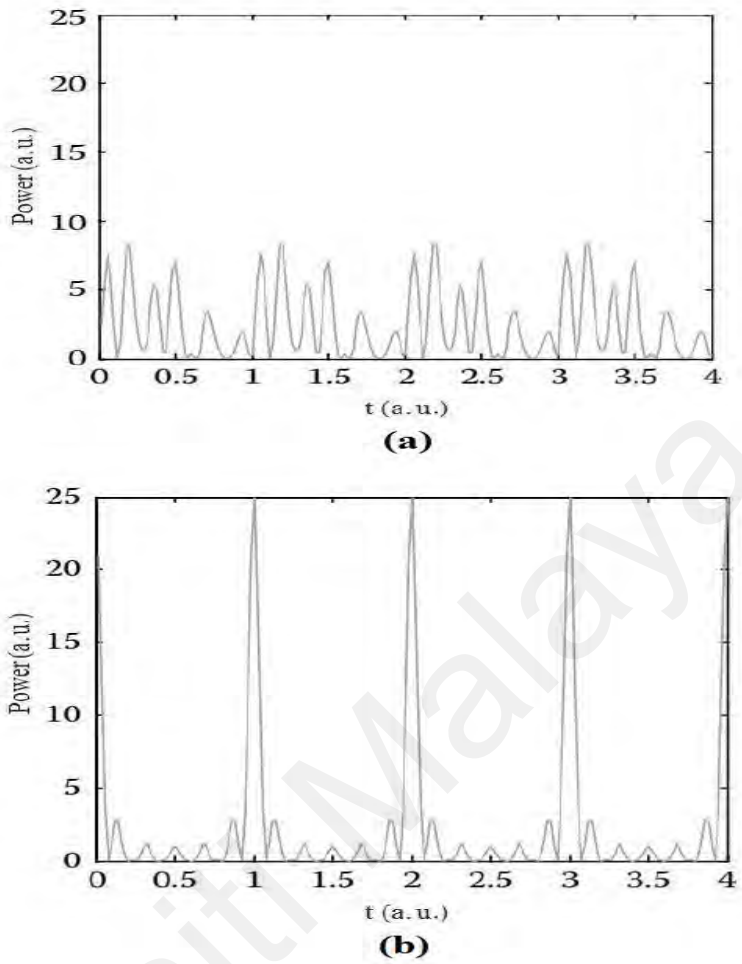

Figure 2.5: Short pulse formation through longitudinal interference, (a) random phase, (b) in phase (Ngo, 2010)

There are several techniques for locking the longitudinal modes of an oscillator and producing ultra-short pulses. It is generally divided into passive and active techniques. In the active technique, an external optical modulator is used to activate the mode-locking operation. The acousto-optic modulator based on the diffraction of light by acoustic wave is normally employed to modulate the resonator losses in exact synchronism with the resonator round-trips (Fermann et al., 1997). Another technique is to use an electro-optic effect, where the refractive index is linear to an applied electric field to get as many of the longitudinal modes lasing in a phase synchronous fashion (Hofer et al., 1990; Zhang et al., 2009).

On the other hand, the passive mode-locking can be achieved by inserting a SA with suitable properties into the laser cavity. In the passive mode-locked case, the mode-locked operation is activated by place the small piece of thin-film SA inside the laser cavity. In this case, the thin film saturation rises after the active gain medium's saturation, where the active medium's energy reaches the sufficient degree of saturation to form emitted ultra-short pulses, also the cavity losses modulated by the thin-film (Solodyankin et al., 2008; Zhang et al., 2011). The pulse will hit the SA every moment, it temporarily reduces the cavity loss due to the saturation of absorption as shown in Figure 2.6. In the steady state, the gain of the laser can be saturated to a level which is just sufficient for compensating the losses for the circulating pulse. Any light of lower intensity which hits the SA at other times will experience higher losses. This allows the SA to suppress weaker pulses, as well as to constantly attenuate the leading and trailing wing of the circulating pulse. Therefore, the SA also function to decrease the pulse duration of the mode-locked pulse.

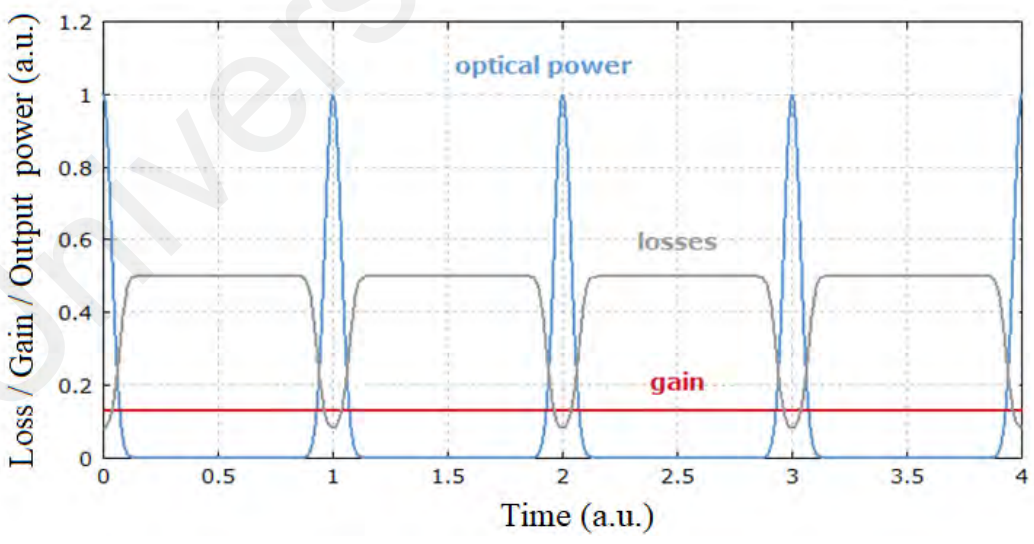

Figure 2.6: Pulse generation mechanism via passive mode-locking (Keller, 2003)

Compared with an active technique, the passive mode-locking tends to generate much shorter pulses, due to the use of SA that can modulate resonator losses considerably faster than any electrical and electronic modulator. The SA also functions to reduce the duration

of circulating pulses. On the other hand, group velocity dispersion (GVD), is a property of dispersive media (e.g. in the context of fiber laser) that is commonly used to assess how the medium will impact the width of an optical pulse flowing through it. The GVD is usually defined as a derivative with respect to wavelength. GVD has several important effects, such as dispersive temporal broadening or squeeze of the ultra-short pulses. Besides GVD, the nonlinear effect also plays an important role in the mode-locked pulse generation (Walmsley et al., 2001). For instance, additional fiber length is normally added into the laser cavity to increase nonlinearity so that it can balance the total cavity dispersion and generates very interesting pulses such as soliton (Lau et al., 2019; Nady et al., 2019). Concerning the soliton, the spectral shape and temporal of ultra-short pulses will be changed during transmission through a fiber because of the self-phase modulation (SPM) resulted from the Kerr effect and chromatic dispersion. However, the effects of dispersion and nonlinearity can perfectly cancel each other, except for a constant phase delay per unit propagation distance, preserving the temporal and spectral form of the ultra-short pulses even over long optical fiber (Hasegawa et al., 1973; Shabat et al., 1972). Consequently, the soliton phenomenon will be observed for light propagating in optical fiber (Mollenauer et al., 1980), where the pulse temporal shape has to be that of an unchipped pulse.

2.6 Saturable Absorber

Saturable absorber (SA) is the type of optical thin-film that used to generate a pulse laser through the laser intensity-dependent. It highly absorbs lower intensity light, and the absorption reduces at a higher intensity of light, and thus promoting pulses generation in a laser cavity. The device is deployed inside a laser cavity to initiate the self-starting and stable short-pulse operation via Q-switching and mode-locking mechanism (Keller, 2003; Zhang et al., 2014). The linear absorption, recovery time and nonlinear absorptions, damage threshold are the main parameters of SAs (Zhang et al., 2014). The linear absorption determines the operating wavelength region of the SA, and it must be coincided with the gain bandwidth of the corresponding lasing medium. Recovery time sets a limit on the switching speed of the device that can affect the duration of the achievable pulses. The saturation intensity and modulation depth of the SA are obtained from the nonlinear absorption curve. The required light intensity in the SA device to saturate the absorption of the material is referred to saturation intensity, whereas the modulation depth is defined as the maximum possible change of absorption. These parameters are controlling pulse dynamics. The damage threshold is the maximum light intensity that a device can tolerate before damage occurs. In choosing a suitable SAs, other characteristics such as environmental stability and the ease and cost of fabrication are also crucial.

To date, different types of SAs with different parameters have been studied and employed to achieve Q-switched and mode-locked lasers. The first SA was introduced in 1965 (Mocker et al., 1965), where the Rhodamine based organic dye was incorporated in a laser cavity to achieve mode-locking pulses with a duration of 10 ns. Figure 2.7 summarizes the historical evolution of the SA technologies (Woodward et al., 2015). After the initial demonstrations of dyes based mode-locked pulses generation, there are not many developments on SA research until the semiconductor saturable absorber mirror

(SESAM) was proposed in the early 1990s (Keller et al., 1992; Keller et al., 1996). Then, SESAMs have quickly become a highly successful technology especially for mode-locking applications due to their many advantages (Okhotnikov et al., 2004). However, SESAMs are costly to fabricate and present only a narrow operating bandwidth. Also, they have a long recovery time and a low damage threshold. These limitations lead research into exploring alternative SAs based on nanomaterials such as carbon nanotubes (Kataura et al., 1999; Margulis et al., 1998) in the late 1990s. The CNTs have attracted considerable attention due to its excellent nonlinear optical characteristic, low cost, and easy fabrication. The first mode-locked fiber laser based on CNTs was demonstrated in 2004 (Set et al., 2004). CNTs exhibited great performance in the applications of ultra-short pulse generation compared to SESAMs (Cheng et al., 2020). However, CNT suffers from its variable nanotube size, which in turn affects its operation bandwidth, band gap and absorption efficiency (Al-Hiti et al., 2021; Chernysheva et al., 2017; Reich et al., 2008; Set et al., 2004).

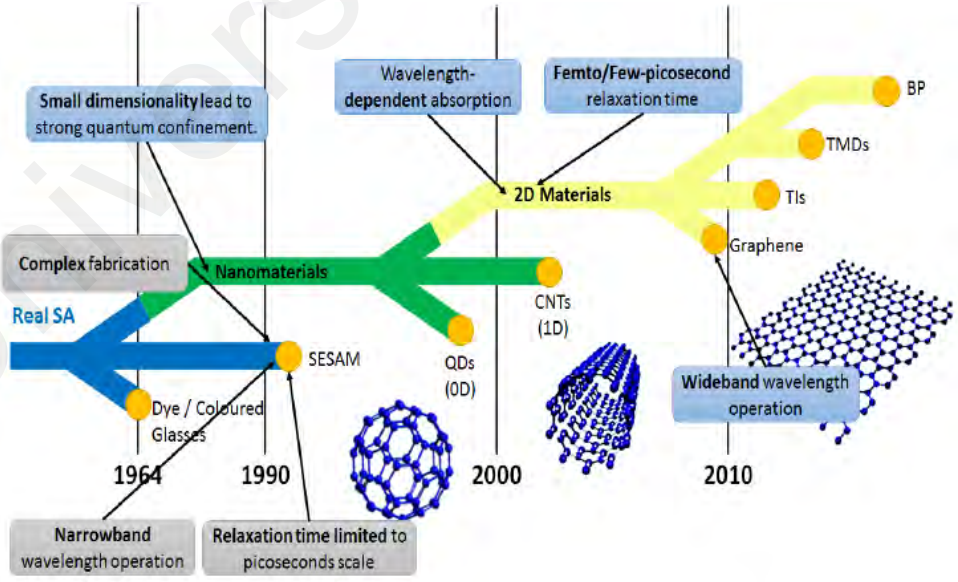

Figure 2.7: SA development stages in fiber laser (Woodward et al., 2015)

The two-dimensional (2D) materials have also received much attention laser applications due to their optical and electronic properties (Ge et al., 2018; Guo et al.,

2019; Li et al., 2020; Liu et al., 2017; Wang, 2017; Zhao et al., 2019). In addition, they have tunable structures that made them to be investigated widely in the ultra-short pulse generation. Graphene (Zhang et al., 2009), black phosphorus (BP) (Ismail et al., 2016) and transition metal dichalcogenides (TMDs) (Niu et al., 2018; Nizamani et al., 2021; Yang et al., 2019) have shown great potential in comparison with SESAMs and CNTs. These materials have a fast recovery time and wide spectral range (Ma et al., 2019), but they suffer from small modulation depth (Bao et al., 2009; Wang et al., 2016) and low band gap (between 0 eV to 1.5 eV) (Jiang et al., 2020; Luo et al., 2016). The graphene and BP also have low damage threshold (Al-Masoodi et al., 2016; Lau et al., 2017; Li et al., 2016). BP is hydrophilic material and thus it also suffers from rapid damage when exposed to water or oxygen.

Tables 2.1 and 2.2 compare the performance of these materials for applications in Q-switching and mode-locking, respectively. These materials were prepared as thin film using a common technique. The highest pulse energy of 531 nJ was achieved in a Q-switched laser, which was configured using multi-walled CNT (MWCNT) SA as shown in Table 2.1 (Ahmed et al., 2015). The high pulse energy is essential for applications in communication engineering, sensing devices, and material processing. The maximum repetition rate of 114.8 kHz was achieved from graphene material (Apandi et al., 2019). The width of the smallest pulse of 2.41 μs was also produced from graphene based SA in a Q-switched laser cavity (Ren et al., 2019).

As shown in Table 2.2, the highest repetition rate of 17.7 MHz was achieved in a mode-locked fiber laser using a single-walled CNT (SWCNT) (Markom et al., 2017). The ultra-short pulse with duration of 570 fs was also realized using BP SA (Ahmed et al., 2016). For mode-locking, the highest pulse energy of 74 nJ was recorded with MoS_2 SA (Wang, 2017). It is shown in Tables 2.1 and 2.2 that the same material may produce

different results if the fabrication methods are different. The mode-locking performance is strongly depended on the fabrication method of SA and cavity design.

Table 2.3 compares the absorption performances including saturable absorption, saturable intensity, non-saturable intensity, and linear absorption for various 2D nanomaterials. For saturable intensity and non-saturable intensity, the MoS_2 and $MoTe_2$ show significant progress in contrast with others. MoS_2 shows the highest saturable absorption of 11.3 % in comparison with other SAs as shown in Table 2.3 (Ahmed et al., 2016). On the other hand, the BP (Chen et al., 2015), reported a considerably high saturable absorption of 8.1 %.

Table 2.1: Q-switching performance for various SA's materials

No.	SAs	Wavelength (nm)	Rept. rate (kHz)	Pulse width (μs)	Pulse energy (nJ)	Ref.
1.	Graphene	1561.13	67.8	6.02	206	(Zuikafly et al., 2018)
2.	Graphene	1562.30	114.8	3.69	30.64	(Apandi et al., 2019)
3.	Graphene	1530	39.85	2.41	N/A	(Ren et al., 2019)
4.	MWCNT	1534.5	48.22	8.3	99.75	(Azooz et al., 2015)
5.	MWCNT	1533.6	33.62	4.2	531.0	(Ahmed et al., 2015)
6.	MWCNT	1568.6	47	4.6	102.1	(Mohammed et al., 2016)
7.	SWCNT	1533.6	33.33	8	291	(Ahmed et al., 2015)
8.	SWCNT	1560.76	41.78	4.73	N/A	(Xu et al., 2014)
9.	BP	1562.35	44.72	9.8	81.5	(Razak et al., 2017)
10	BP	1552.9	44.33	7.04	134	(Ahmed et al., 2017)
11.	MoS_2	1551.4	38.43	5.02	141.3	(Ahmed et al., 2017)
12.	WS_2	1559.8	104.1	9.6	123.2	(Razak et al., 2017)

Table 2.2: Mode-locking performance for various SA's materials

No.	Thin-film SA	Wavelength (nm)	Rept. Rate (MHz)	Pulse Width	Pulse Energy (nJ)	Ref.
1.	Graphene	1562	1.85	2.24ps	0.86	(Hammadi et al., 2018)
2.	Graphene	1557.7	11	820 fs	0.42	(Ahmed et al., 2017)
3.	Graphene	1565	1.79	0.756 ps	-	(Bao et al., 2009)
4.	SWCNT	1533.6	15.3	1.8 ps	0.28	(Ahmed et al., 2014)
5.	SWCNT	1564.2	17.7	0.77 ps	51.4	(Markom et al., 2017)
6.	MWCNT	1550	4.54	1.28 ps	-	(Cheng et al., 2013)
7.	BP	1562	5.426	1.23 ps	-	(Mao et al., 2018)
8.	BP	1560.7	6.88	570 fs	0.74	(Ahmed et al., 2016)
9.	BP	1571.45	5.96	0.946 ps	-	(Chen et al., 2015)
10.	MoS_2	1598.94	17.1	0.83 ps	74	(Ahmed et al., 2016)
11.	$MoTe_2$	1559	1.8	2.46 ps	-	(Wang, 2017)

Table 2.3: SA absorption properties for various materials

No.	SAs	Linear absorption	Saturable absorption (%)	Saturable intensity (MW/cm^2)	Non-Saturable absorption (%)	Ref.
1.	Graphene	-	6.1	21	47	(Ahmed et al., 2017; Hammadi et al., 2018)
2.	Graphene	-	6.2%	0.61	33.5	(Bao et al., 2009)
3.	BP	60 %	0.3	-	-	(Mao et al., 2018)
4.	BP	-	8.1	6.55	-	(Chen et al., 2015)
5.	BP	-	7	0.20	58	(Ahmed et al., 2017)
6.	MoS_2	-	8.6	100	8.2	(Ahmed et al., 2017)
7.	MoS_2	35 %	11.3	23.5	23.0	(Ahmed et al., 2016)
9.	$MoTe_2$	-	1.46	3.5	51	(Wang, 2017)

2.7 Pulsed Laser Importance Parameters

2.7.1 Repetition Rate

Repetition rate, f_{rep} is defined as the number of pulses emitted from the laser cavity per second. Figure 2.8 (a) shows the typical pulse train of a mode-locked laser, which indicates that a pulse repetition rate can be calculated by using the following equation:

$$f_{rep} = 1/\Delta t \tag{2.7}$$

where Δt represents the pulse period. The Q-switching approach may produce pulses with repetition rate in kHz regime while mode-locking generates pulses in MHz regime. The repetition rate of a Q-switched laser varies with pump power while a mode-locked laser has a fixed repetition rate, which is determined by a cavity length. The increase of cavity length reduces the repetition rate. Figure 2.8 (b) shows the typical frequency spectrum captured by a radio frequency spectrum analyser by using the fast photodetector. The pulse train's repetition rate was represented by the first fundamental frequency peak. The signal-to-noise ratio (SNR) representing the first fundamental peak refers to the difference in the intensity between a peak and the signal floor of a spectrum. The optimal SNR should be higher than 30 dB that represents the stability of the pulse.

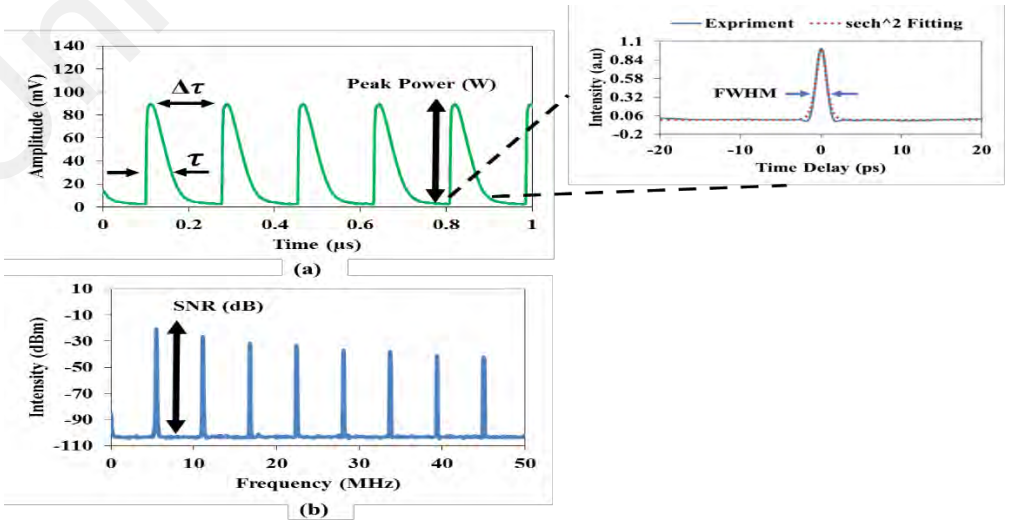

Figure 2.8: Output pulse train from a mode-locked laser in (a) time domain, and (b) frequency domain. Inset of (a) shows a typical autocorrelator trace.

2.7.2 Pulse Width

Pulse width is defined as τ, is based on the full width at half-maximum (FWHM) of the optical power against the time, as shown in the inset of Figure 2.8 (a). The pulse width of the laser is depended on the pulsing techniques. For instance, the Q-switching generates pulse width in the range of microsecond and nanosecond while mode-locked pulses are in a range from few picoseconds to femtoseconds regime. The shape of the pulse could be designed by a bell-shaped function, where the outline of pulse shape either Gaussian or Hyperbolic secant ($sech^2$) function. The Gaussian pulse shape is usually generated by the normal dispersion regime, while $sech^2$ by anomalous dispersion regime, a well-known working regime for soliton laser.

The product of the pulse width and spectral bandwidth is known as the time-bandwidth product (TBP). The TBP value is calculated by using the FWHM value for width and the bandwidth. Typically, the value of TBP is higher than 0.3, also, it is depended on the shape of the pulse and precision in defining the pulse width and bandwidth, where the laser cavity that generated ultra-short pulses have a large bandwidth.

The pulse width that generated from the laser cavity can be examined by using photodiode in combination with oscilloscope, where can observe the pulses which have width between microsecond and nanosecond. To measure ultra-short pulses, an autocorrelator can be used.

2.7.3 Pulse Energy

The pulse energy is defined as E_p and it represents the total energy that available in the pulse. Mathematically the pulse energy can be computed using the following equation:

$$E_p = \frac{P_o}{f_{rep}} \tag{2.8}$$

where the P_o represents the average output power. Usually, the energy generated from the laser cavity depends on the characteristics of the laser cavity and laser pulsing techniques. In addition, the range of pulse energy between millijoules to picojoules. The pulse energy of mode-locked operation usually in the range of the nanojoules and picojoules due to the high repetition rate from the laser cavity.

2.7.4 Output Power

The pulse's average output power P_o is created by the laser cavity's output. The output power will be affected by the design of the laser, where the mode-locked cavity generates lower output power in comparison with the Q-switched laser. This is due to the additional length of the cavity that degrades the laser performance. However, the estimation of output power is totally different with peak power, where peak power P_p represent the pulse energy divided by pulse width as shown in the following equation:

$$P_p = 0.88\frac{E_p}{\tau} \tag{2.9}$$

CHAPTER 3: PREPARATION AND CHARACTERIZATION OF SATURABLE ABSORBER

3.1 Introduction

Saturable absorber (SA) is a kind of optical thin-film that used to adjust the Q-factor of the cavity to generate the pulse laser. (Salam et al., 2019). SAs' absorption levels are varied and depending on their characteristics, such as spectral range. (Ismail et al., 2016), saturation fluence (Salam et al., 2019), linear absorption (Jafry et al., 2021), and nonlinear absorption (Baharom et al., 2019). SAs are frequently utilized in the generation of passive pulse lasers because of their advantages as compact, inexpensive, versatile, and simple in design. (Keller, 2003). SAs mostly consists of the elements and the compounds of the Boron and Carbon groups. Many of nanomaterials had fabricated as SA, such as, transition metal dichalcogenides (TMDs), black phosphorus (BP), graphene, and carbon nanotube (CNT). Graphene-based SAs have a broad spectrum absorption. However, it has a small modulation depth and low damage threshold. (Dong et al., 2012). CNT-based SAs are simply fabricated and inexpensive (Hasan et al., 2009; Li et al., 2014). However, they have a narrow band absorption which is significantly impacted by the nanotube diameter. (Wang et al., 2015). BP-based SAs, typically have a large bandwidth spectrum. However, they suffer from small modulation depth, also low optical threshold, and complicated fabrication procedures. (Chen et al., 2015). SAs of the TMD materials compounds such as Ws_2 (Mao et al., 2015; Yang et al., 2019), SnS_2 (Niu et al., 2018), and $MoSe_2$ (Liu et al., 2018), they showed to have excellent absorption properties. Nevertheless, they are restricted via low damage tolerance threshold, and an intricate manufacturing process. Therefore, many works have been devoted in the recent years to explore new materials as SA. This chapter presents the fabrication and characterization of three types of SA devices based on two different materials: 8-Hydroxyquinolino cadmium chloride hydrate (8-HQ$CdCl_2H_2O$) and chromium aluminum carbide (Cr_2AlC).

3.2 Exfoliated 8-HQCdCl$_2$H$_2$O over Scotch Tape

Organic materials have also attracted much interest in recent years for various electronic and photonics applications since they have an ultrafast nonlinear response and wide spectral tunability (Al-Hiti et al., 2020; Li et al., 2019). Moreover, they have excellent qualities such as low fabrication cost (Ji et al., 2020), good electrical conductivity (Sheberla et al., 2014), mechanical flexibility (Park et al., 2015) and thermal stability (Zhao et al., 2006). The organic materials have good electrical properties which make them suitable for the applications in various electronic devices such as photovoltaic in the solar panel (Spalatu et al., 2017), organic light-emitting diode (OLED) (Meftah et al., 2020; Puniredd et al., 2013), and field-effect transistor (FET) (Sun et al., 2017). For instance, 8-Hydroxyquinolino cadmium chloride hydrate (8-HQCdCl$_2$H$_2$O) is widely used in electronic devices (Shahedi et al., 2017). Also, the 8-HQCdCl$_2$H$_2$O has excellent properties that make it useful for different applications, these characteristics include good conductivity (Salyulev et al., 2016), thermal stability (Baraker et al., 2018), reliability (Gurnani et al., 2003) and simple fabrication (Fung et al., 2012). In this thesis, the generation of passively Q-switched and mode-locked pulses at 1.5 μm region using the newly developed 8-HQCdCl$_2$H$_2$O based SA. The SA is fabricated by two different techniques: mechanical exfoliation and drop-casting. This section discusses the fabrication and characterization of 8-HQCdCl$_2$H$_2$O SA, which was obtained through the mechanical exfoliation technique.

3.2.1 Preparation of the SA Device

The 8-HQCdCl$_2$H$_2$O SA was prepared by mechanical exfoliation because it is a simple and authoritative method formerly utilized for materials such as BP (Chen et al., 2015), graphene (Chang et al., 2010) and TI (Sotor et al., 2014). The fabricating started by adding 50 mg of 8-Hydroxyquinolino (8-HQ) powder into 5 ml of methanol to produce solution A, and 50 mg of cadmium chloride hydrate (CdCl$_2$H$_2$O) powder into 2.5 ml of methanol

to produce solution B. Subsequently, both solution A and B were left for 10 hours stirring separately. After that, the solutions were combined and stirred for about 7 hours to form mixture C (i.e. 8-HQCdCl_2H_2O). Then, solution C was poured into the petri dish to dry under normal room temperature for about 3 days to form the 8-HQCdCl_2H_2O powder. The preparation of the 8-HQCdCl_2H_2O powder is shown in Figure 3.1 (a). The 8-HQCdCl_2H_2O powder was then exfoliated by utilizing scotch tape. The scotch tape was folded and pressed persistently to form evenly distributed 8-HQCdCl_2H_2O powder over it. Finally, a small piece of 8-HQCdCl_2H_2O over scotch tape was inserted onto fiber ferrule to form SA, as illustrated in Figure 3.1 (b).

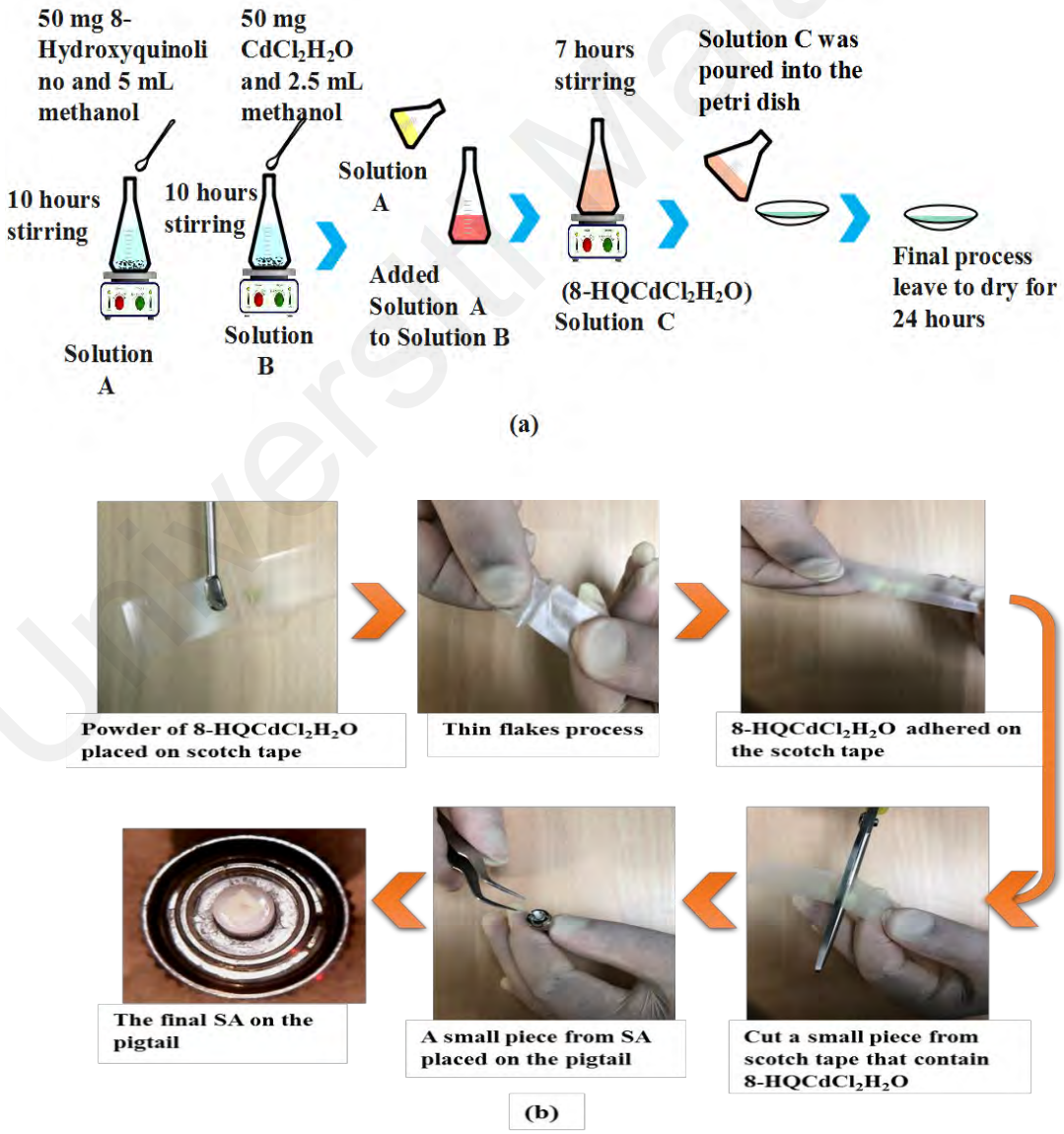

Figure 3.1: SA fabrication procedure, (a) material fabrication process, and (b) mechanical exfoliation of SA.

3.3 Physical and Chemical Characterization

The exfoliated 8-HQCdCl2H2O had examined by using the energy-dispersive X-ray spectroscopy (EDX), then it was scanned by scanning electron microscopy (SEM). SEM determined the structural mapping of the materials, while EDX revealed the elemental constituent of the materials. Figure 3.2 (a) shows the SEM image, which indicates the uniform distribution of 8-HQCdCl$_2$H$_2$O molecules. Figure 3.2 (b) shows the chemical elements of our SA analyzed by the EDX. The exfoliated 8-HQCdCl$_2$H$_2$O consists of carbon (C), nitrogen (N), oxygen (O), chloride (Cl), and cadmium (Cd) elements as tabulated in the inset of Figure 3.2 (b). As seen, 38.28 weight % of carbon was detected whereas nitrogen 4.26 weight %. Both elements are originated from the scotch tape. The content of oxygen, chloride and cadmium element was 6.22, 17.93 and 33.31 weight %, respectively. Hence, it confirmed the elemental distribution of the 8-HQCdCl$_2$H$_2$O SA.

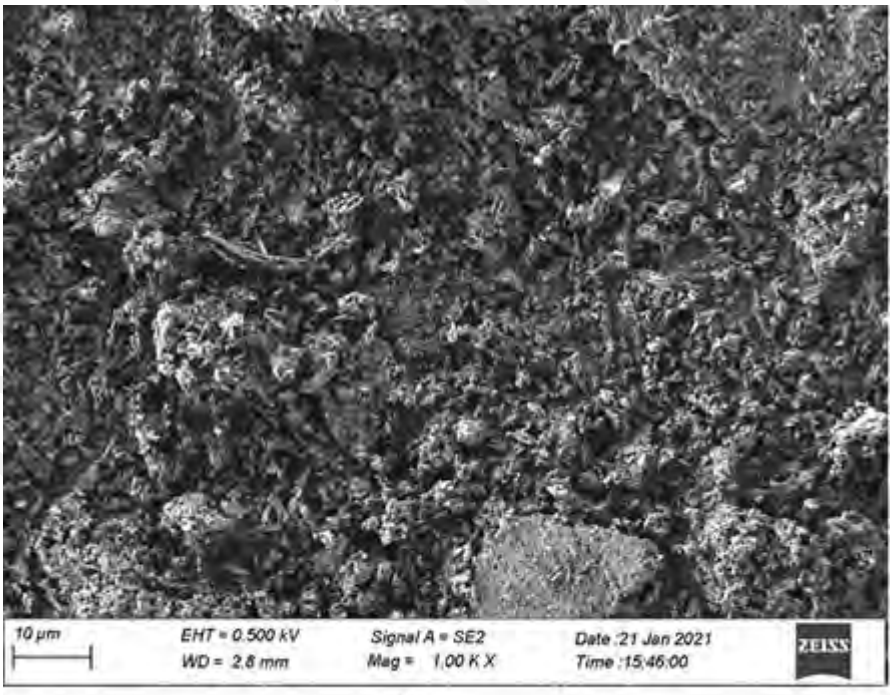

(a)

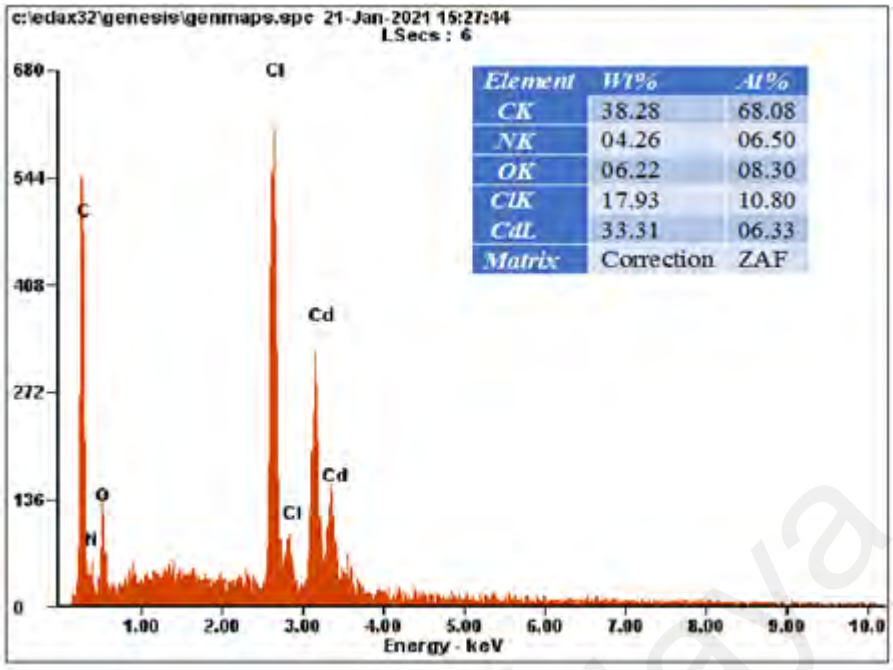

(b)

Figure 3.2: The physical and chemical characteristics of the 8-HQCdCl$_2$H$_2$O over scotch tape, (a) SEM image, and (b) EDX analysis

3.3.1 Optical Characterization

The two main analyses that determine the optical properties of the SA devices are linear absorption and nonlinear optical response. By illuminating the SA material with a laser source at a broad wavelength, one may detect the working wavelength of such material. This work investigates the absorption of material in the near-infrared region, specifically the 1.55 µm region. The availability of an optical spectrum analyzer (OSA) that covers from 1.2 to 1.6 µm region gives the ability to probe material's absorption at this regime. A good saturable absorber needs to own sufficient normal absorption at the working wavelength, while also providing the nonlinear absorption in the same region. The latter is normally determined by using a Z-scan technique, which provides a useful understanding of the material's optical properties such as nonlinear index (Kerr nonlinearity) and nonlinear absorption coefficient (Gu et al., 2006). However, due to the limited equipment in the working wavelength of 1.55 µm regime, this method can be replaced with a balanced-twin detector technique. This homemade method allows the

detection of a few important parameters in pulsed laser generation which are saturable absorption, non-saturable absorption, and saturation intensity.

Concerning the linear absorption, a white light source (WLS) (YOKOGAWA, ANDO AQ-4303B) with a wavelength range between 700 nm and 1700 nm was employed to carry out the linear absorption test. Two patch cord of single mode fiber (SMF) were used for linear absorption. The first patch cord of SMF was a reference and connected between the WLS and OSA. The second patch cord of SMF, is linked between the input of SMF to the WLS, and the output of SMF was connected to an OSA. In addition, the second SMF contain the FC/PC connector to carry the 8-HQCdCl_2H_2O SA. The broadband light was launched from the WLS passed through the FC/PC that contain the 8-HQCdCl_2H_2O SA to reach the OSA with a 1nm resolution and a video bandwidth (VBW) of 10 Hz, as shown in Figure 3.3 (a). The result is shown in Figure 3.3 (b), where the linear absorption recorded at a wavelength range between 1200 nm and 1600 nm. It indicates the linear absorption of 2.1 dB at 1550 nm wavelength.

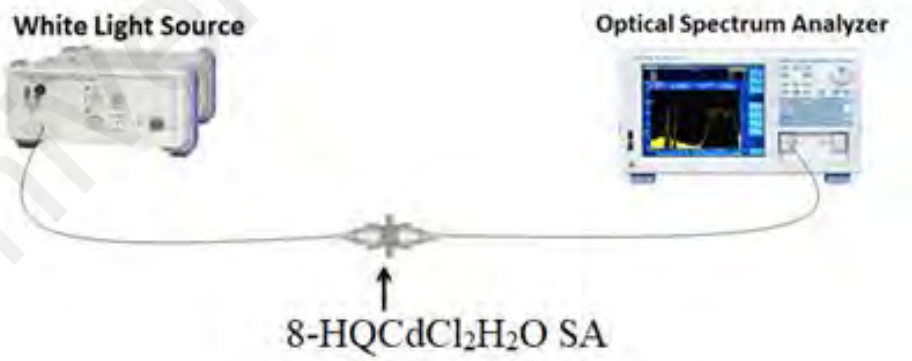

(a)

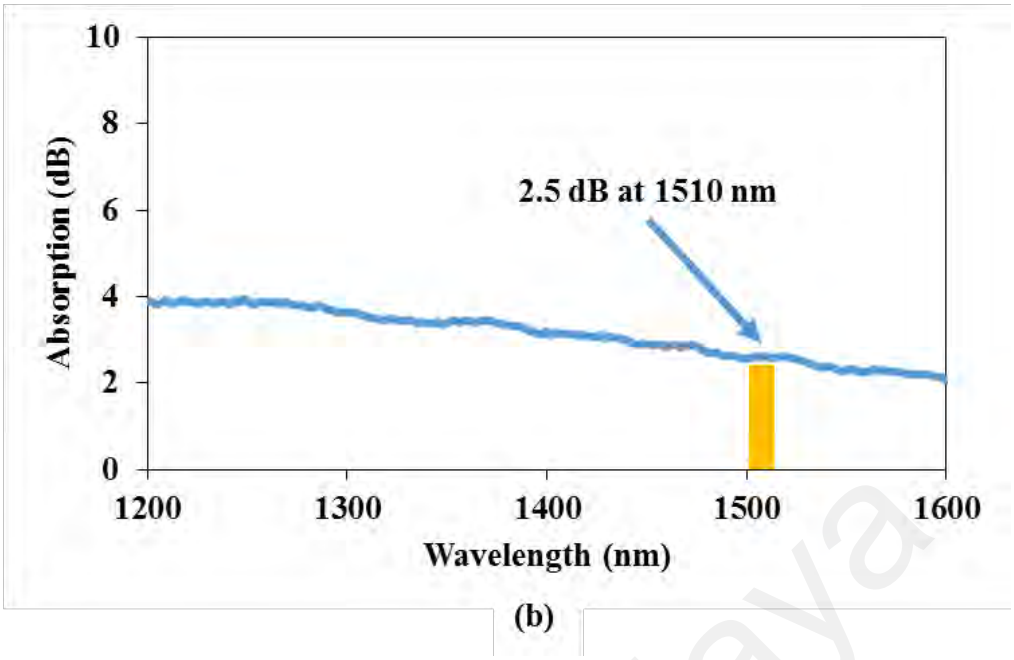

Figure 3.3: Linear absorption measurement, (a) experimental setup, (b) the obtained result

Next, the nonlinear absorption of the SA device was measured by using a balanced twin-detector measurement. A mode locked erbium-doped fiber laser with a pulse width of 3.0 ps, corresponds to the repetition rate of 1.9 MHz was constructed as laser source. The center wavelength of the mode locked EDFL was captured at 1559 nm. The mode locked EDFL was converged to an erbium-doped fiber amplifier (EDFA), which was then connected to an optical attenuator. The intensity of the signal was controlled by rotating the knob at the attenuator. The laser output power of the attenuator is split by an optical coupler (OC) of 50/50. The 50% of the laser was launched to the 8-HQCdCl_2H_2O SA for the evaluation of the absorption properties, and another 50% of the laser output was kept as a reference. The signal was measured using an optical power meter. The data were recorded and fitted using the following equation:

$$\alpha\,(I) = \frac{\alpha_0}{\left(1+\frac{I}{I_S}\right)} + \alpha_{ns} \tag{3.1}$$

where α_0 represents modulation depth or saturable absorption, I is the intensity-dependent input, I_s is the saturation intensity, and α_{ns} is the nonsaturable absorption. The experimental setup for measuring the nonlinear optical response was depicted in Figure 3.4 (a). The nonlinear absorption curve obtained is shown in Figure 3.4 (b). It indicates that the 8-HQCdCl$_2$H$_2$O SA exhibits a non-saturable absorption of 78 %, saturable absorption of 11 %, and saturable intensity of 2 MW/cm^2. High non-saturable absorption is attributed to the rough morphology of the exfoliated 8-HQCdCl$_2$H$_2$O tape as well as the impurity.

The optical absorbance spectrum of the 8-HQCdCl$_2$H$_2$O tape is also measured at UV and visible wavelength range as shown in Figure 3.5. The peak spotted at 470 nm could correspond to the 8-HQCdCl$_2$H$_2$O absorption. The optical band gap was calculated using formula $(\alpha hv)n = B(hv - Eg)$ as B is a constant relative to the material, hv is the photon energy and n equals 2 for direct transition. While Alpha (α) is the absorption coefficient which was calculated from the Beer-Lambert's law as $\alpha(v) = 2.303 \times Abs(\lambda)/d$ as d is the thickness of the thin film. The band gap is estimated at 2.6 eV by extrapolation at the horizontal axis of the linear region of $(\alpha hv)^2$ against hv, see the inset of Figure 3.5.

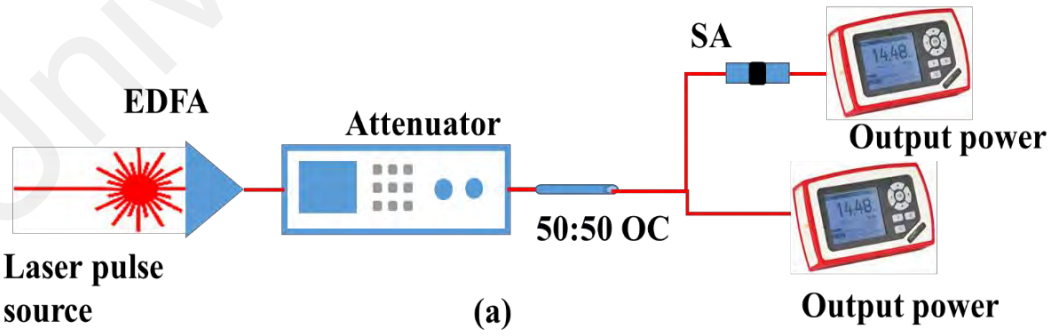

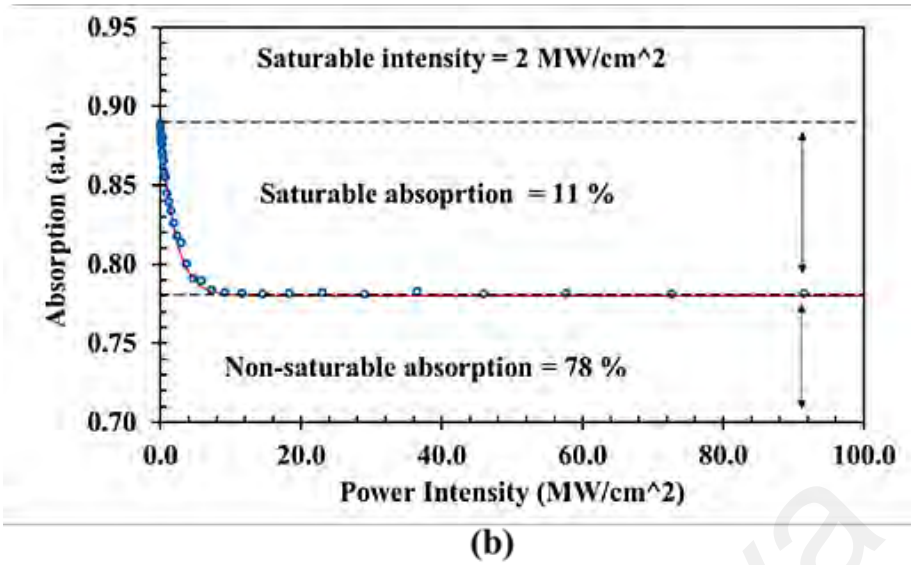

Figure 3.4: Measurement of the nonlinear optical response, (a) experimental arrangement, (b) results.

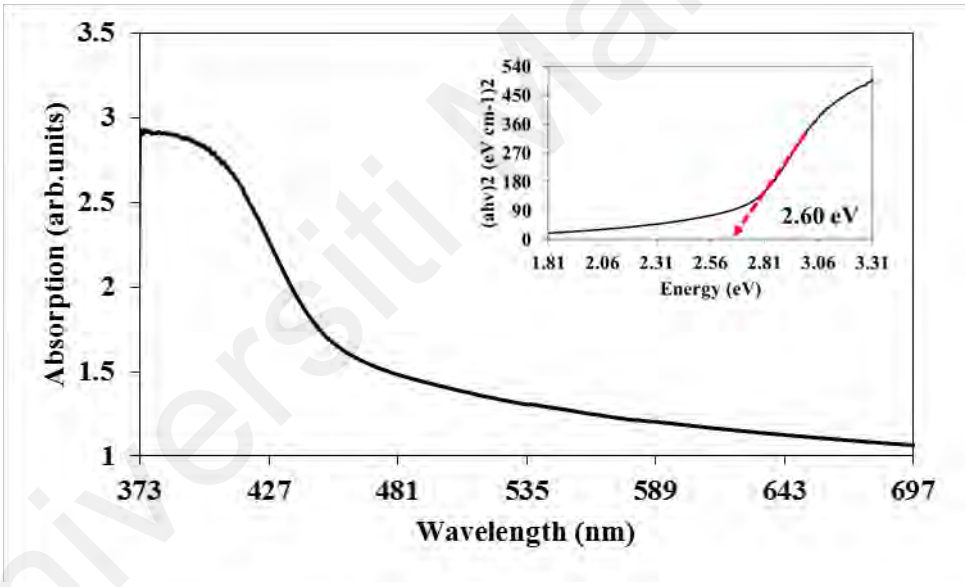

Figure 3.5: The absorption spectrum in UV and visible range. Inset shows the estimation of the optical bandgap for the 8-HQCdCl$_2$H$_2$O SA.

3.4 8-HQCdCl$_2$H$_2$O PVA Thin-Film

The fabrication of 8-HQCdCl$_2$H$_2$O thin-film SA is presented in this section. It uses polyvinyl alcohol (PVA) compound as a host polymer due to several advantages such as high flexible thin-film forming ability and excellent physical properties and chemical resistance (Wu et al., 2015). The first step in the fabrication process of 8-HQCdCl$_2$H$_2$O

thin-film is to add 50 mg of 8-Hydroxyquinolino powder into 5 ml of methanol to prepare solution A. Then, 50 mg of $CdCl_2H_2O$ powder was added into 2.5 ml of methanol to make solution B. Both solutions A and B are left separately for 10 hours stirring. Subsequently, the solution A was mixed with solution B and stirred for about 7 hours to prepare solution C. On the other hand, PVA solution was prepared by adding 1 g of PVA into 100 ml of distilled water, and the solution was stirred for about an hour. Finally, 2.5 ml of PVA solution was thoroughly mixed with solution C through both stirring and sonicating processes. The mixed solution was then left to dry under normal room temperature for twenty-four hours to allow the forming of 8-HQ$CdCl_2H_2O$ PVA thin film. The whole preparation process is summarized as illustrated in Figure 3.6. The trinocular compound microscope (AmScope) was used to measure the thickness of the prepared 8-HQ$CdCl_2H_2O$ PVA thin-film. Thickness of thin film was about 60 μm and the same thin film has been used for Q-switched and mode-locked pulse generation experiments.

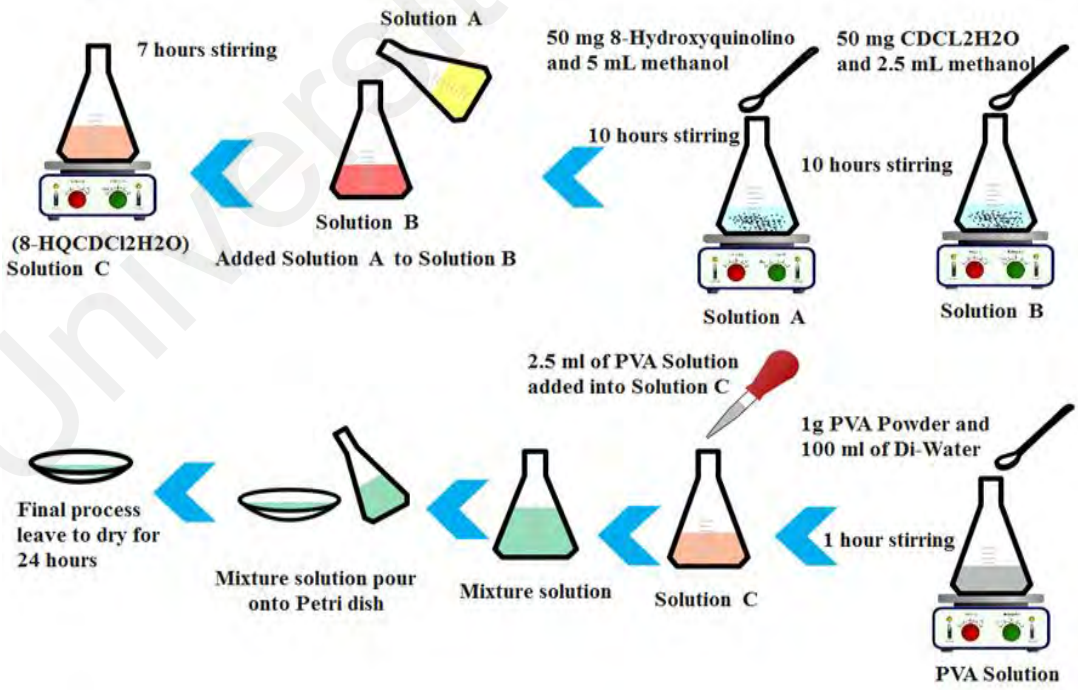

Figure 3.6: Procedures in preparing 8-HQ$CdCl_2H_2O$ PVA thin-film

To find out the structure of 8-$HQCdCl_2H_2O$ thin film, it is characterized by SEM. Figure 3.7 (a) shows the SEM image, which indicates the uniform distribution of 8-$HQCdCl_2H_2O$ molecules along with the polymer. As seen, the size of 8-$HQCdCl_2H_2O$ particles varies from 200 to 300 nm. Figure 3.7 (b) shows the chemical elements of our thin film analyzed by the EDX. The thin film consists of carbon (C), oxygen (O), cadmium (Cd), chloride (Cl), and silicon (Si) elements. The result indicates that the materials utilized are pure since no other elementary peaks are detected. The chemical composition and molecule structure of thin film investigated by Perkin Elmer Spectrum 400 Fourier Transform Infrared Spectroscopy (FTIR), and the spectrum obtained based on transmission mode is shown in Figure 3.7 (c). The FTIR spectrum was obtained within the range of wavenumber from 4000 to 500 cm^{-1}. There is a strong absorption between the two points of 3000–3600 cm^{-1}, which peaks at 3325.99 cm^{-1}. This is due to the symmetrical stretching of N-H from the intramolecular hydrogen bonds (Shukla et al., 2003). The stretching peaks of C–H, C=H, C=C, C-H, and C-O were observed at 2937.99, 1732.38, 1498.87, 1297.78, and 1023.93 cm_{-1}, respectively (Coates, 2006; Hamdalla et al., 2016; Lei et al., 2017). Nitrogen bonds assign to various forms as N=N and N-O were found at 1576.72 and 1515.55 cm^{-1} (Nandiyanto et al., 2019). The fingerprint region of FTIR is between 500 and 1500 cm^{-1} for the 8-$HQCdCl_2H_2O$ while the heavier elements are detected between 780 and 400 cm^{-1}. The peaks of 639.23 and 543.76 cm^{-1} represent the bond of O-Cl in the thin-film (Ezema, 2005).

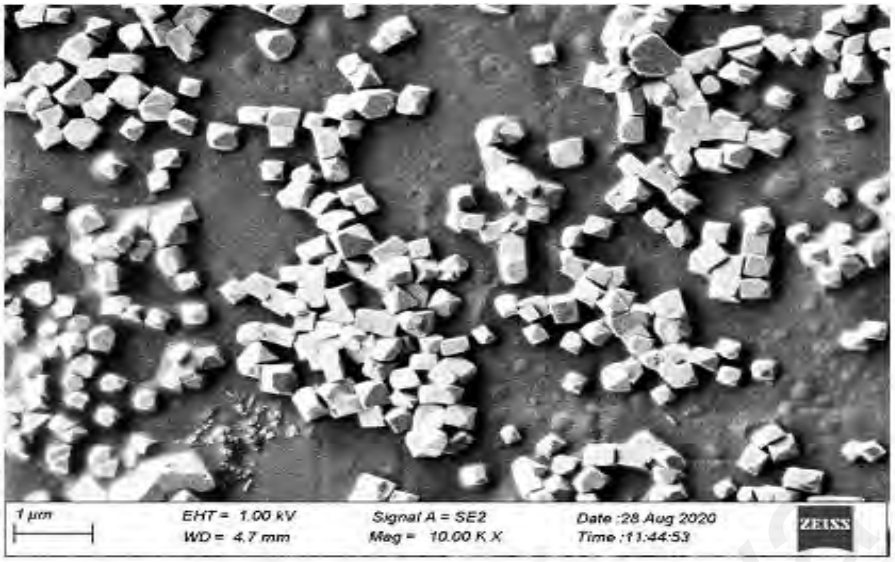

(a)

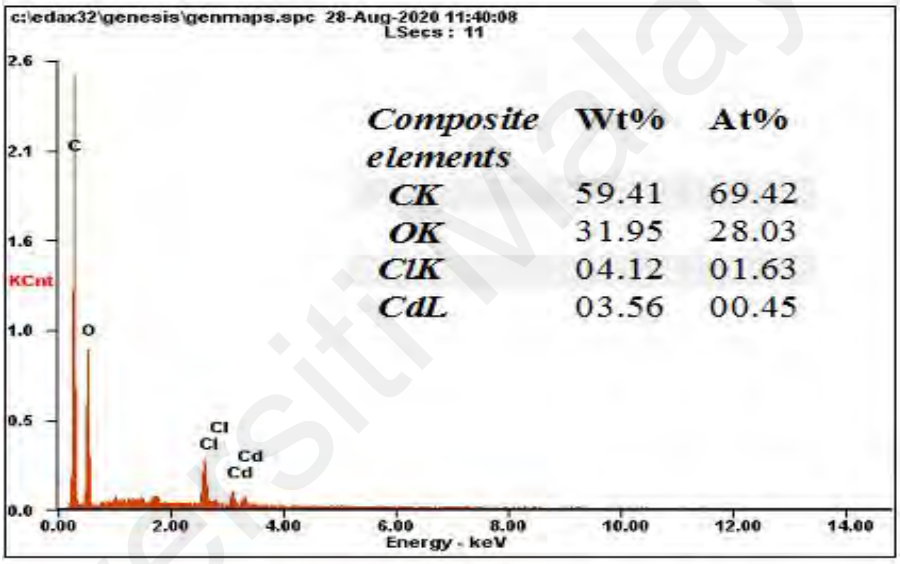

(b)

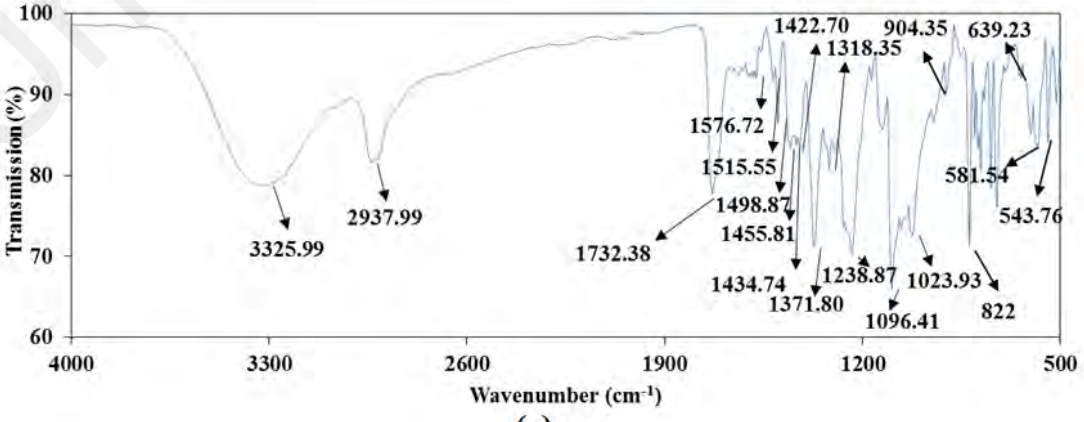

(c)

Figure 3.7: Characterization of 8-HQCdCl$_2$H$_2$O thin film, (a) SEM image, (b) EDX profile, and (c) FTIR analysis

The linear absorption of the 8-HQCdCl$_2$H$_2$O PVA thin-film was then evaluated by launching a broadband light from a WLS into the prepared film and recorded the output spectrum by OSA as described in Figure 3.3 (a). Figure 3.8 (a) shows the experimental result. The linear absorption of about 4 dB was observed at 1540 nm wavelength. Nearly the same material absorption could be observed in L-band. The nonlinear absorption was also measured using the experimental arrangement of Figure 3.4 (a) for the prepared 8-HQCdCl$_2$H$_2$O thin film. It used a mode-locked laser pulse source with a 3.6 MHz of repetition rate, 1.02 ps of pulse width, and 1562 nm of wavelength, respectively. Figure 3.8 (b) shows the nonlinear absorption curve, which was obtained by launching the light source into the prepared 8-HQCdCl$_2$H$_2$O PVA film. It indicates that the 8-HQCdCl$_2$H$_2$O film exhibits a saturable absorption, non-saturable absorption, and saturable intensity of 18 %, 70 %, and 0.1 MW/cm^2, respectively. The low saturation intensity of the SA allows the laser to self-starts at low optical intensity.

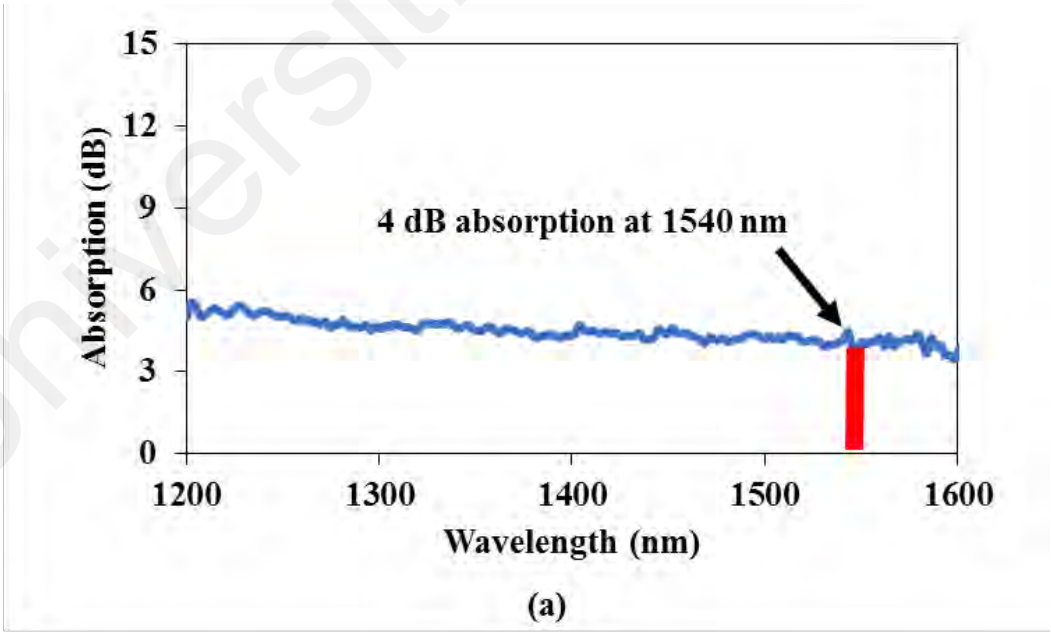

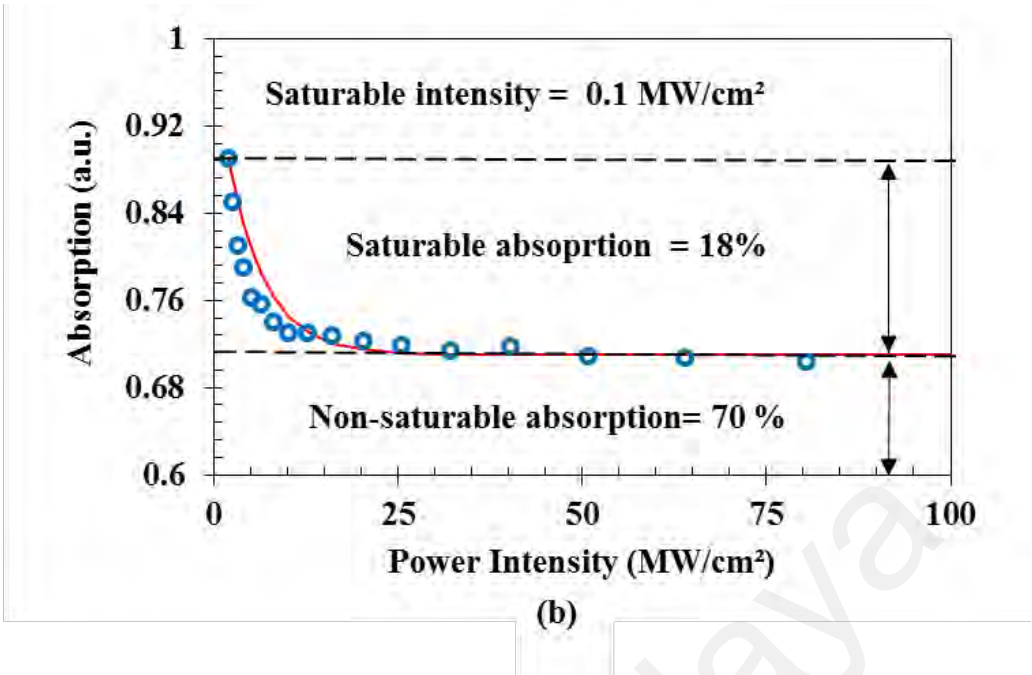

Figure 3.8: 8-HQCdCl$_2$H$_2$O PVA film absorption properties, (a) linear absorption, and (b) nonlinear absorption

3.5 Chromium Aluminum Carbide Thin Film

MAX phases compounds are hexagonal carbides and nitrides (Tallman et al., 2013). They consist of a single element of an early transition metal (i.e. that represents M), an element of group A (i.e. chemical elements of groups 13–14) and an X that represents either carbon or nitrogen to form the MAX compound (Gonzalez-Julian et al., 2016). MAX phases have a mixture of chemical (Schneider et al., 2004), electrical (Tian et al., 2006), and mechanical properties (Li et al., 2011) of ceramic and metal under different circumstances (Tian et al., 2007). They have a good electrical and thermal conductivity (Xiao et al., 2011), a good thermal shock resistance and a high damage threshold due to their electronic structure and chemical bonding (Gonzalez-Julian et al., 2018).

Nowadays, various research studies have reported MAX phases as SAs due to their excellent compatibilities in laser applications (Jafry et al., 2020; Kwon et al., 2021). The optical capabilities of MAX phases such as a large effective nonlinear absorption coefficient (Ahmad et al., 2019), a fast optical-switching capability (Lee et al., 2019) and a high optical damage tolerance (Jafry et al., 2020) make it a preferable SA, in comparison

to other 2D-based materials. In this work, the chromium aluminum carbide (Cr_2AlC) from the MAX phases family is chosen as the main compound for a SA, due to its excellent mechanical and chemical properties, such as enhanced ductility and durability (Al-Khazrajy et al., 2015). Lee et al. reported that Cr_2AlC oxidized only at the extreme temperatures of above 1300 °C (Lee et al., 2007). The Cr_2AlC compounds have attractive characteristics as they contain both metals and ceramics, which made the Cr_2AlC to have high hardness (Barsoum, 2000) and the heat stability (Drulis et al., 2006). Cr_2AlC also has excellent electrical resistivity resulting the material to be an good electrical conductor at high temperatures (Gorshkov et al., 2019). One of the objectives of this thesis is to experimentally demonstrate the process of generation of the mode-locked and the Q-switched laser pulses by a new SA based on Cr_2AlC-PVA. This section presents the preparation process and characterization of Cr_2AlC film SA.

In this work, The PVA was utilized as a host polymer due to its various benefits, such as chemical resistance, outstanding physical properties, and high flexibility (Wu et al., 2015). The Cr_2AlC nano-powder was obtained from Laizhou Kai Kai Ceramic Materials Company Ltd which has a purity above 98 % with a particle size of 200 nm. The whole preparation process of Cr_2AlC film SA is shown in Figure 3.9. Initially, PVA solution was prepared by dissolving 1 g of PVA powder in 100 ml of deionized (DI) water, then they were left stirring for 1 hour at 500 RPM using a magnetic stirrer. Then, 50 mg of Cr_2AlC powder was added into 8 ml of final PVA solution for 2 hours stirring at 800 rpm under normal room temperature to obtain a solution mixture. Eventually, the mixture was poured into a petri dish and placed under normal room temperature to dry for seven days. A tiny piece of Cr_2AlC PVA thin-film was cut, then placed between two FC/PCs to form an optical SA device in the fiber laser.

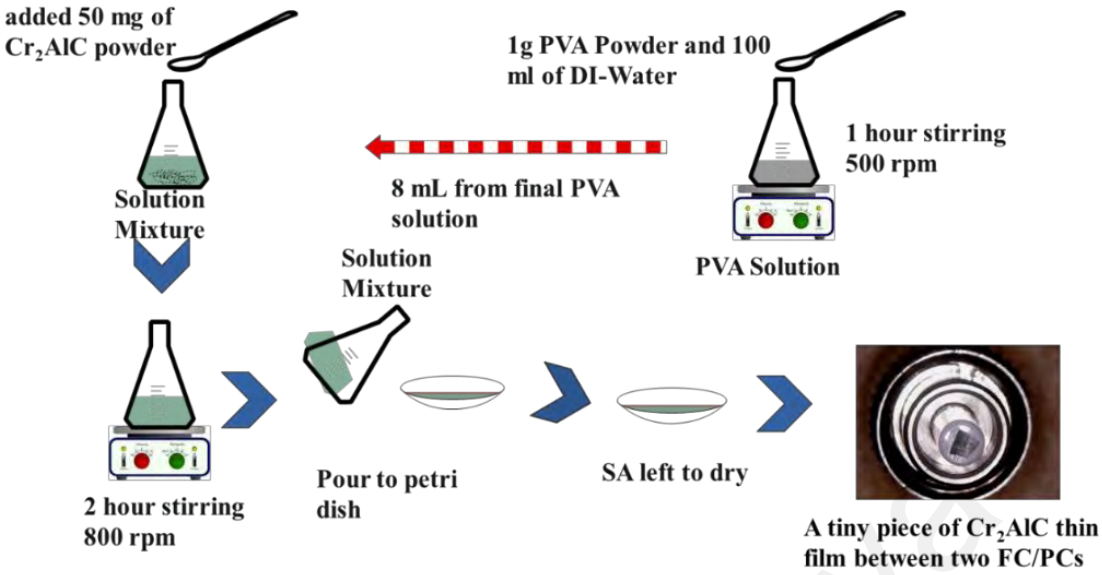

Figure 3.9: Cr_2AlC SA fabrication steps

Figure 3.10 describes the morphological and elemental characterization of Cr_2AlC particles in the host of PVA. The surface of Cr_2AlC thin film had scanned using a SEM and then analyzed using an EDX. Figure 3.10 (a) describes the Cr_2AlC particles dispersed throughout the polymer. Also, the SEM image was acquired with a 1 nm of resolution. The surface examination with the EDX had performed to confirm the existence of Cr_2AlC molecules in the thin film. Figure 3.10 (b) shows several peaks with 53.43% weight of carbon (C), 23.99% weight of oxygen (O), 8.05% weight of aluminum (Al) and weight of 14.52% chromium (Cr). The EDX analysis also proved that the material used is pure because no other elementary peaks were detected.

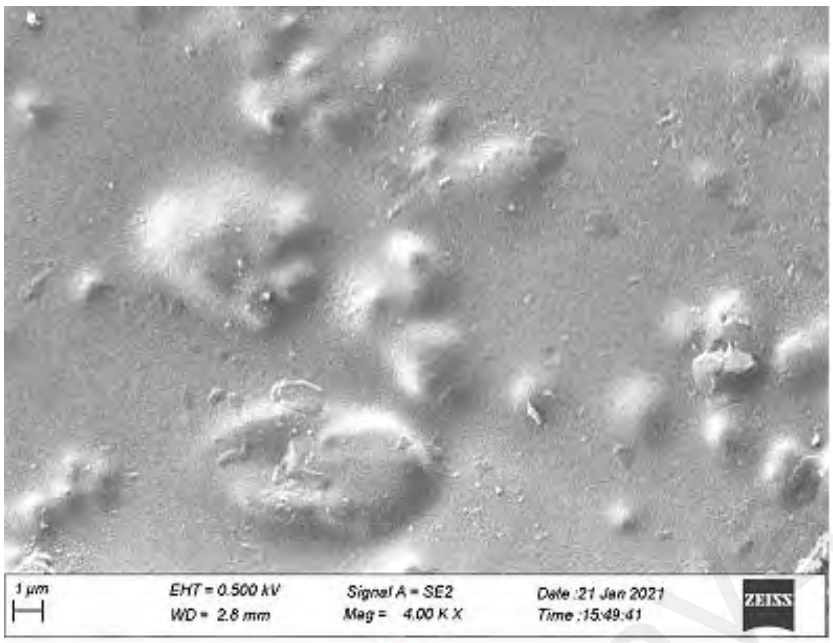

(a)

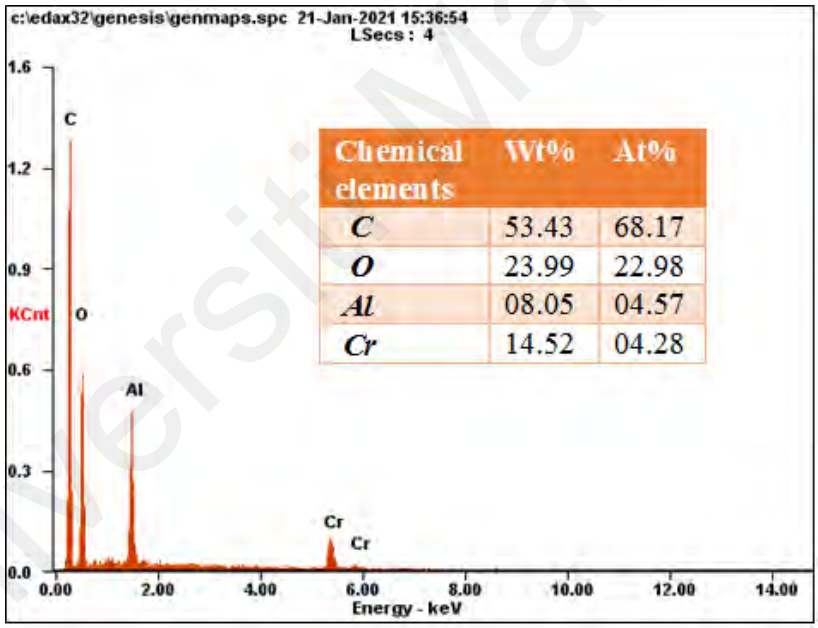

(b)

Figure 3.10: Characterization of Cr_2AlC, (a) SEM image, and (b) EDX analysis

The Cr_2AlC film was also examined for nonlinear and linear absorption characteristics as shown in Figure 3.11. The linear absorption of Cr_2AlC was obtained by launching a light source to the thin-film and then the wavelength data were recorded by an OSA, see Figure 3.11 (a). The linear absorption was realized at 12 dB with a wavelength of 1555 nm and a wavelength regulation of 1 nm. The properties of nonlinear absorption of

Cr_2AlC PVA thin-film was obtained by amplifying mode-locked pulse laser in the EDFA and sent to the attenuator as described in section 3.2, see Figure 3.4 (a). The attenuator output was split by 50/50 optical coupler, 50% output of SA film, and other 50% output reference. The mode-locked pulse laser parameter recorded a pulse width of 2.5 ps, the repetition rate of 1.88 MHz, and wavelength 1558 nm. Figure 3.11 (b) demonstrates the findings of the nonlinear absorption for Cr_2AlC film that achieved 40 MW/cm^2 of saturable intensity, 3.2% saturable absorption, and 28.4% non-saturable absorption. The optical absorbance spectrum of the Cr_2AlC in UV and visible range is shown in Figure 3.11 (c). It shows the peak spotted at 388 nm could correspond to the Cr_2AlC. The optical band gap was calculated using formula $(\alpha hv)n = B(hv - Eg)$ as B is a constant relative to the material, hv is the photon energy and n equals 2 for direct transition. While Alpha (α) is the absorption coefficient which was calculated from the Beer-Lambert's law as $\alpha(v) = 2.303 \times Abs(\lambda)/d$ as d is the thickness of the thin film. The band gap is estimated at 2.76 eV by extrapolation at the horizontal axis of the linear region of $(\alpha hv)^2$ against hv, see Figure 3.11 (d).

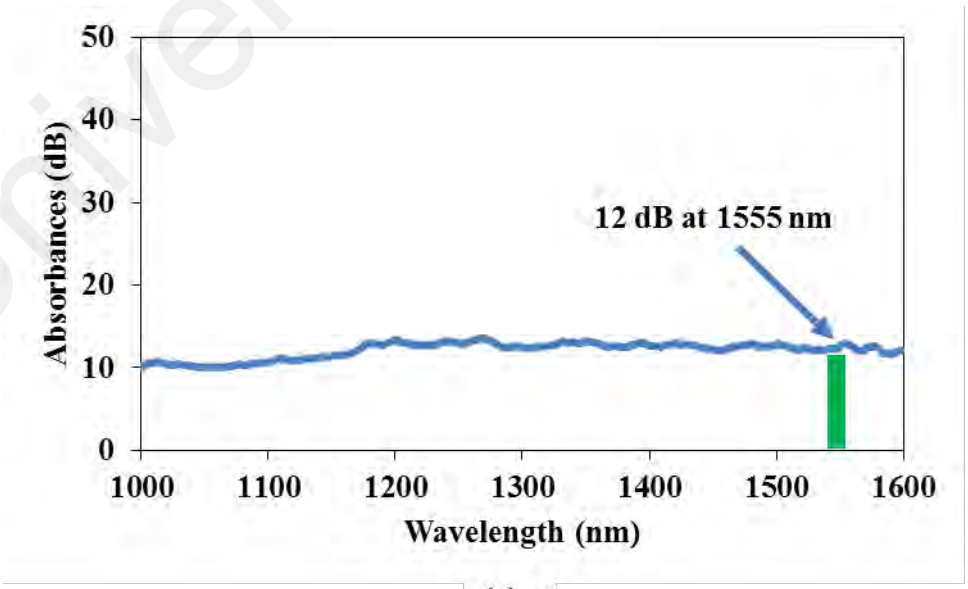

(a)

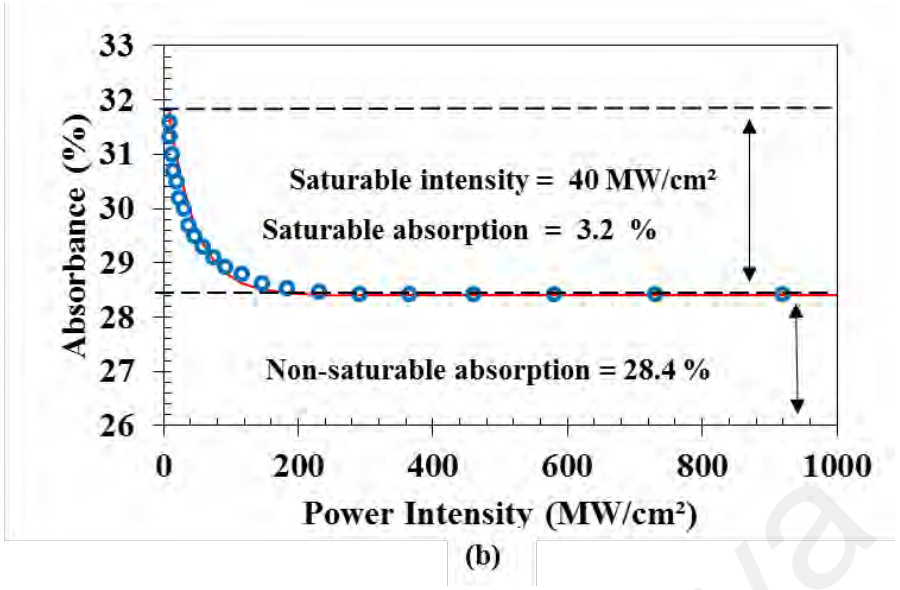

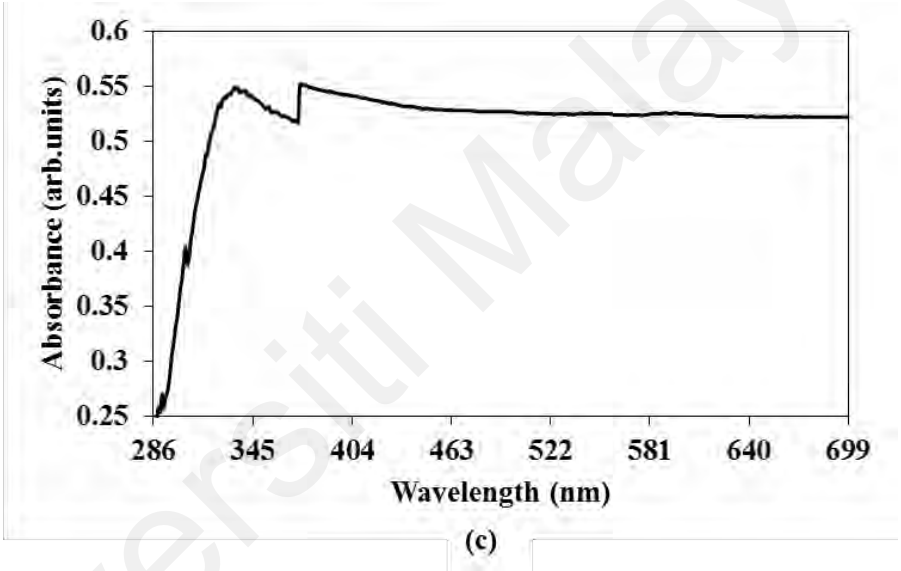

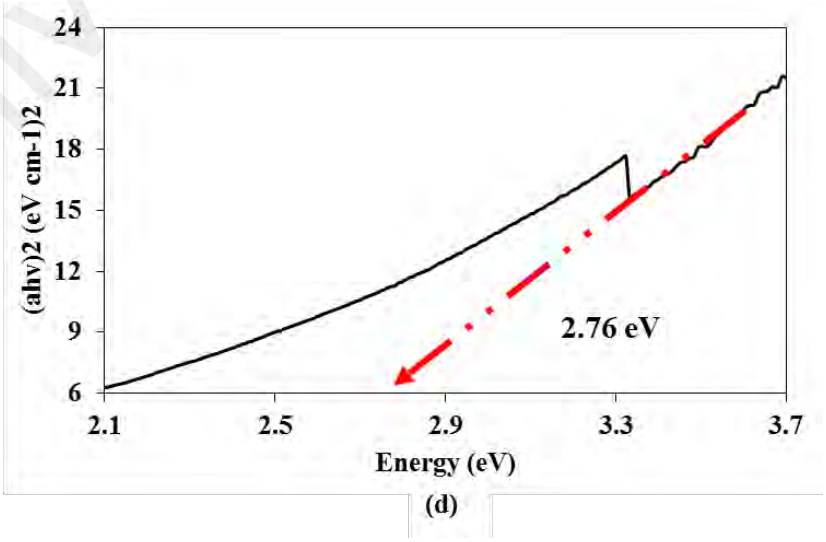

Figure 3.11: The absorption characterizations of Cr_2AlC film, (a) linear absorption, (b) non-linear absorption, (c) absorption spectrum in UV and visible range, and (d) optical band gap of Cr_2AlC

3.6 Summary

The three different types of SAs were successfully developed based on two different materials: 8-HQCdCl_2H_2O and Cr_2AlC, which belong to the organic and MAX phases family, respectively as a based material. 8-HQCdCl_2H_2O SA was prepared based on two methods: mechanical exfoliation and drop-casting while the Cr_2AlC also was prepared by drop-casting. The PVA was used as a host polymer in preparing the thin films. These SAs were also successfully characterized in terms of physical and chemical characteristics as well as linear and nonlinear absorption properties. The exfoliated 8-HQCdCl_2H_2O on scotch tape, 8-HQCdCl_2H_2O thin film, and Cr_2AlC thin film have a saturable absorption or modulation depth of 11 %, 18 %, and 3.2 %, respectively, and thus suitable for Q-switching and mode-locking applications. The linear absorption of exfoliated 8-HQCdCl_2H_2O, 8-HQCdCl_2H_2O PVA, and Cr_2AlC PVA of 2.1 dB, 4 dB, and 12 dB, respectively.

CHAPTER 4: NANOSECOND Q-SWITCHED PULSES GENERATION

4.1 Introduction

The generation of short-pulse laser technology has been getting a high demand in the medical and optoelectronics applications due to their promising advantages (Pile, 2013). This type of laser pulsing generation could achieve through a Q-switching technique. This technique can be classified into passive and active schemes. The passive scheme is realized by placing a saturable absorber (SA) device in the laser cavity and it has several advantages like cost-effectiveness, simplicity in the design, flexible configuration, and compactness (Guoyu et al., 2015; Rahman et al., 2019). The addition of external driven modulators makes active schemes more complex, resulting in high cost (Al-Hiti et al., 2019; Samsamnun et al., 2020).

To date, several types of SAs have reported for generating passive Q-switching pulses from a fiber laser cavity, such as such as semiconductor saturable absorber mirrors (SESAMs) (Zhang et al., 2010), graphene (Haris et al., 2020; Jiang et al., 2013), carbon nanotubes (CNTs) (Harun et al., 2012; Set et al., 2004), and black phosphorous (BP) (Ismail et al., 2016). Graphene, CNT, and BP are the most attractive materials for optoelectronic applications due to their excellent conductive properties (Fei et al., 2014; Huang et al., 2011; Kang et al., 2010; Sun et al., 2012). Besides, they have a wide spectral response bandwidth (Heo et al., 2019; Ma et al., 2020; Su et al., 2016), and low manufacturing cost, making them distinguished from other SAs (Ahmad et al., 2016; Qin et al., 2015) while they have a fast recovery time as well (Jung et al., 2012; Salam et al., 2020; Wang et al., 2015). Nonetheless, these SAs face disadvantages that made their popularity limited. As SESAMs required complex fabrication, restricted bandwidth tuning, and high cost (Salam et al., 2019; Yusoff et al., 2019). Graphene has a low optical saturation absorption per layer (Baharom et al., 2019), and low modulation depth (R.

Rosdin et al., 2019). CNT has its response spectral range depending on the chirality and diameter of the nanoparticles (Chen et al., 2016). BP also lacks in few properties such as low damage threshold (Han et al., 2019), complex fabrication process (Wang et al., 2019), and it does not have ample purity and less-uniformity (Latiff et al., 2017).

Transition metal dichalcogenides (TMDs) are another family of transition metals that have received great attention from many authors due to ultrahigh multi-electron transfer and high electrical conductivity such as vanadium Diselenide (VSe_2) (Ahmad et al., 2021), niobium disulfide (NbS_2) (Li et al., 2020), and $W_xNb_{(1-x)}Se_2$ (Li et al., 2021). However, they have some defects as low damage threshold (Mao et al., 2017; Pan et al., 2020).

On the other hand, the latest studies aimed at manufacturing organic materials as a Q-switching to be used as a high-performance thin-film SA in various fiber laser cavities (Salam et al., 2019; Salam et al., 2019; Samsamnun et al., 2020; Soboh et al., 2020). It has advantages as the ultrafast nonlinear optical response (Yang et al., 2013), wide spectral tunability (Clark et al., 2010), low fabrication cost (Salam et al., 2019), good electrical conductivity (Sheberla et al., 2014) and thermal stability (Dalton et al., 2007). The presence of electrical properties in the organic materials motivated the technology field to utilized materials in the different electronic device applications, such as, photovoltaic in the solar panel (Spalatu et al., 2017), organic light-emitting diode (OLED) for manufacture the screens of television and mobile phones (Meftah et al., 2020; Puniredd et al., 2013), also field-effect transistor (Yefet et al., 2013), that use as electronic elements for manufacturing radio-frequency identification (RFID) (Isyanto et al., 2017; Ren et al., 2017). Organic materials contribute in the pharmacological applications field where it treats anti-cancer (Xu et al., 2015), severe acute respiratory syndrome coronavirus 2 (SARS-CoV-2) (Liu et al., 2020) and anti-HIV (Al-Busafi et al., 2014).

MAX phases compounds are hexagonal carbides and nitrides (Tallman et al., 2013). They consist of a single element of an early transition metal (i.e. that represents M), an element of group A (i.e. chemical elements of groups 13–14), and an X that represents either carbon or nitrogen to form the MAX compound (Gonzalez-Julian et al., 2016). MAX phases have a mixture of chemical (Schneider et al., 2004), electrical (Tian et al., 2006), and mechanical properties (Li et al., 2011) of ceramic and metal under different circumstances (Tian et al., 2007). They have good electrical and thermal conductivity (Hettinger et al., 2005; Xiao et al., 2011), good thermal shock resistance and, a high damage threshold due to their electronic structure and chemical bonding (Gonzalez-Julian et al., 2018). The stimulus behind using the MAX phases as a SA is due to several research studies reported about its capabilities in laser applications, such as a large effective nonlinear absorption coefficient (Ahmad et al., 2019), a fast optical-switching capability (Lee et al., 2019), a high optical damage tolerance (Jafry et al., 2020), and an excellent damage threshold makes it a preferable SA, in comparison to other 2D-based materials. In addition, the MAX phases show a contribution for generating Q-switched and mode-locked pulses that have a pulse with the smallest width and a high rate of pulse repetition (Jafry et al., 2020; Kwon et al., 2021).

In chapter 3, the fabrication and characterization of three types of SA devices were successfully demonstrated based on two different materials: 8-Hydroxyquinolino cadmium chloride hydrate (8-HQCdCl_2H_2O) and chromium aluminum carbide (Cr_2AlC). The 8-HQCdCl_2H_2O and Cr_2AlC were chosen for our study due to their similar characteristics include good electrical conductivity (Pan et al., 2008; Salyulev et al., 2016; Zhou et al., 2009), thermal stability (Baraker et al., 2018; Drulis et al., 2006; Shahedi et al., 2017), reliability (Gurnani et al., 2003; Liu et al., 2018), mechanical flexibility (Jomaa et al., 2020; Tian et al., 2007), and simple fabrication (Fung et al., 2012; Kindeel et al., 2013; Ta et al., 2021). Besides that, the 8-HQCdCl_2H_2O as organic material is considered

to be environmental friendly (Grabowski et al., 2011). The Cr_2AlC has ductility and durability (Al-Khazrajy et al., 2015). It has a high chemical attack resistance and high-temperature oxidation in the air (Lee et al., 2007). The Cr_2AlC compound have attractive characteristics as containing metals and ceramics, which made the Cr_2AlC have high hardness (Barsoum, 2000), and high purity (Ge et al., 2019). It has excellent electrical resistivity resulting material is an electrical conductor at high temperature (Gorshkov et al., 2019). This chapter aims to demonstrate the generation of nanosecond Q-switched pulses using the newly developed SAs.

4.2 Exfoliated 8-HQCdCl_2H_2O SA for Generating Q-Switching Pulses

In this section, the generation of passively Q-switched pulses is demonstrated in 1.5 μm region using the newly developed 8-HQCdCl_2H_2O based SA. The SA was fabricated by a mechanical exfoliation technique as described in the previous chapter. Figure 4.1 shows an experimental setup of Q-switched pulses generation. A 1 m length of erbium-doped fiber (EDF) was used as a gain medium with ion absorption of 23 dB/m at 980 nm. The EDF has core diameter, cladding diameter, and numerical aperture of 4 μm, 125 μm, and 0.16, respectively. A continuous wave (CW) of laser diode (LD) operating at the wavelength of 980 nm was used to pump the gain medium through the wavelength division multiplexer (WDM). The previously prepared transparent tape with the exfoliated 8-HQCdCl_2H_2O was inserted into the laser cavity between two fiber ferrules to form pulses of Q-switching. The isolator (ISO) was used to maintain the light propagation in one direction into the ring cavity. In this study, the Q-switching performance was investigated based two different output couplers (OCs). The 50/50 and 95/05 OC were used to extract 50% and 5% of the lasing output for analysis measurements and remaining 50% and 95 % were connected to WDM for feedback. The total cavity length was about 3 m for both arrangements. The output laser was measured by using an optical spectrum analyzer (OSA) (MS9710C), while optical power meter

(OPM) (Thorlabs: PM100D) was used to measure the average output power. The temporal behavior of generated Q-switched pulses and laser stability were analyzed utilizing a 350 MHz digital oscilloscope (GWINSTEK: GDS-3352), and a 7.8 GHz radio frequency spectrum analyzer (RFSA) (Anritsu: MS2683A), respectively. Both RFSA and oscilloscope were connected via a fast photo-detector (Thorlabs: DET01CFC).

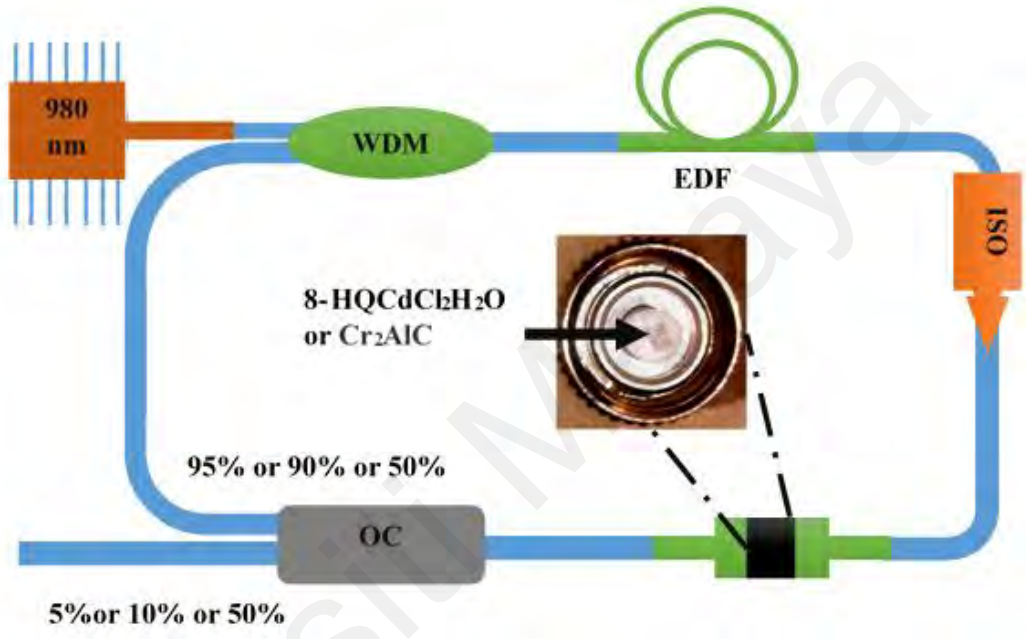

Figure 4.1: Experimental setup of Q-switched EDFL using the 8-HQCdCl$_2$H$_2$O tape as SA

4.2.1 Q-switching Performance Using 50/50 OC

At first, a CW emission was generated at a pump power of 10 mW. Stable Q-switched EDFL operation was recorded at a pump power of 50 mW. Figure 4.2 (a) compares the pulse trains of the Q-switched EDFL at five different input LD powers from 50 mW to 167 mW. The pulse train observed that the pulse repetition frequency increases with an increment of input LD pump power. By using the oscilloscope, the pulse width was recorded to be 4.007 µs, 3.026 µs, 2.817 µs, 2.484 and 2.076 µs, and with the repetition rate of 74.36 kHz, 93.46 kHz, 106.4 kHz, 117.2 kHz and 136 kHz, respectively. The output spectra were taken using an OSA at different input LD powers of 50 mW, 75 mW,

127 mW, 152 mW, and 167 mW, see Figure 4.2 (b). The optical spectra pulses have central wavelengths of 1530.74 nm, 1530.49 nm, 1530.74 nm, 1530.49 nm and 1530.49 nm, with 3 dB bandwidths of 2.516 nm, 3.52 nm, 3 nm, 3.522 nm, and 4 nm, respectively which indicate that the Q-switched EDFL operation has high stability.

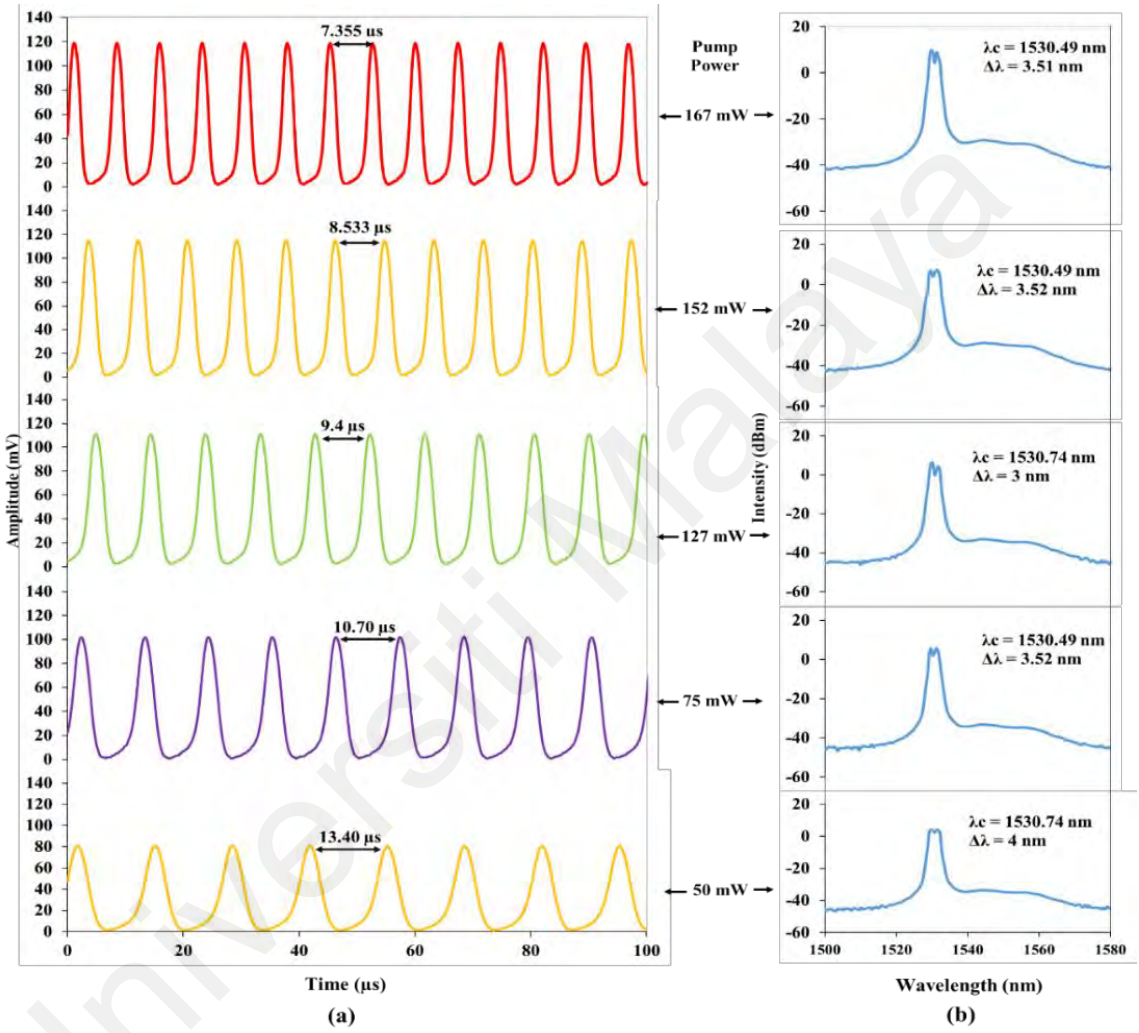

Figure 4.2: Exfoliated 8-HQCdCl$_2$H$_2$O SA EDFL operation using 50/50 OC, (a) typical pulse trains, and (b) optical spectra at a different pump power

Figure 4.3 (a) shows the repetition rate and pulse duration with respect to incident pump power. As expected, the pulse rate incremented linearly from 74 kHz to 136 kHz while the pulse width dropped from 4.007 µs to 2.076 µs as pump power varies from 50 mW to 167 mW, respectively. Figure 4.3 (b) gives the average output power and pulse energy versus pump power. Maximum average output power and pulse energy were observed to be 23.4 mW and 172 nJ, at the maximum input power of 167 mW. The slope

efficiency of the laser is calculated to be around 14 %. Figure 4.3 (c) shows the RF spectrum of Q-switched EDFL operation at 167 mW pump power. At the repetition rate of 136 kHz, the signal-to-noise ratio (SNR) was 81 dB with a span around 2000 kHz. The RF spectrum has a resolution bandwidth (RBW) and video bandwidth (VBW) of 1 kHz and 100 Hz, respectively, which indicating that the laser was highly stable.

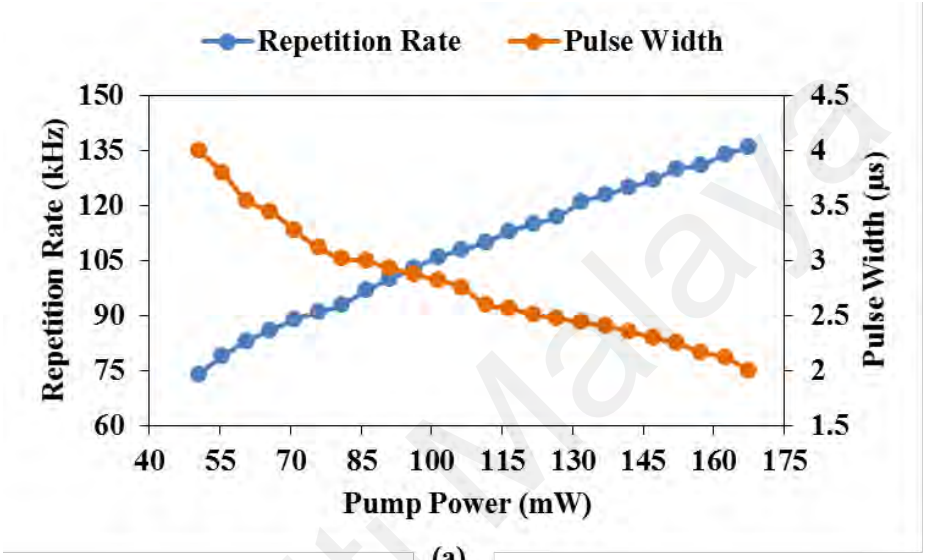

(a)

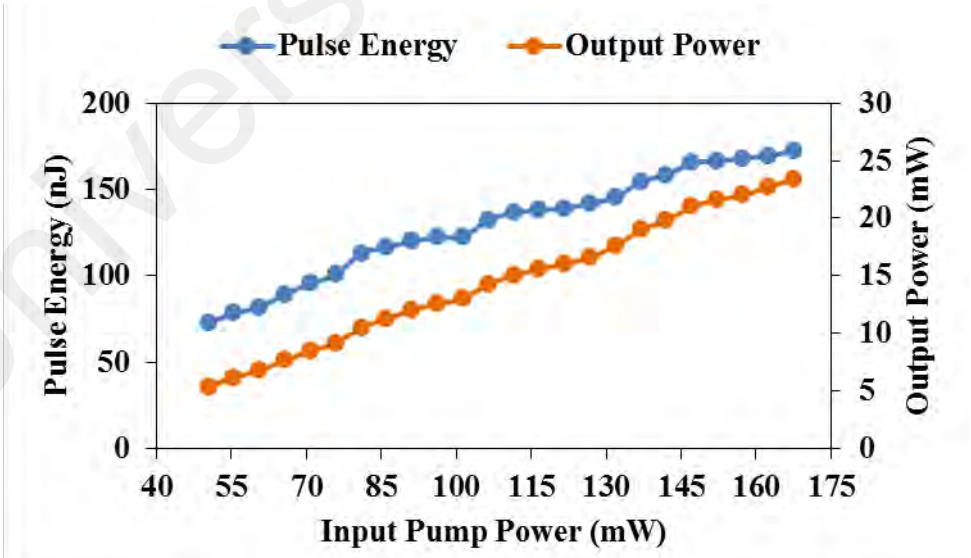

(b)

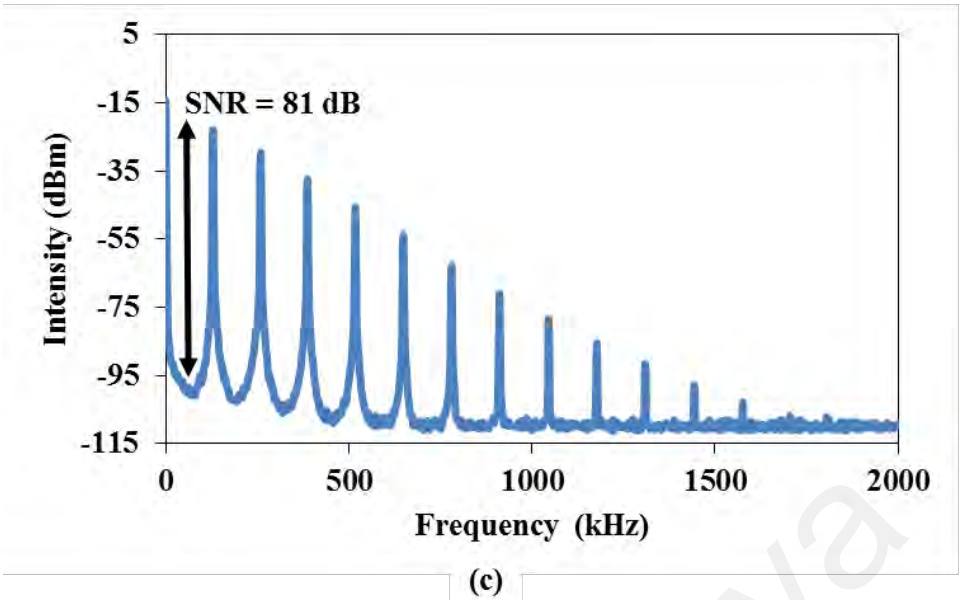

Figure 4.3: Exfoliated 8-HQCdCl$_2$H$_2$O SA Q-switched performance using 50/50 OC, (a) pulse repetition rate and pulse width versus input pump power, (b) output power and pulse energy versus input pump power, and (c) RF spectrum at a repetition rate of 136 kHz

4.2.2 Q-switched Performance Using 95/05 OC

In this setup, the OC was changed from 50/50 to 95/05 OC in the laser cavity. The pulse width was reduced, and the pulse repetition rate was increased, impacting both the average output power and pulse energy. Also, the threshold and maximum input power for producing the Q-switched were 101 mW to 167 mW, respectively. Figure 4.4 (a) shows the temporal characteristics at 101 mW, 122 mW, 142 mW, and 167 mW pump power. The different pulse trains are taken in the time domain using an oscilloscope and it shows pulse intensity. The different repetition rates were achieved to be at 145 kHz, 155 kHz, 163 kHz, and 173 kHz with the pulse widths of 2.4 µs, 2.1 µs, 1.88 µs and 1.66 µs at the pump powers of 101-167 mW**.** Figure 4.4 (b) compares the output spectra of the Q-switched EDFL at different pump powers of 101 mW, 122 mW, 142 mW, and 167 mW with center wavelengths of 1530.74 nm, 1530.74 nm, 1530.49 nm, and 1530.49 nm.

The repetition rate and pulse width against pump power are shown in Figure 4.5 (a). The repetition rate increased from 145 kHz to 173 kHz and pulse width was decreased

from 2.4 µs to 1.66 µs, as pump power was incremented at the same range. The pulse repetition rate improved as compared to the other experiment with a 50/50 coupler, since the change in OC resulted in a shorter time for pulse to travel in the cavity. Also, the SA saturation became faster as compared to the 50/50 OC cavity, resulting in a shorter pulse duration keeping a 95 % of input power to oscillate in the laser cavity. The average output power was decreased in comparison to the previous setup because it extracted 5 % of used power and keeping the rest into the cavity. This setup realized average output power from 1.04 mW to 1.8 mW, see Figure 4.5 (b). While pulse energy is produced from 7 nJ to 10 nJ which is less than the previous setup. Figure 4.5 (c) shows the RF spectrum, which was measured to analyze Q-switched EDFL operation stability in the range of 2000 kHz with 1 kHz of RBW and 100 Hz of VBW. The SNR for Q-switched laser is at 75 dB which corresponding to the repetition rate of 173 kHz.

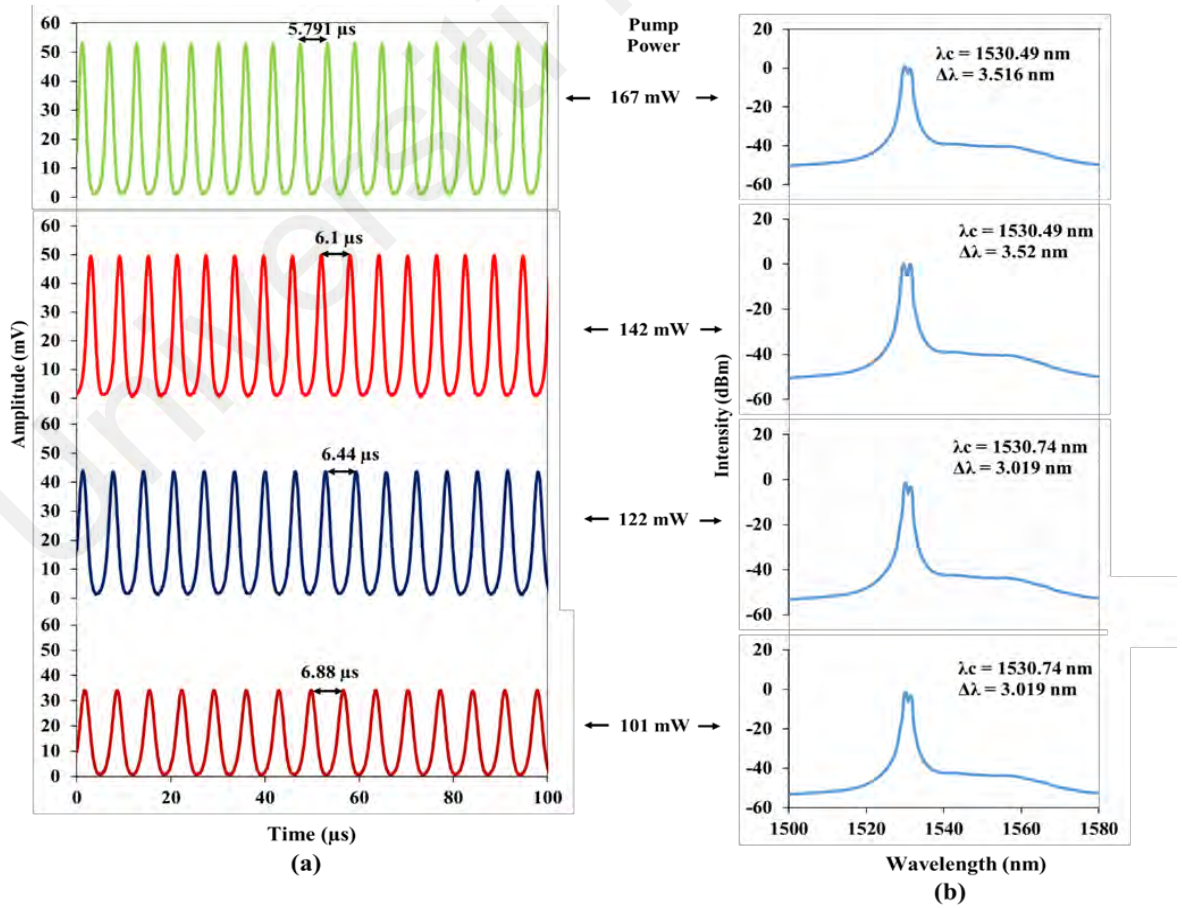

Figure 4.4: Exfoliated 8-HQCdCl$_2$H$_2$O SA EDFL operation using 95/05 OC, (a) typical pulse trains, and (b) The optical spectra at a different pump power

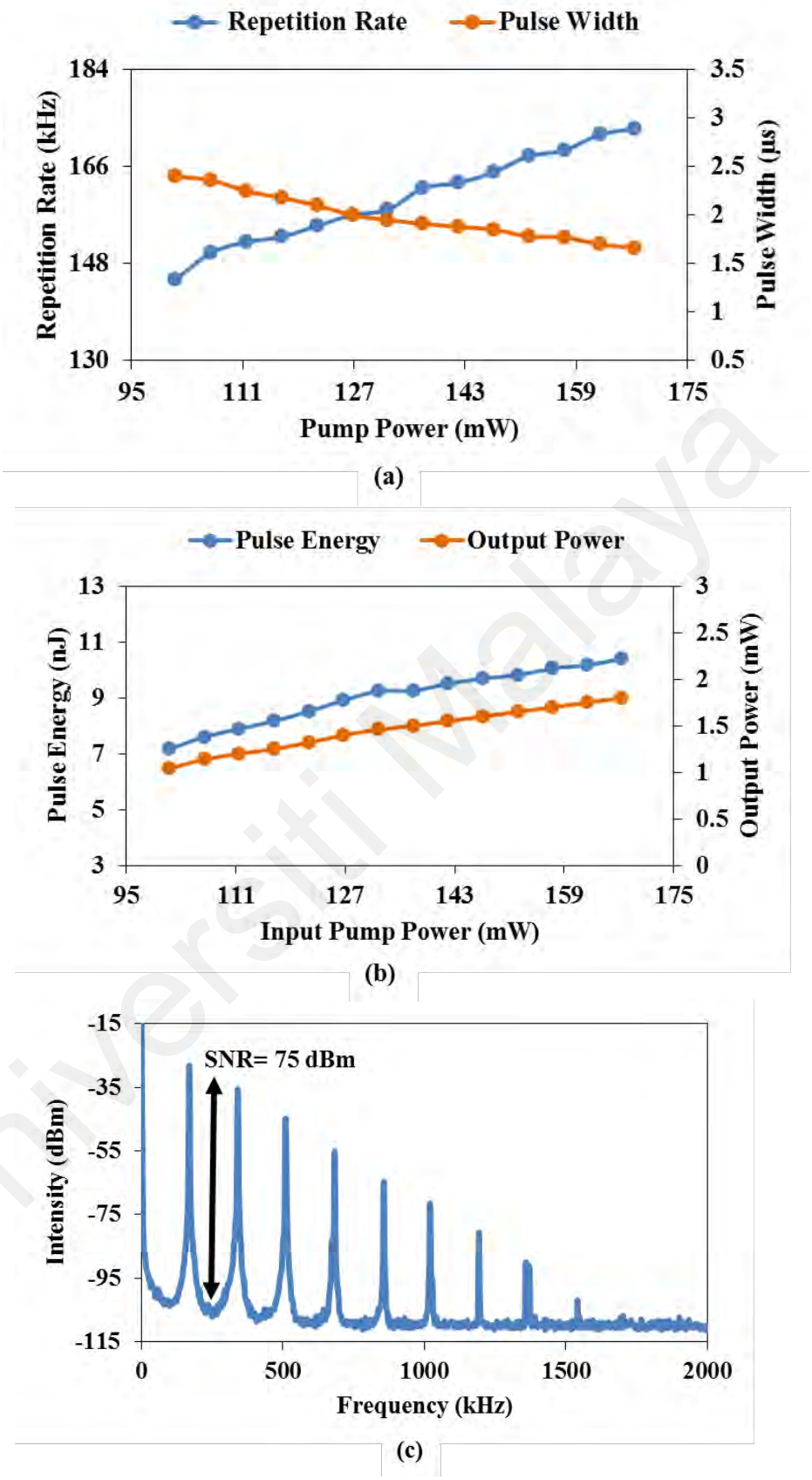

Figure 4.5: Exfoliated 8-HQCdCl$_2$H$_2$O SA Q-switched performance using 95/05 OC, (a) the pulse repetition rate and pulse width against input pump power, (b) output power and pulse energy versus input pump power, and (c) RF spectrum at a repetition rate of 173 kHz

The impact of changing the output ratio of the couplers used in EDFL is highlighted in this work. Our findings suggest that a 95/5 coupler with 95% of output set to feedback is best suitable to get a shorter pulse width. Much shorter pulses having low pulse energy can be achieved by lowering the output ratio of coupler. However, on the other hand, a very high output power of around 23.5 mW is extracted using a 50/50 coupler which resulted in the pulse energy of 172 nJ.

4.3 8-HQCdCl$_2$H$_2$O Thin Film as Q-switcher for Generating Nanosecond Pulses

In the preceding section, the Q-switched EDFL operation was successfully achieved utilizing the mechanically exfoliated 8-HQCdCl$_2$H$_2$O as a SA. However, the shortest pulse width was only attainable at 1.66 μs. In this study, the Q-switched EDFL operation is experimentally explained to generate a much shorter pulse by using the similar 8-HQCdCl$_2$H$_2$O material, but it was prepared based on drop-casting approach. The 8-HQCdCl$_2$H$_2$O was embedded in polyvinyl alcohol (PVA) to fabricate the thin-film, which has then employed in the Q-switched EDFL cavity for passively generating nanosecond pulses. 8-HQCdCl$_2$H$_2$O was elected to be apart from our thin-film, since it is widely used in applications of electrical and electronic devices (Shahedi et al., 2017). It has excellent solubility in the water and good conductivity (Salyulev et al., 2016), also it is used for electroplating and photocopying (Hebboul, 2018; Prakash et al., 2013). Moreover, it has high thermal stability for the formation of the thin-film in the optoelectronic applications (Baraker et al., 2018). The cavity design of the nanosecond Q-switched EDFL is like Figure 4.1 except for the OC ratio. A 10 dB OC was used to extract 10% of the lasing output for analysis while allowing the remaining 90% to oscillate in the cavity. The prepared 8-HQCdCl$_2$H$_2$O PVA thin-film was inserted between two fiber ferrules via an adaptor to form a fiber-compatible SA. It was incorporated in the EDFL cavity for nanoseconds pulse generation.

The Q-switched laser operation in the EDFL was obtained within the pump power range of 101 mW to 167 mW. It generates nanosecond pulse train with a varying repetition rate and pulse width. The repetition rate increased from 123 kHz to 150 kHz and pulse width decreased from 976 ns to 726 ns when the pump power was raised from 101 mW to 167 mW as shown in Figure 4.6 (a). In the same magnitudes of laser pump power, as illustrated in Figure 4.6 (b), the pulse energy and output power increased from 3.6 nJ to 4.5 nJ and 0.44 mW to 0.7 mW, respectively. The laser's optical-to-optical efficiency is estimated to be around 0.41 %. Compared to the previous laser with exfoliated 8-HQCdCl$_2$H$_2$O, this value is smaller due to the higher linear absorption.

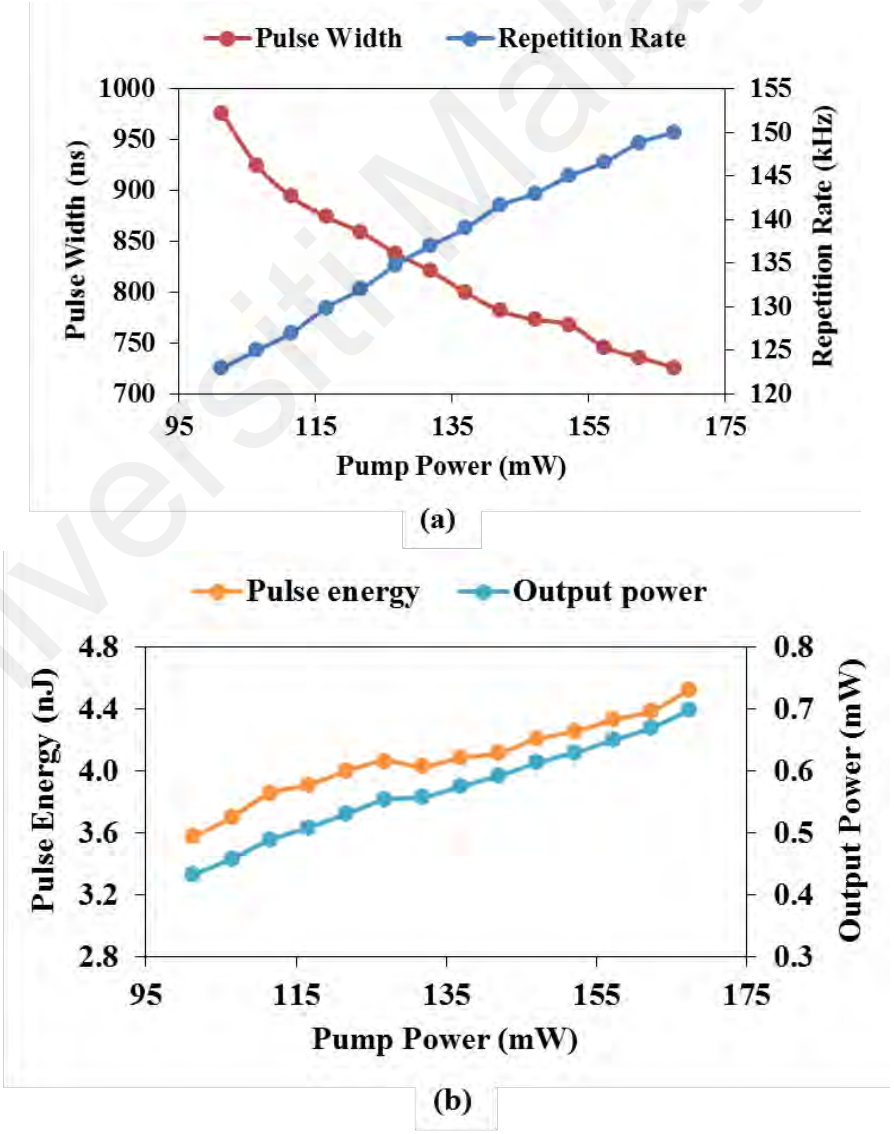

Figure 4.6: Performance of the nanosecond Q-switched EDFL with 8-HQCdCl$_2$H$_2$O SA, (a) pulse width and pulse repetition against pump power, and (b) pulse energy and output power against pump power

Figure 4.7 (a) shows the typical oscilloscope trace for the Q-switched laser, which was captured in the range of 200 µs at the highest pumping power of 167 mW. As seen, the laser's temporal performance has been stable with a pulse width of 726 ns, corresponding to the highest frequency of 150 kHz. The enlarged image shows two pulses measured of a full-width half-maximum of 726 ns, and the distance between peak to peak of 8.9 µs. Figure 4.7 (b) displays the frequency with a SNR of 72 dB determined in the span of 3000 kHz. The RF spectrum has a resolution bandwidth RBW and VBW of 3 kHz and 100 Hz, respectively. The first peak shows a frequency of 150 kHz which is in good alignment with the oscilloscope trace.

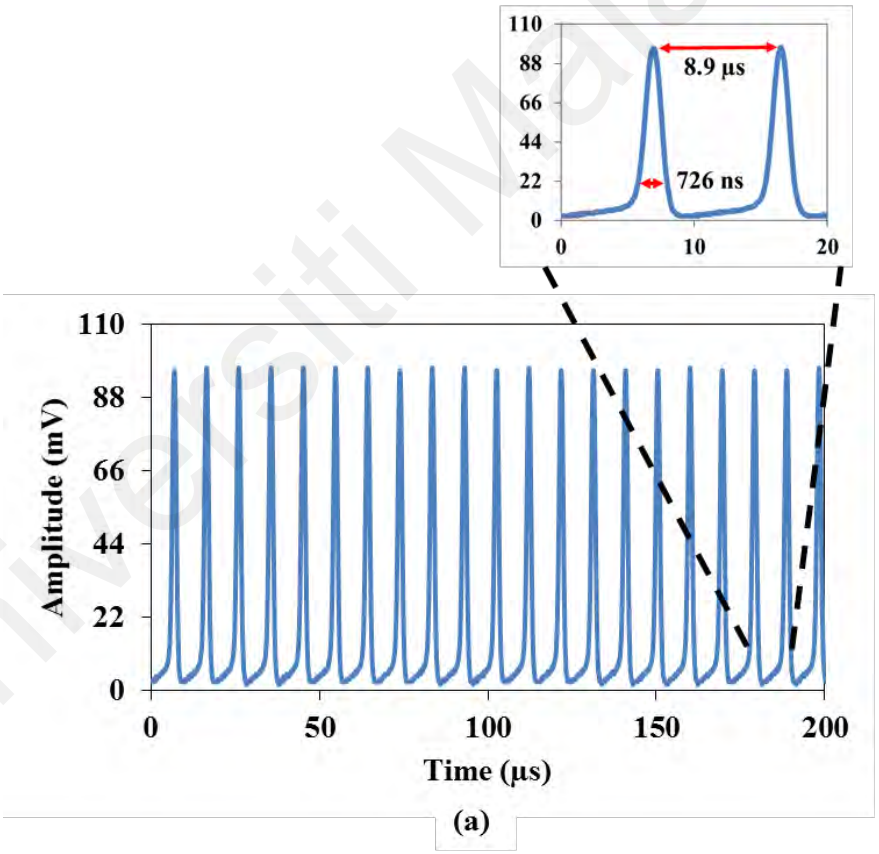

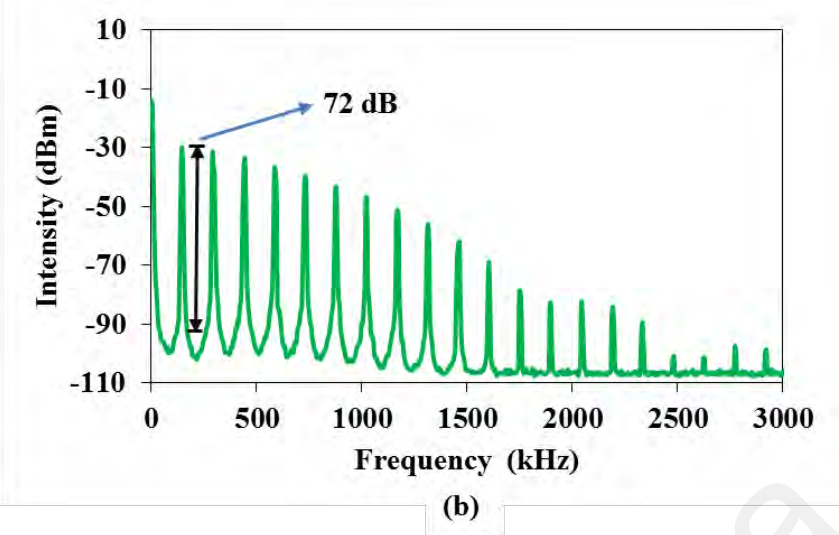

Figure 4.7: The temporal characteristics of the nanosecond Q-switched EDFL with 8-HQCdCl$_2$H$_2$O SA, (a) typical pulse train, and (b) frequency spectrum

Figure 4.8 shows the output spectra of the EDFL, which operates in Q-switching and CW regime as it was configured with and without SA. Without the SA, the optical spectrum of the EDFL cavity operated at the center wavelength of 1566 nm with 1.2 nm, 3 dB bandwidth and power intensity of −2 dBm. However, the spectrum of EDFL shifted to the shorter wavelength when the SA inserted into the cavity due to the increase in cavity loss. The operating wavelength centered at 1530 nm with 3 dB bandwidth of 1.6 nm, and power intensity of −6 dBm, as depicted in Figure 4.8.

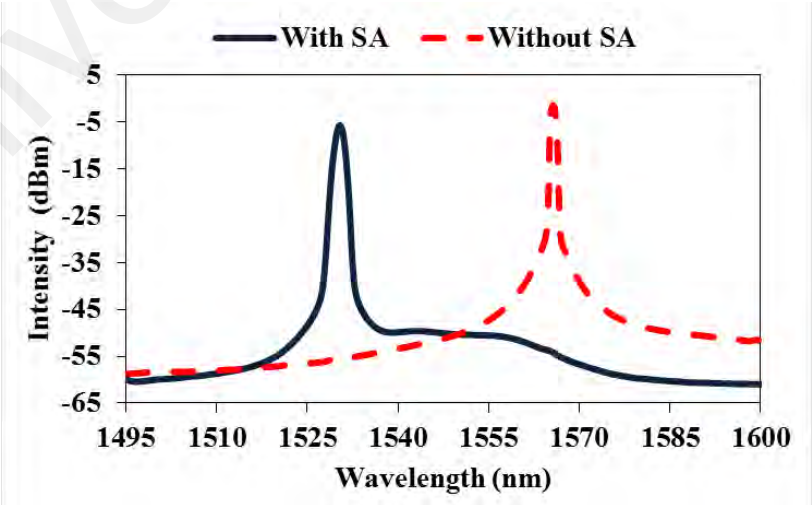

Figure 4.8: The output spectra of the EDFL with and without the deployment of 8-HQCdCl$_2$H$_2$O SA inside the cavity

4.4 Cr_2AlC Thin Film for Generating Nanosecond Q-Switched Pulses

In this section, a thin-film SA from the MAX phases compounds was utilized to create nanosecond Q-switched laser pulse. In the fabrication steps of the SA film, the Cr_2AlC powder is mixed with PVA solution before being dried to create the Cr_2AlC thin-film. The manufacturing steps and characterization of Cr_2AlC thin film had done described in the previous chapter. A tiny piece of Cr_2AlC PVA thin film was surrounded by two EDFL laser cavity fiber ferrules, as shown in Figure 4.1, to generate a Q-switching pulse in the wavelength range of 1531 nm. Like the previous 8-$HQCdCl_2H_2O$ thin film-based laser, a 10 dB OC (90/10) was used. It lets 10% of the laser light will be released out of the cavity for laser pulse performance analysis, and 90% laser will keep circulating inside the EDFL cavity. The length of the total ring cavity is 3 m. The Cr_2AlC film saturation rise before the active medium saturation, where the saturation occurs when the gain medium energy reaches a level adequate. During that period, the Cr_2AlC thin-film modulates the cavity loss, then will allow the passive Q-switching operation achieved and then generate nanosecond pulses. It is worthy to note that the proposed experimental setup does not include any polarization controller (PC). The self-started Q-switched laser pulses appeared just by the insertion and adjustment of Cr_2AlC thin-film between the fiber ferrules. However, the addition of PC only contributed to intra-cavity loss. This reduced the Q-switched laser performance by generating wider pulses and lower average output power. Thus, the PC was excluded from our experimental setup.

The Q-switching pulses appeared at the input pump power of 117 mW and they remained available until the input pump power was increased into 167 mW. Figure 4.9 (a) shows the relationship between pulse width, repetition rate with laser pump power. The pulse width dropped from 995 to 780 ns, and the repetition rate increased from 108 to 132 kHz, as the pump power rises gradually from 117 mW to 167 mW. The very short pulse may be predicted when the additional reductions in the overall length of the cavity

and increasing the modulation depth of the SA. With the enhancement of the preparation procedure of SA, the depth of modulation may be improved.

Figure 4.9 (b) shows the oscilloscope pulse train for an interval of 100 μs for the shorter pulse width with the highest repetition rate were 780 ns and 132 kHz, repecively, as well as, the distance between pulse to pulse was 7.7 μs, at 167 mW of the maximal laser input power. Figure 4.9 (c) shows the pulse energy and output power increased from 7 nJ to 9 nJ and 0.79 mW to 1.134 mW, respectively, in the same laser pump power range. Based on the relation between the output power and pump power, the optical efficiency is calculated to be around 0.67 %. This value is slightly higher than the previous laser with 8-HQCdCl_2H_2O thin film. Figure 4.9 (d) shows the SNR that obtained by the RFSA over the span of 2000 kHz was 67 dB, where the first peak corresponds to 132 kHz of repetition rate with a maximum input laser pump power of 167 mW. The Cr_2AlC thin-film has been replaced with only PVA thin film to avoid the potential of pulse generation using only PVA or any nonlinear polarization rotation (NPR) action within the cavity. Then, the pump power raised to the LD's maximum sustainable limit. In the case of only PVA thin film, there were no pulses were observed through the oscilloscope throughout the whole range of pump power. It also demonstrates that Q-switching operation cannot be accomplished using a pure PVA thin film or cavity phase self-modulation.

Figure 4.9 (e) exhibits the EDFL spectra of CW laser and Q-switch operations. In the spectrum of CW laser, the wavelength observers at 1566 nm with a 3 dB bandwidth of 1.6 nm, and spectrum intensity of -5 dBm. However, the spectrum of the Q-switch operations shifts to a shorter wavelength of 1531 nm with a 3 dB bandwidth of 2.8 nm and power intensity of -19 dBm. The spectrum shifted to the shorter wavelength because of the loss introduced by adding the SA in EDFL. It is worthy to note that the pulse laser began to fade once the laser input pump power reached 167 mW, because of over-

saturation of the Cr_2AlC thin-film resulted from higher input pump power. However, when the pump power was reduced to 167 mW, the Q-switched nanosecond pulses returned and indicating that SA did not burn. Therefore, it can be deduced that the damage threshold of the Cr_2AlC SA is higher than 200 mW pump power. Nevertheless, the laser's optical efficiency can be improved, because of small output coupler ratio released 10%, and 90% of laser continue circulating in laser cavity. In addition, the intra-cavity loss restricted optical efficiency and output power.

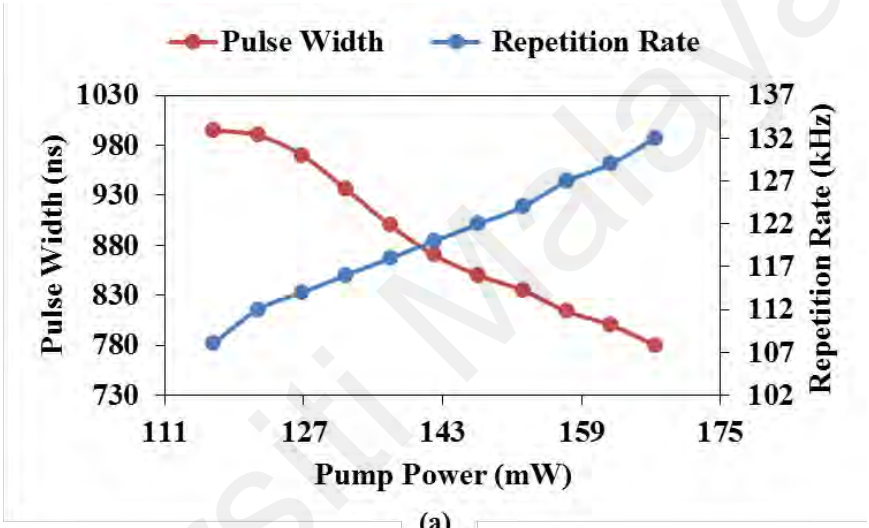

(a)

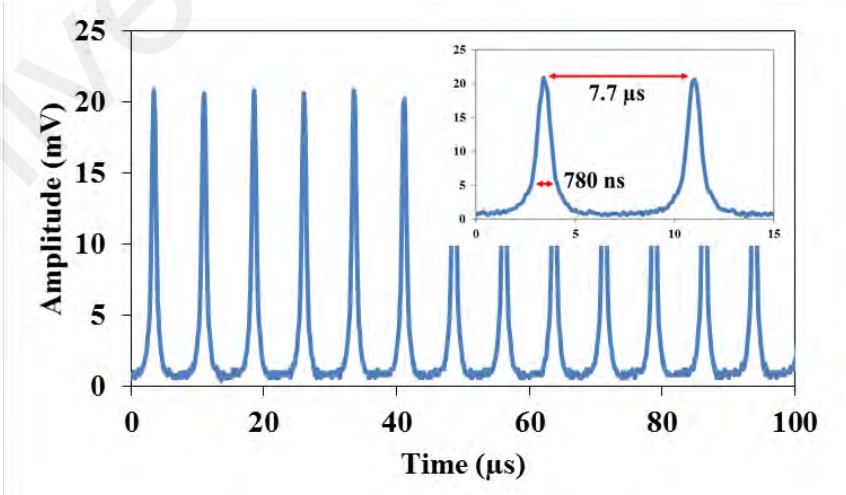

(b)

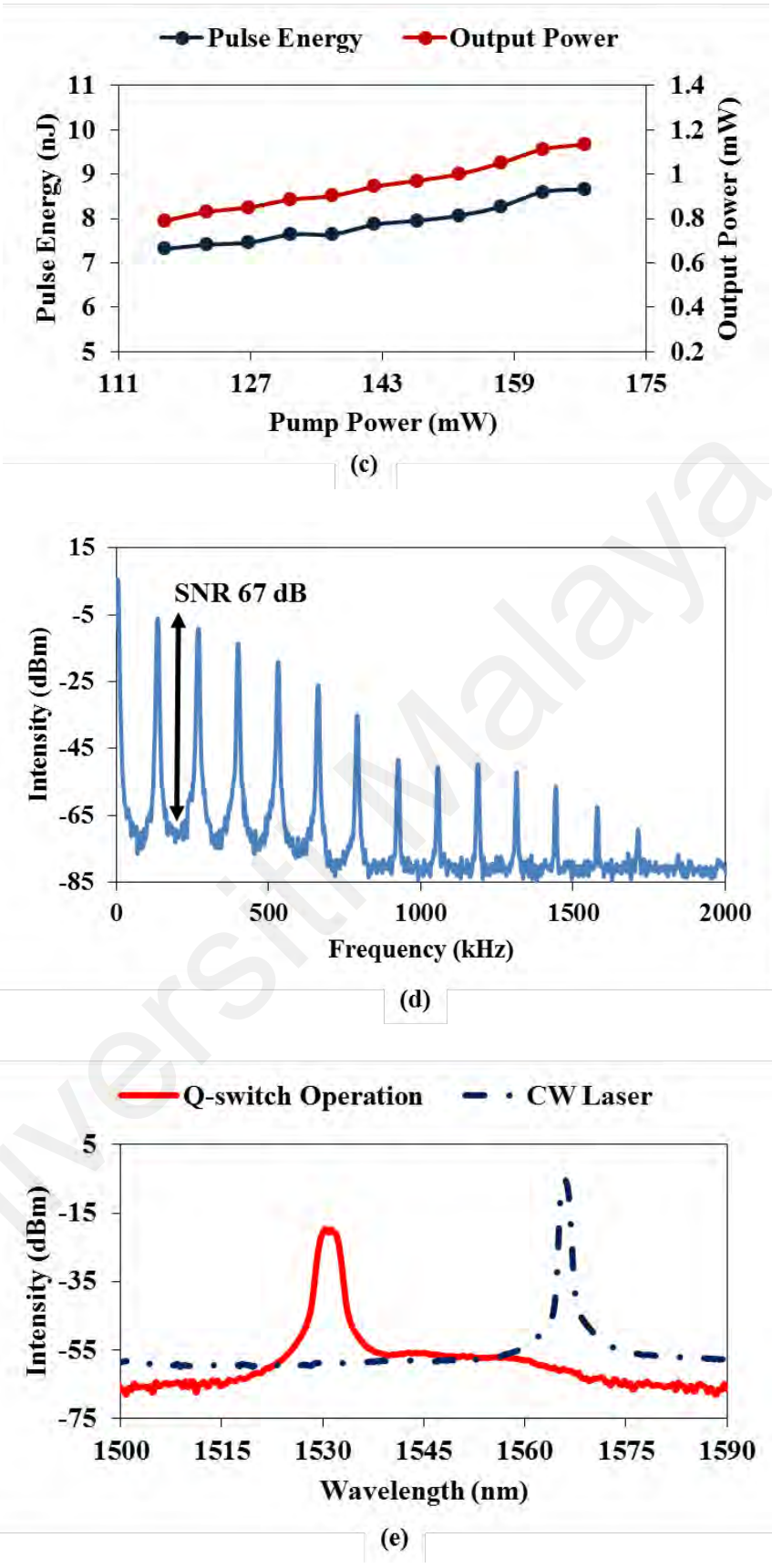

Figure 4.9: The nanosecond Q-switching performance with Cr_2AlC thin-film SA, (a) repetition rate and pulse width against pump power, (b) pulse energy and output power against pump power, (c) typical pulse train, (d) radio frequency spectrum, and (e) EDFL spectra with and without SA

Table 4.1 shows a comparison of Cr_2AlC SA Q-switching performance with prior SAs based on a range of different materials (Ahmad et al., 2017; Ahmed et al., 2017; Al-Hayali et al., 2017; Chen et al., 2016; Chen et al., 2015; Jafry et al., 2020; Lee et al., 2019; Liu et al., 2020; Liu et al., 2013; Liu et al., 2019). The elements that were utilized to compare Cr_2AlC SA performance are listed in Table 4.1 as: saturation intensity, modulation depth, repetition rate, pulse energy, pulse width, operating wavelength (λ), maximum pump power, output power, and SNR. The proposed Cr_2AlC SA demonstrated the performance of the Q-switched laser generated in the region of 1.5-micron. The Q-switched laser by our proposed SA showed a relatively high SNR of about 67 dB, which proves that the lasing was stable. Among only few nanoseconds pulse Q-switched lasers reported in literature, our results showed some outstanding performance of the new SA. Previously, Liu et al. have reported Q-switched EDFL having a very short pulse width of about 583 ns by using tungsten ditelluride (WTe_2) as a SA. However, the shortest pulse width of 583 ns was achieved at a very high pump power of 630 mW. The increase of such a high pump power in EDFL ring cavity can either damage the SA or the LD in a long run. On the other hand, the output power of Q-switched laser was achieved to be higher than molybdenum disulfide (MoS_2), titanium aluminium carbide (Ti_2AlC) and Si-PVA based SA. The corresponding pulse energy of 9 nJ was achieved in our work, related to the fact that the maximum repetition rate was achieved to be 132 kHz, producing a very narrow pulse width of 780 ns. It is also worthy to note that a high energy pulse is expected to be realized by the proposed SA through pulse-shaping technique (Gao et al., 2019). In addition, adjusting the coupling ratio and further improving the EDFL cavity loss might enhance the output power, which will directly increase the pulse energy and the pulse peak power.

Table 4.1: Performance comparison with various SA materials

SA	Mod. Dep. (%)	Sat. Intensity	Max pump power (mW)	Rep. rate (kHz)	Pulse width (μs)	Pulse energy (nJ)	Output Power (mW)	λ (nm)	Ref.
CNT	-	-	209.6	70.4	4.5	81.3	5.7	1563	(Liu et al., 2013)
BP	7	0.20 MW/cm^2	170	44.3	7.04	134	5.94	1553	(Ahmed et al., 2017)
MoS_2	2.15	129.4 MW/cm^2	170	41.4	13.5	184.7	0.71	1560	(Chen et al., 2015)
WSe_2	3.5	103.9 MW/cm^2	300	49.6	3.1	33.2	1.23	1560	(Chen et al., 2016)
Ti_3AlC_2	2	1.69 MW/cm^2	94	112	3.93	75	8.4	1560	(Jafry et al., 2020)
Ti_2AlC	6.3	31.2 MW/cm^2	74	27.4	4.88	22.58	0.62	1560	(Lee et al., 2019)
Al_2O_3	-	-	330	81	2.8	56.7	4.5	1560	(Al-Hayali et al., 2017)
WTe_2	31.06	0.515 MW/cm^2	630	240	0.58	58.625	14.07	1531	(Liu et al., 2019)
MoS_2	7.7	0.002 MW/cm^2	45.6	25.3	3.3	90	2.27	1562	(Ahmad et al., 2017)
Si-PVA	20.1	5.78 MW/cm^2	164	58.7	2.32	-	0.89	1567	(Liu et al., 2020)
Cr_2AlC	2	100 MW/cm^2	167	132	0.78	9	1.134	1531	This work

4.5 Summary

The generation of nanosecond Q-switched pulses had successfully achieved in the EDFL cavity using the newly developed SAs. At first, the exfoliated 8-HQCdCl_2H_2O SA was experimentally demonstrated to produce different Q-switched EDFL pulses in two different experimental setups. A high-performance and stable Q-switched operation was realized in both setups. First, the Q-switched fiber laser produce pulses by a 50/50 OC, with the EDFL cavity to generate the high pulse energy of 172 nJ, at the highest output power of 23.4 mW. Then, after modifying the 50/50 OC to 95/05 OC, the width of pulses was dropped to 1.66 μs, then the repetition rate pulses rose to 173 kHz. The 8-HQCdCl_2H_2O SA using mechanical exfoliation showed good results as a passive Q-switcher in the EDFL, but the lowest pulse width cannot reach nanosecond regime. Nevertheless, the nanosecond pulse generation was successfully realized using the 8-HQCdCl_2H_2O film as SA. At the maximum input pump power of 167 mW, the Q-switched laser produced pulses at a repetition rate of 150 kHz with pulse width of 726 ns. This work also demonstrated the MAX phases compound (Cr_2AlC), which is utilized as a SA thin-film to generate the nanosecond Q-switched pulses The obtained results demonstrate that Cr_2AlC film can generate a very short laser pulse, where it produced a 780 ns of pulse width, with 132 kHz of repetition rate of the pulse at 167 mW of the maximal laser input power. As well as, the high pulse energy reported 9 nJ and the highest output power reached 1.134 mW.

CHAPTER 5: ULTRA-SHORT PULSE GENERATION VIA MODE-LOCKING

5.1 Introduction

Fiber lasers have been extensively applied in different fields such as biomedical imaging, material processing, and optical communication (Keller, 2003; Okhotnikov et al., 2004; Wise et al., 2008) due to their advantages of good beam quality, short-pulses, and high peak power. A passively mode-locked laser is the most common technology that has been used to produce ultra-short pulse emission in fiber lasers based on saturable absorbers (SAs) (Ahmed et al., 2017) due to its unique characteristics such as ease of use and cheapness.

In recent years, SA has played a significant role in the development of pulsed lasers. The semiconductor saturable absorber mirrors (SESAMs) have been used as SA to produce pulse lasers in the laser cavity (Zhang et al., 2010). The SESAM has shown great progress for generating ultra-short pulses due to its precise control of absorption wavelength (Keller et al., 1996). However, SESAM's popularity has dwindled as a result of its limited operating bandwidth (Al-Hiti et al., 2020).

The two-dimensional (2D) materials have received much attention in nonlinear optics and ultra-short pulse laser applications due to their optical and electronic properties (Ge et al., 2018; Guo et al., 2019; Li et al., 2020; Liu et al., 2017; Wang, 2017; Zhao et al., 2019). In addition, 2D materials have tunable structures that made them to be investigated widely in the ultra-short pulse laser applications. 2D materials are the dominating materials that were employed in the laser cavity as thin-film based SAs. Graphene (Zhang et al., 2009), black phosphorus (BP) (Ismail et al., 2016) and transition metal dichalcogenides (TMDs) (Niu et al., 2018; Nizamani et al., 2021; Yang et al., 2019) have shown great potential in comparison with SESAMs. TMDs (Su et al., 2016), BP (Wang

et al., 2015) and graphene (Xing et al., 2010; Zhang et al., 2009) have a fast recovery time and wide spectral range (Ma et al., 2019), but they suffer from small modulation depth (Bao et al., 2009; Chen et al., 2015; Wang et al., 2016; Zhang et al., 2019) and low band gap (between 0 eV to 1.5 eV) (Jiang et al., 2020; Luo et al., 2016; Mak et al., 2010; Sotor et al., 2015). The BP and graphene also have low damage threshold (Al-Hiti et al., 2020; Al-Masoodi et al., 2016; Hammadi et al., 2018; Lau et al., 2017; Li et al., 2016; Luo et al., 2010). Over recent years, carbon nanotubes (CNTs) had distinguished properties that made their popularity grown in innovative electronics and photonic applications (Scardaci et al., 2007; Yamashita, 2011). In addition, CNTs exhibited great performance in the applications of ultra-short pulse generation compared to SESAMs (Cheng et al., 2020). However, CNT suffers from its variable nanotube size, which in turn affects its operation bandwidth, band gap and absorption efficiency (Al-Hiti et al., 2021; Chernysheva et al., 2017; Reich et al., 2008; Set et al., 2004).

Recently, organic materials were fabricated and deployed in different applications because they have ultrafast nonlinear activity and wide spectral tenability (Al-Hiti et al., 2020; Li et al., 2019). Moreover, they have excellent properties such as low fabrication cost (Ji et al., 2020), good electrical conductivity (Sheberla et al., 2014), mechanical flexibility (Park et al., 2015), thermal stability (Zhao et al., 2006), and light-weight (Heiber et al., 2019). On other side, MAX phases materials reported numerous capabilities in fiber laser applications, including a large effective nonlinear absorption coefficient. (Ahmad et al., 2019), a fast optical Q-switching capability (Lee et al., 2019), a high optical damage tolerance (Jafry et al., 2020) and an excellent damage tolerance threshold, hence, it is a preferable SA when compared to other 2D-based materials..

In this work, the organic thin film developed and fabricated based on 8-Hydroxyquinolino cadmium chloride hydrate (8-HQCdCl_2H_2O), and chromium

aluminum carbide (Cr_2AlC) had fabricated as MAX phases thin-film. The generations of soliton mode-locked pulses in an erbium-doped fiber laser (EDFL) cavity were demonstrated using the newly developed passive SAs. The 8-$HQCdCl_2H_2O$ with good solubility in an organic solvent is selected to be a part of our SA research since it was widely deployed in electrical and electronic fields (Shahedi et al., 2017), and electroplating and photocopying (Hebboul, 2018; Prakash et al., 2013). Cr_2AlC considered as one of the good materials to resist high temperatures and contains good oxidation (Go et al., 2019; Sokol et al., 2019). Also, it is characterized by high elastic stiffness and lightweight (5.24 g/cm^3). In addition, the Cr_2AlC has physical, chemical and optical properties comparable to graphene and TMDs (Gonzalez-Julian et al., 2016; Gorshkov et al., 2019; Malic et al., 2013; Voiry et al., 2013; Wen et al., 2017; Xue et al., 2014).

5.2 Mode-locked Erbium-Doped Fiber Laser With 8-$HQCdCl_2H_2O$ Thin Film SA

5.2.1 Laser configuration

Figure 5.1 shows the proposed EDFL cavity used to achieve mode-locked pulse generation using the newly developed 8-$HQCdCl_2H_2O$ thin film as a SA. A 980 nm laser diode is used to pump an erbium-doped fiber (EDF) inside the ring resonator consisting of an optical isolator, SA device and output coupler (OC) via a wavelength division multiplexing (WDM). The cavity length was about 3 m without the additional single-mode fiber (SMF). The EDF used is 1 m long which has ion absorption of 23 dB/m at 980 nm, with group velocity dispersion (GVD) of 27.6 ps^2/km. The 10% output was extracted using 90/10 OC. A small piece of 8-$HQCdCl_2H_2O$ thin-film was placed inside the cavity as an SA. The radio frequency spectrum analyzer (RFSA) (Anritsu: MS2683A) having bandwidth of 7.8 GHz, and oscilloscope (GWINSTEK: GDS-3352) having 350 MHz bandwidth were connected via a fast photodetector of (Thorlabs: DET01CFC).

Optical power meter (OPM) (Thorlabs: PM100D) was used to report the average output power. OSA (MS9710C), Oscilloscope and RFSA were used to measure the output of laser wavelength, the resulting pulse train, and radio-frequency spectrum, respectively.

The mode-locked EDFL operation was achieved by incorporating three different lengths of SMF with GVD of -21.7 ps^2/km. The length of EDFL cavity was extended with the addition of 30 m, 50 m, and 100 m SMF to design three different cases of mode locked EDFL cavity. The total length of each case for mode-locked EDFL cavity becomes 33 m, 53 m, and 103 m, with group delay dispersion (GDD) of -0.6802 ps^2, -1.1142 ps^2 and -2.1992 ps^2, respectively. The addition of SMF also increased the cavity nonlinearity, which functions to the balance the nonlinearity and dispersion factors of the cavity and assists in soliton pulse generation.

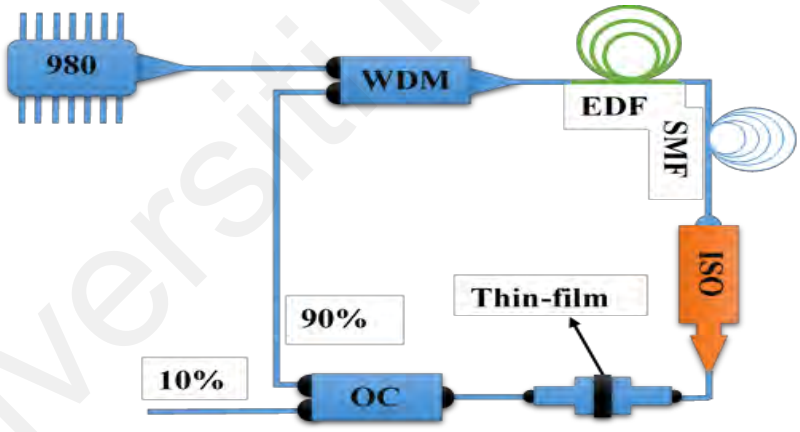

Figure 5.1: Laser cavity configuration for mode-locked pulse generation with 8-HQCdCl$_2$H$_2$O thin-film as SA

5.2.2 Mode-locking Performance with 8-HQCdCl$_2$H$_2$O Thin Film as SA

By incorporating the prepared SA and increasing the cavity length with addition of 30 m, 50 m, and 100 m of SMF to original length of EDFL cavity, the pulses of the mode-locked appeared when the LD power was in the range of 91-167 mW. Figure 5.2 (a) shows the width of pulses that measured separately from EDFL cavity at the oscilloscope for each length of 33 m, 53 m, and 103 m were 46 ns, 48 ns, and 52 ns, respectively. As well

as the period of pulse-to-pulse recorded were 177 ns, 277 ns and 525 ns, which matches very well to the cavity length of 33 m, 53 m, and 103 m, respectively. Figure 5.2 (b) shows the pulse repetition rate obtained over RFSA for each length in the span of 100 MHz. The repetition rates were observed to be 5.6 MHz, 3.6 MHz, and 1.9 MHz, with signal-to-noise ratio (SNR) of 83 dB, 85 dB, and 70 dB at a maximum input pump power of 167 mW. The repetition rate corresponds well with the oscilloscope measurement of Figure 5.2 (a). The high SNR indicates the stability of the pulse train.

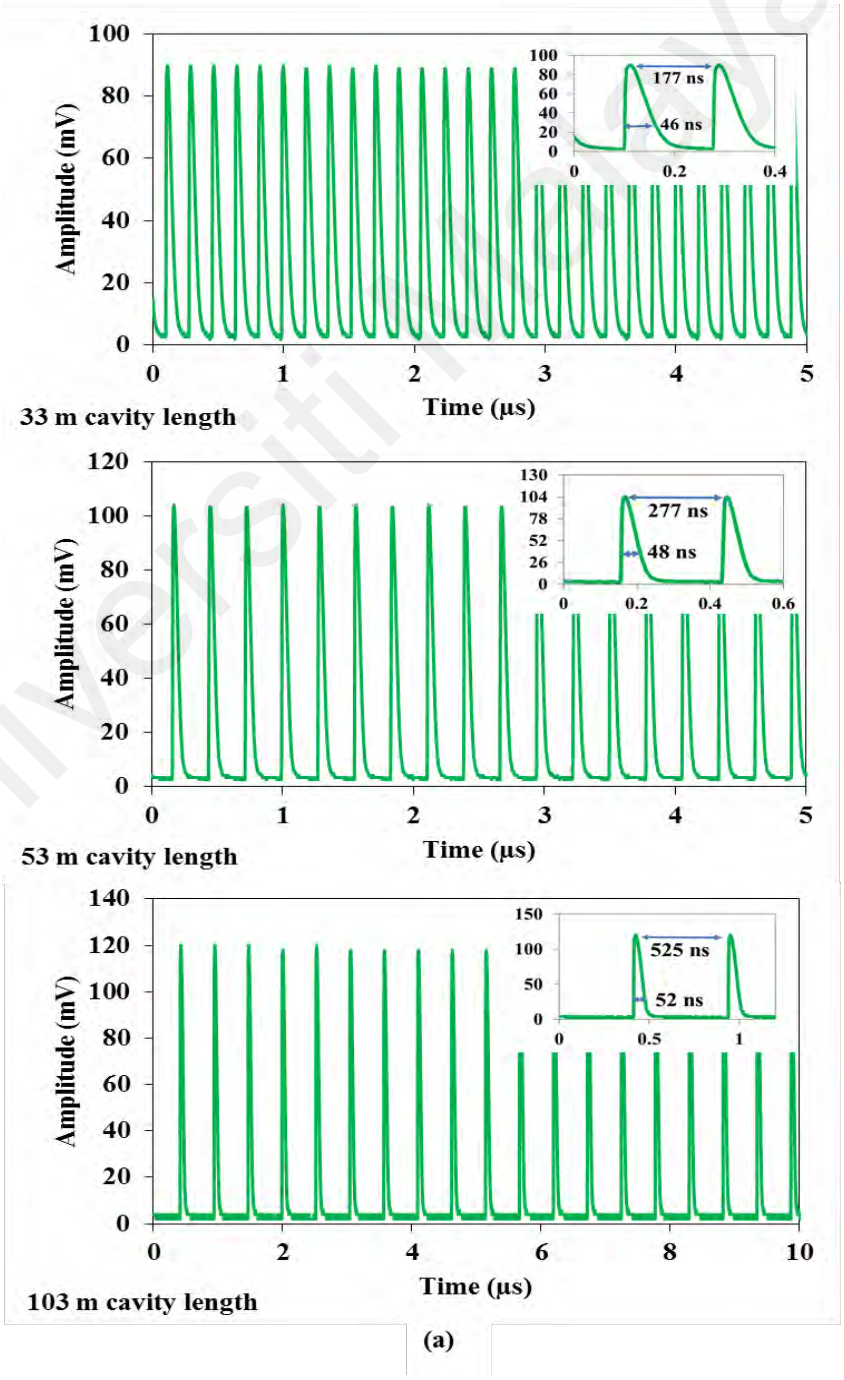

(a)

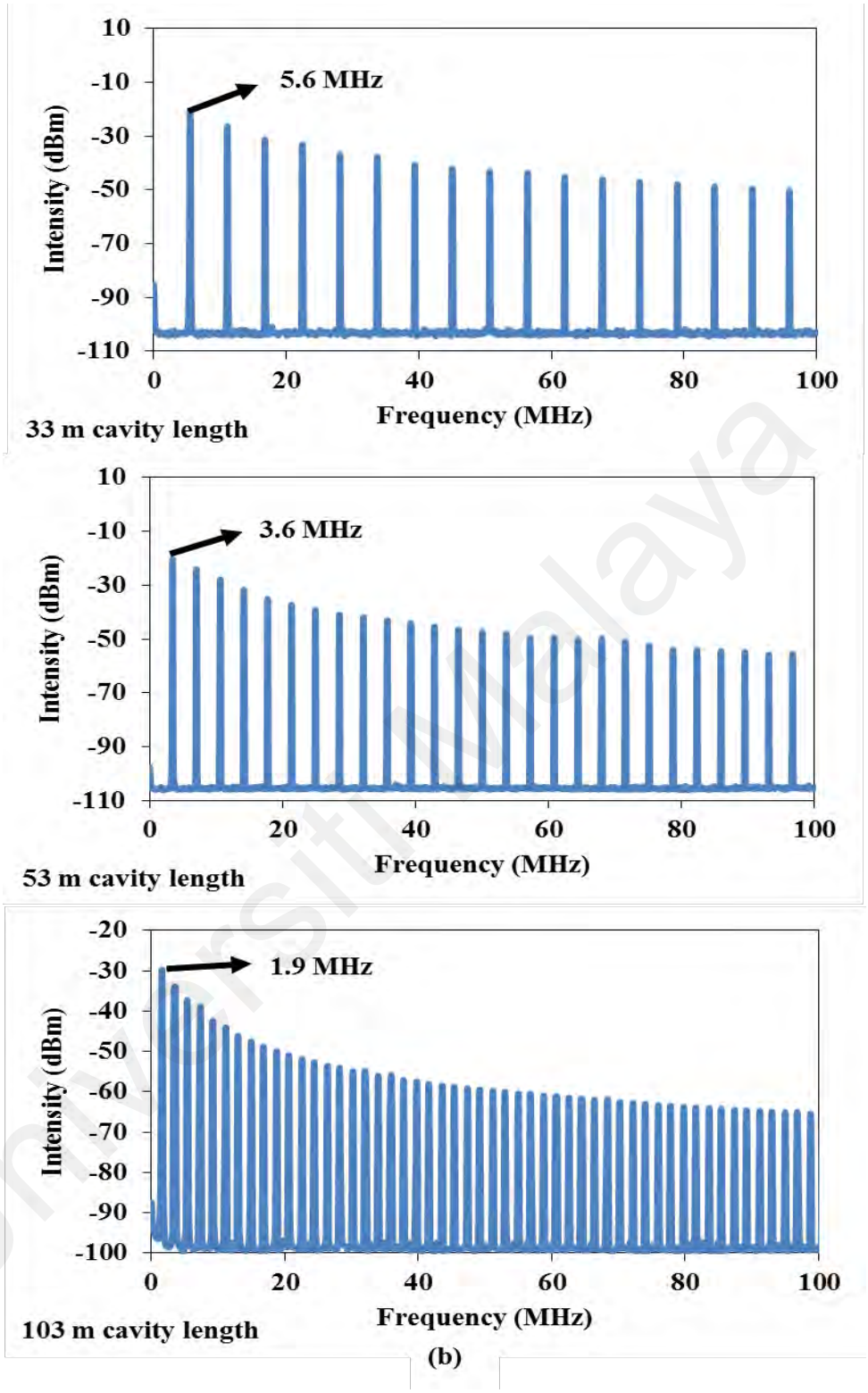

Figure 5.2: The oscilloscope and RFSA characteristics, (a) typical pulse train, and (b) RF spectrum at different cavities lengths

Figure 5.3 (a) shows the relationship between the average output power of the mode-locked laser and input pump power at three different EDFL cavities. The power linearly increased with the pump power and a slope efficiency of 4.3 %, 3.4 %, and 3.2 % was

obtained for EDFL cavities of 33 m, 53 m, and 103 m, respectively. It shows that the laser efficiency slightly reduced with the increase of SMF length in the cavity. This is due to the SMF which induces additional loss and degrades the efficiency of the laser.

Figure 5.3 (b) shows the pulse energy in the same range of input pump power for three different cavities. The pulses held energies were 1.3 nJ, 1.6 nJ, and 3 nJ at maximum output powers of 7 mW, 5.6 mW, and 5.1 mW, where were obtained with laser cavities of 33 m, 53 m, and 103 m, respectively. The highest energy was obtained with 103 m long cavity due to the inverse correlation between pulse energy with a high pulse repetition rate that generated from the effects increment of SMF length in the EDFL cavity (Salam et al., 2019). As the pump power was increased above 167 mW to the maximum pump power of 200 mW, the mode-locked pulses disappear for all cases of different EDFL lengths, and the CW laser operation was retained. Later, the laser pump power was reduced to 167 mW, and the mode-locked operation was restored without any damages or burn on the SA. We believe the damage threshold of the 8-HQCdCl_2H_2O thin-film is beyond our operating regime of 200 mW pump power.

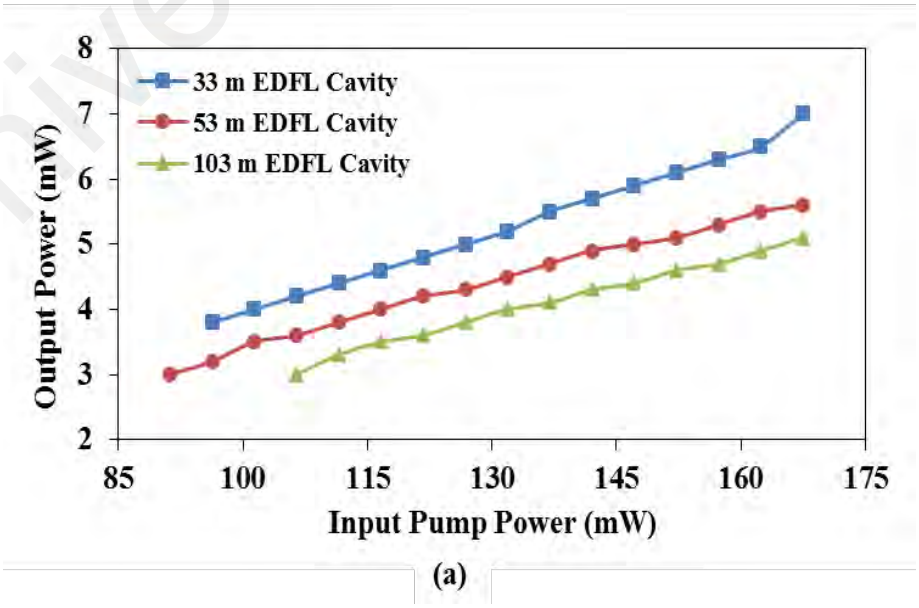

(a)

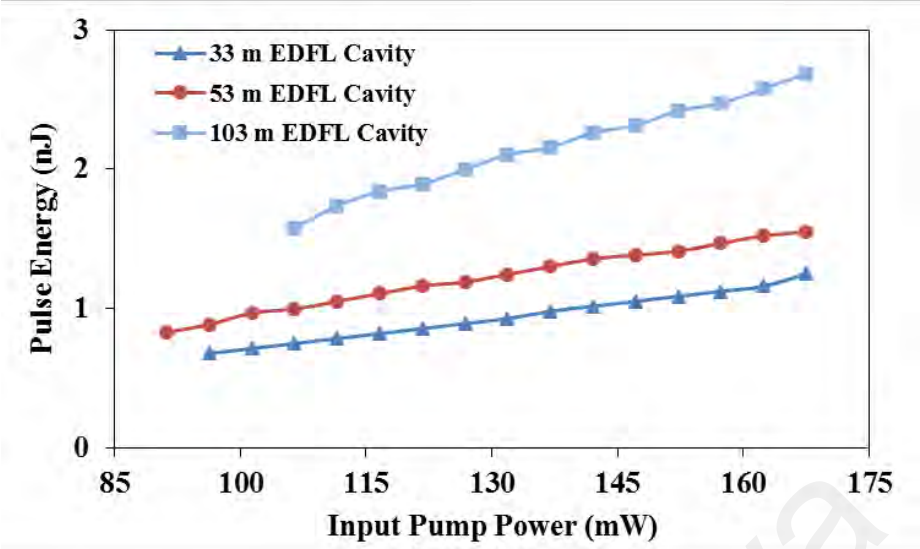

Figure 5.3: Mode-locked performance based on different cavities lengths, (a) Pulse output, and (b) pulse energy against input pump power for different EDFL cavities

Figures 5.4 (a), (b) and (c) describe the output spectra obtained from the EDFL cavities of 33 m, 53 m, and 103 m, respectively, as it was measured by OSA within a range between 1515 nm and 1600 nm. The pump power was fixed at 167 mW in the experiment. The output spectrum with no SA is also included in the figures for comparison purpose. It is observed that the EDFL operates at 1565 nm regardless of cavity lengths. As shown in Figure 5.4 (a), with the incorporation of SA, the EDFL operated at the center of wavelength 1562 nm, with -8 dBm intensity of peak power, and spectral bandwidth of 3 dB of 6.03 nm when the cavity length is fixed at 33 m. Figure 5.4 (b) indicates the operating wavelength of EDFL with 53 m length at center of 1564 nm, with 3 dB spectral bandwidth of 6 nm and intensity of -4 dBm. In Figure 5.4 (c), the wavelength is 1555 nm, at 3 dB spectrum bandwidth of 12.8 nm and power intensity of -4 dBm of EDFL cavity with 103 m. The Kelly sidebands were verified over the OSA and appeared in the case of EDFL cavity with 33 m. This indicates the mode-locked laser operated in soliton regime. However, in the case of cavity 53 m, the Kelly sidebands were less prominent due to the increment in the SMF length, which increase the GDD further from zero. However, the

Kelly sidebands were disappeared, and the 3 dB spectral width was broadened with further increase of SMF length to 100 m. This forced the mode-locked laser to generate stretched pulses due to the large GDD in the EDFL cavity. The increased GDD resulted in an imbalance in the nonlinearity and dispersion generates from the EDFL cavity (Ismail et al., 2016).

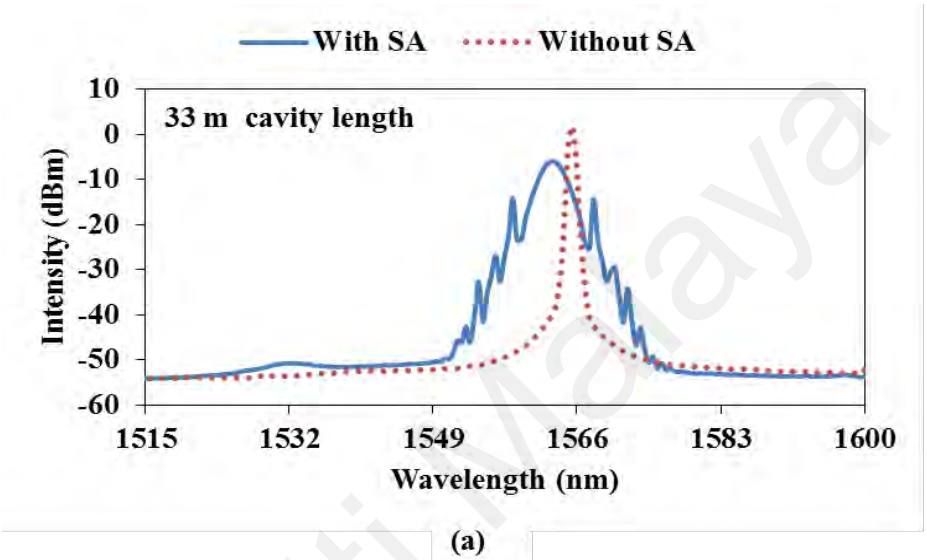

(a)

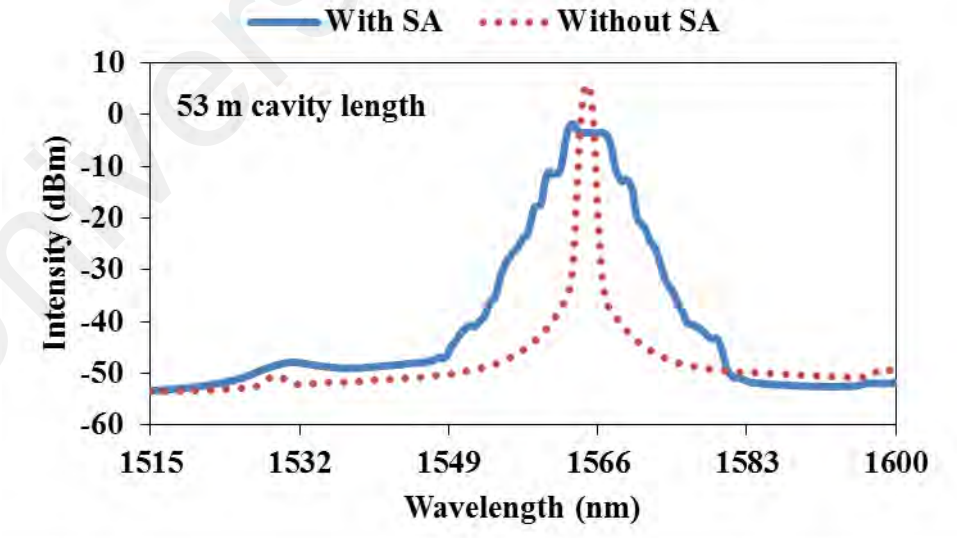

(b)

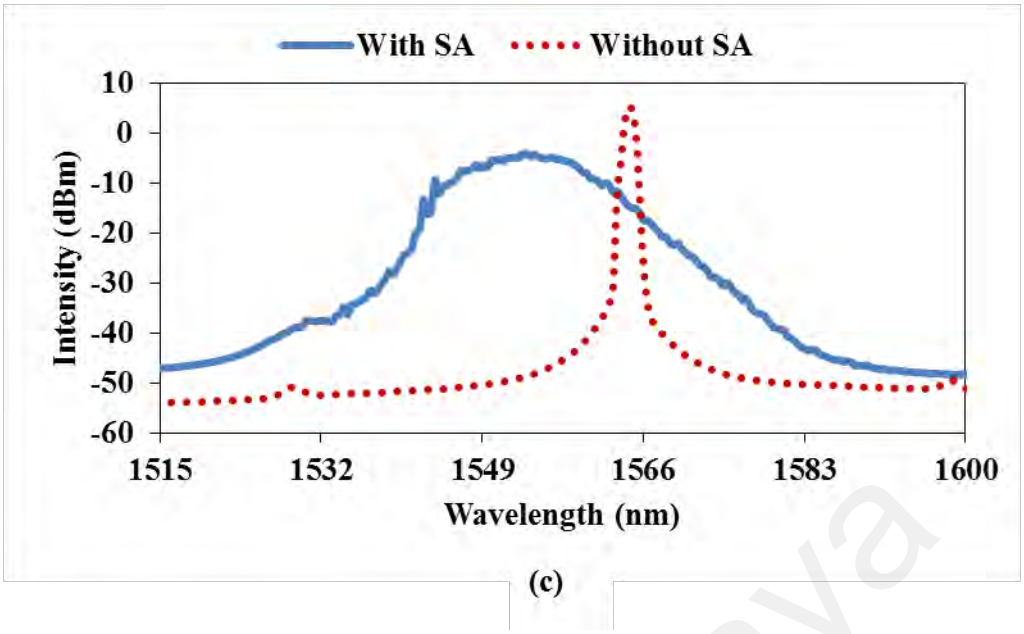

Figure 5.4: Optical spectra from the mode-locked EDFL configured with additional SMF of (a) 33 m, (b) 53 m, and (c) 103 m. The output spectra without the SA are also included as a comparison

Figure 5.5 compares the autocorrelation traces obtained from the mode locked EDFLs configured with different SMF lengths, at a maximum input pump power of 167 mW. The autocorrelation trace has a full width at half-maximum (FWHM) of 950 fs, 1.02 ps, and 1.53 ps for EDFL cavities of 33 m, 53 m, and 103 m, as shown in Figures 5.5 (a), (b) and (c), respectively. The time-bandwidth product (TBP) was calculated mathematically, and it is obtained that the TBP for all cavities are approximately 0.644, which indicates the mode-locked pulse was slightly chirped. The EDFL having total cavity length of 33 m generated the optimum results with a sharp appearance of Kelly sidebands achieving shortest pulse width of 950 fs. Also, the stability performance of the mode-locked EDFL configured with 33 m of cavity length was also examined by operating the mode-locked operations for 180 minutes and recorded the cavity spectrum every 30 minutes. The samples of soliton Kelly sidebands kept the same wavelengths and optical intensities throughout the process of the mode-locked stability evolution. Figure 5.6 describes the spectra samples obtained from 33 m cavity mode-locked that demonstrates first order had intensities of –14 dBm and −14 dBm (at 1558.41 nm and 1567.97 nm), the second-order

had intensities of −26.82 dBm and −29.50 dBm (at 1556.4 nm and 1570.48 nm), and the third-order had intensities of −32.55 dBm and −34 dBm (at 1554.38 nm and 1571.99 nm), and the forth-order had intensities of −42.55 dBm and −42.74 dBm (at 1552.87 nm and 1573.50 nm), respectively.

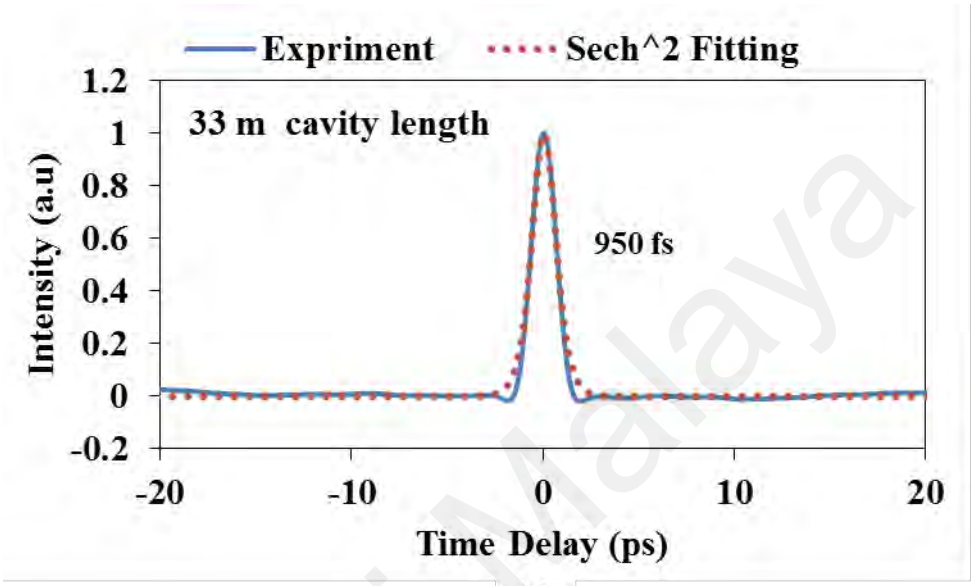

(a)

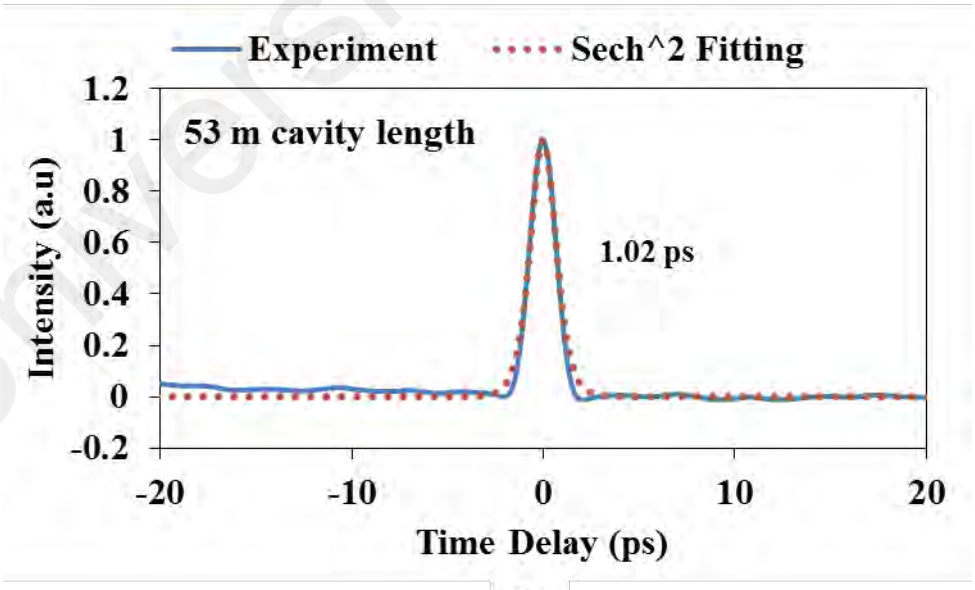

(b)

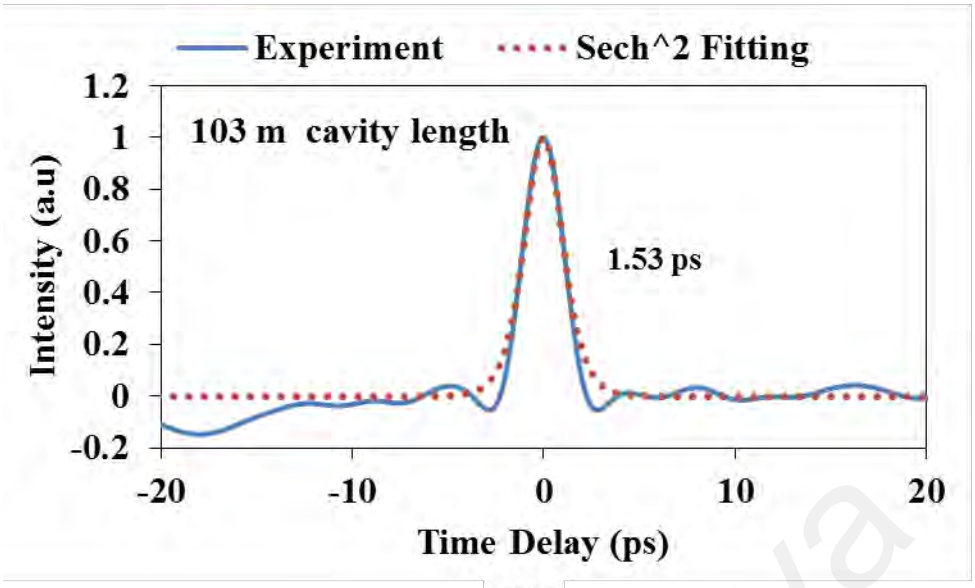

(c)

Figure 5.5: Autocorrelator trace of the mode-locked pulses with the addition of (a) 33 m, (b) 53 m, and (c) 103 m long SMF inside the EDFL cavity

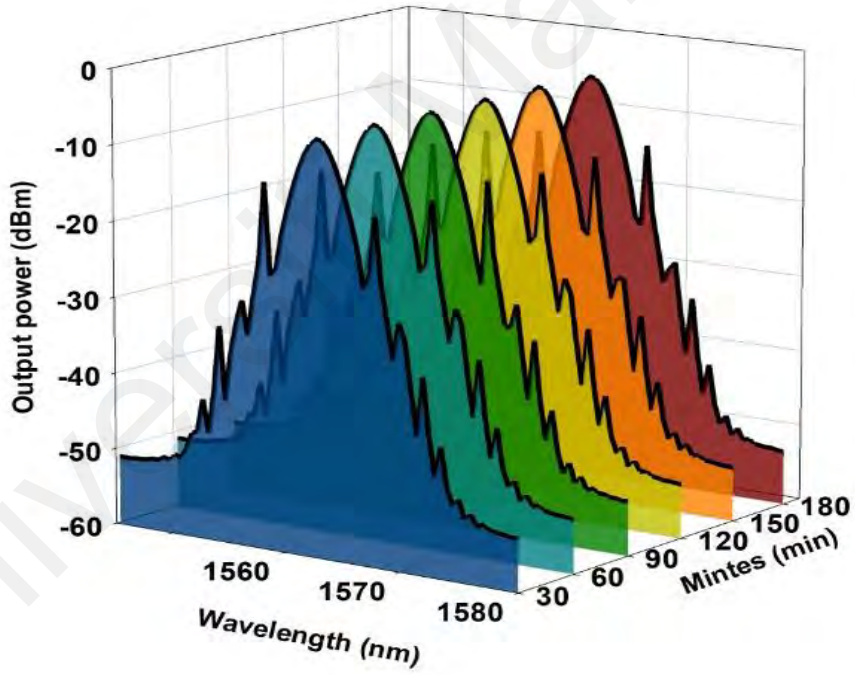

Figure 5.6: Spectrum stability of EDFL of 33 m cavity length

The performance comparisons of 8-HQCdCl$_2$H$_2$O-based mode-locked erbium-doped fiber laser with other SAs are shown in Table 5.1. (Ahmed et al., 2017; Ahmed et al., 2014; Al-Hiti et al., 2020; Al-Hiti et al., 2020; Al-Hiti et al., 2019; Baharom et al., 2019; Hammadi et al., 2018; Mao et al., 2018; Nady et al., 2017; Nady et al., 2018; Salam et al., 2019; Samsamnun et al., 2020; Yan et al., 2017; Zhang et al., 2018; Zulkipli et al., 2020).

By comparison, the SNR of the 8-HQCdCl_2H_2O film SA is impressive and has a good performance by using casting method due to high stability for mode-locking laser with different cavity lengths. Besides, the repetition rate and pulse width can be compared with other SAs which have also good performance.

Table 5.1: Performance comparison of proposed mode locked EDFL with other SAs

SA Material	Cavity length	Mod. depth	Saturation intensity	Rep. rate	Pulse width	SNR	Ref.
Graphene (film)	105 m	6.1%	21 MW/cm2	3.43MHz	2.24 ps	52 dB	(Hammadi et al., 2018)
Graphene (film)	17.3 m	5.9%	21 MW/cm^2	11 MHz	820 fs	45 dB	(Ahmed et al., 2017)
CNT (film)	8.4 m	-	-	15.3 MHz	1.8 ps	-	(Ahmed et al., 2014)
BP (film)	31.8 m	0.3 %	-	5.426 MHz	1.23 ps	50 dB	(Mao et al., 2018)
FIrpic (film)	60 m	12.8 %	5.5 MW/cm^2	3.43 MHz	120 ns	38.3 dB	(Salam et al., 2019)
WS_2	424.8 m	15.1 %	157.6 MW/cm^2	487 kHz	1.49 ps	71.8 dB	(Yan et al., 2017)
$PtSe_2$	8.7 m	4.90-1.11 %	0.34 -1.23 GW/cm^2	23.3 MHz	1.02 ps	61 dB	(Zhang et al., 2018)
Lu_2O_3 (film)	202.5 m	10 %	72 MW/cm^2	0.97 MHz	2.12 ps	61 dB	(Baharom et al., 2019)
V_2O_3 (film)	201 m	7 %	71 MW/cm^2	1 MHz	3.14 ps	-	(Nady et al., 2018)
Ho_2O_3 (film)	11.7 m	45 %	140 MW/cm^2	17.1 MHz	0.65 ps	75 dB	(Al-Hiti et al., 2019)
NiO	202.5 m	39 %	0.04 MW/cm^2	0.96 MHz	0.95 ps	-	(Nady et al., 2017)
P_3HT (film)	113.5 m	11 %	80.45 MW/cm^2	1.838 MHz	2.62 ps	55.23 dB	(Samsamnun et al., 2020)
Eu_2O_3 (film)	113.5 m	20 %	10 MW/cm^2	1.8 MHz	3.51 ps	70 dB	(Zulkipli et al., 2020)
WO_3 (film)	102.5 m	20 %	0.04 MW/cm^2	1.85 MHz	2.69 ps	53 dB	(Al-Hiti et al., 2020)

Table 5.1: continued

SA Material	Cavity length	Mod. depth	Saturation intensity	Rep. rate	Pulse width	SNR	Ref.
Turmeric	52.5 m	23 %	0.16 MW/cm^2	3.383 MHz	920 fs	77 dB	(Al-Hiti et al., 2020)
8-HQCdCl$_2$H$_2$O (film)	103 m	18 %	0.1 MW/cm^2	1.9 MHz	1.53 ps	70 dB	This work
	53 m	18 %	0.1 MW/cm^2	3.6 MHz	1.02 ps	85 dB	
	33 m	18 %	0.1 MW/cm^2	5.6 MHz	950 fs	83 dB	

5.3 Mode-locked Erbium-Doped Fiber Laser with Cr_2AlC Thin Film SA

In this section, passively mode locked EDFL pulses generations were demonstrated using Cr_2AlC thin film as SA for operation at the 1.5 μm region. The Cr_2AlC film prepared by a drop-casting approach was inserted between two FC/PCs to produce two mode-locked laser pulses at a central wavelength of 1558 nm and 1559 nm. Among two mode locked fiber lasers produced in this work, highest repetition rate was obtained at 1.88 MHz corresponding to the cavity length of 103 m. The SA fabrication process was simple and cheap as described in the Chapter 3. This the first demonstration of Cr_2AlC MAX phases as SA in EDFL which operates at 1.5-μm wavelength.

5.3.1 Laser Configuration of the Mode-locked Laser with Cr_2AlC Thin Film SA

The proposed laser cavity for the mode-locked EDFL cavity is illustrated in Figure 5.7. A 980 nm pump source and a piece of 1 m heavily EDF were connected into the laser cavity as a gain medium through 980/1550 nm WDM. The EDF with ion absorption of 23 dB/m at 980 nm, core diameter of 4 μm, cladding diameter of 125 μm, and numerical aperture of 0.16 was used as a gain medium. ISO was utilized to force the unidirectional operation into the laser cavity. While an 80:20 OC was used to let 20% extract out and retains the other 80% into the cavity.

Two different additional lengths of SMF were integrated with the laser cavity to create two different states of mode-locked EDFL operation with the lengths of 100 m and 200 m. The GVD values of the SMF, WDM, and EDF are -21.7 ps^2/km, -48.5 ps^2/km and 27.6 ps^2/km, respectively. The total lengths of the cavities were 103 m and 203 m with the total cavity dispersion of -2.19 ps^2 and -4.36 ps^2, respectively. However, the Q-switched operation cannot be observed in these experiments using this cavity arrangement. By significantly reducing the cavity length, the Q-switching operation can realize as described in the previous chapter.

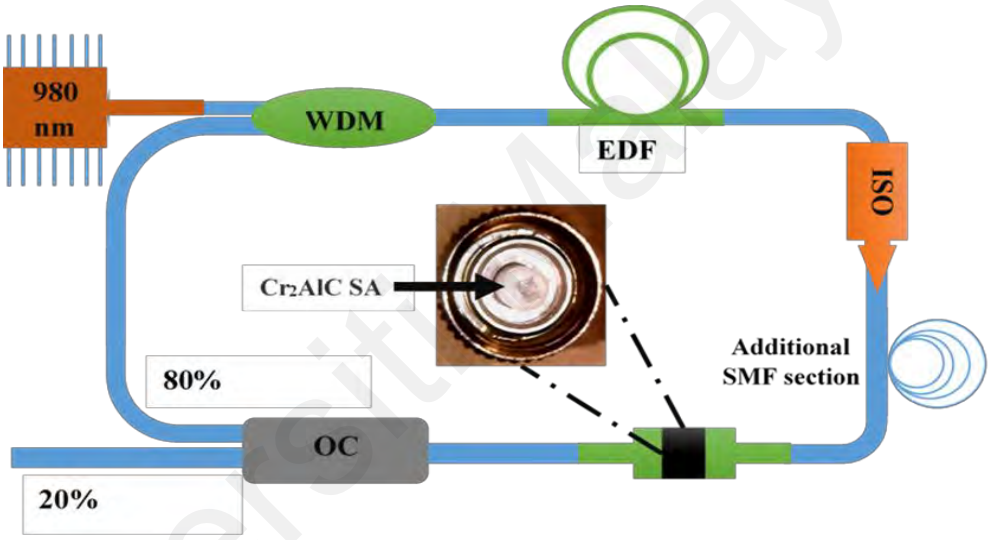

Figure 5.7: Laser cavity configuration of the passively mode locked EDFL using Cr_2AlC film SA.

5.3.2 Mode-locked Laser Performance with Cr_2AlC Thin Film SA

In this work, both cavities (with length of 103 m and 203 m) generated the continuous wave (CW) laser at a threshold pump power of 10 mW, then the pump power was increased between the 121.69 to 167 mW, mode-locked pulses were produced. Figure 5.8 (a) depicts a regular pulse train consisting of the two mode-locked operations, which were measured separately by an oscilloscope at the highest input laser pump power of 167 mW. It describes the 535 ns and 999 ns of the pulse period, this corresponds to the repetition rate of 1.88 MHz and 1 MHz at cavity lengths of 103 m and 203 m, respectively, see

Figure 5.8 (b). Figure 5.8 (c) shows the output spectra of the two mode locked EDFL operations obtained from cavity lengths of 103 m and 203 m with a resolution of 0.07 nm. They show lasing spectra centered at 1558 nm and 1559 nm with 3-dB bandwidth of 2.4 nm and 0.8 nm. Both spectra showed Kelly sidebands, which indicated the lasers operated in soliton regime. However, the Kelly sidebands are less prominent in 203 m cavity due to excessive nonlinearity caused via long cavity length and high pump power (Samsamnun et al., 2019). While the non-SA wavelength spectrum was centered at 1561 nm with 3-dB bandwidth of 1.2 nm. The laser operation wavelength could be tuned by incorporating tunable filter inside the cavity. However, the filter may also destroy the soliton pulses if the spectral bandwidth is wider than the filter bandwidth. In our experiment, the wavelength is shifted when we changed the cavity length (203 m to 103 m), due to the variation in cavity loss and the dispersion characteristics.

Initially, the oscilloscope reveals pulse widths of 179 ns and 345 ns for two mode locked EDFL operations. Despite the limitations of oscilloscope resolution, and made these pulse durations are not actual. Therefore, the autocorrelation (Alnair Labs Hac-200) was utilized to precisely evaluate the FWHM with high precision for two mode-locked EDFL operations, as shown in Figure 5.8 (d) and Figure 5.8 (e). The FWHM of the two mode-locked operations were about 2.5 ps and 4.45 ps with cavity lengths of 103 m and 203 m. Also, the TBP was estimated at 0.741 and 0.439 for 103 m and 203 m cavity lengths which are higher than the transform-limited prediction of 0.315. This indicated the generated pulses are slightly chirped.

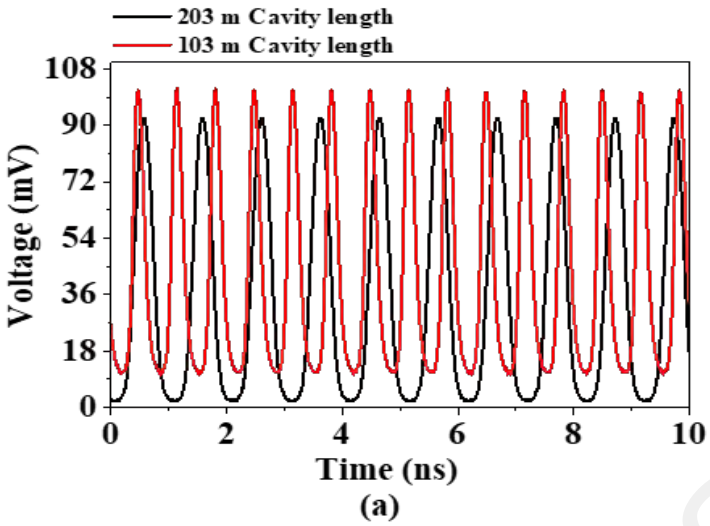

(a)

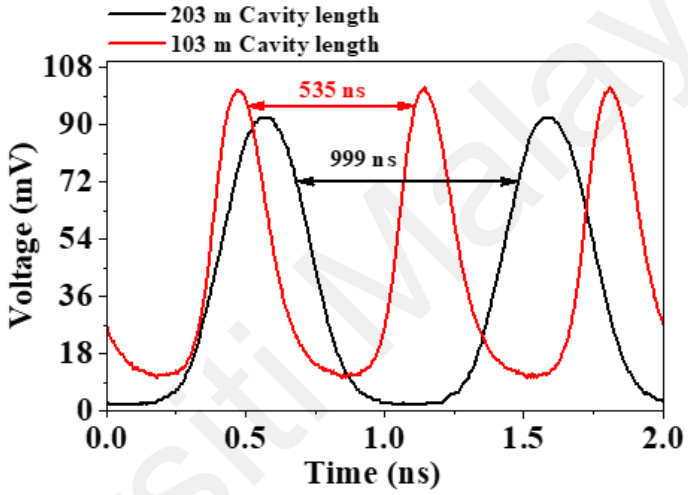

(b)

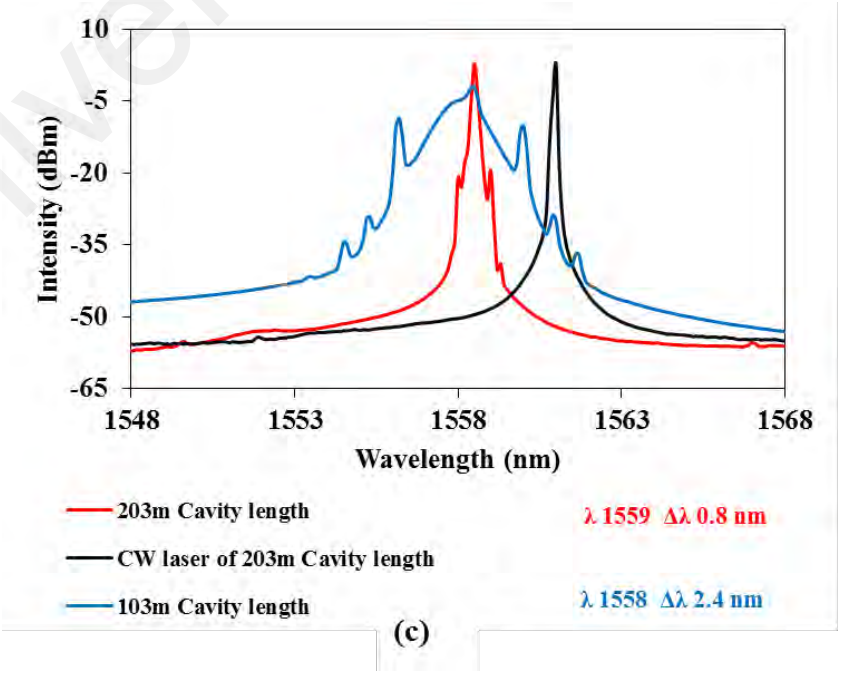

(c)

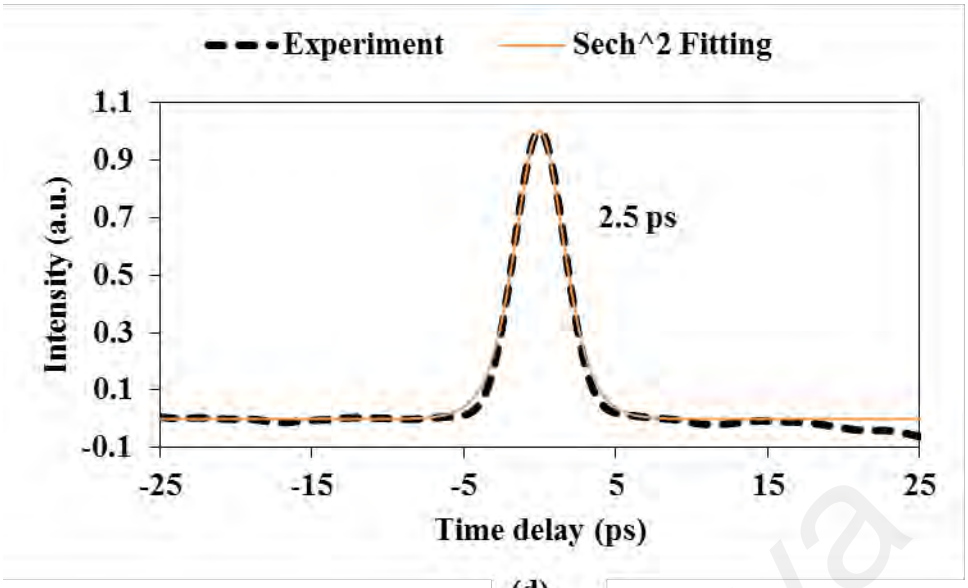

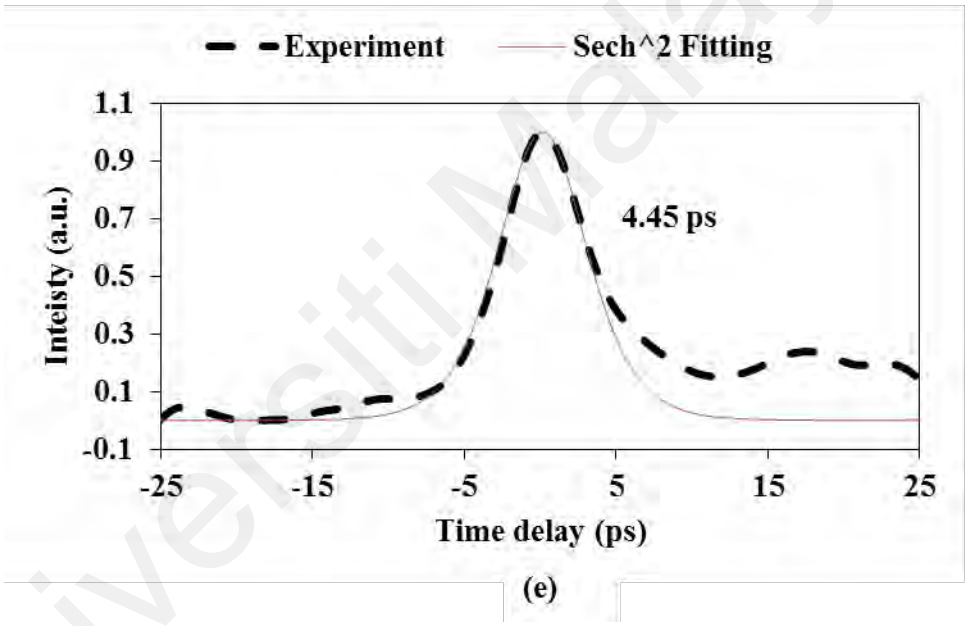

Figure 5.8: The oscilloscope, optical spectra, and autocorrelator characteristics of two mode locked EDFL operations, (a) pulse train, (b) pulse period, (c) output spectra, (d) FWHM using 103 m cavity length, and (e) FWHM using 203 m cavity length

The mode-locked fiber lasers were also analyzed by the RFSA, see Figure 5.9 (a). The SNR of two mode-locked EDFLs was achieved using cavity lengths of 103 m and 203 m at 70 dB and 73 dB which corresponded to repetition rates of 1.88 MHz and 1 MHz. As compared to other previous works (Hammadi et al., 2018; Salam et al., 2019), the SNR obtained is significantly higher which indicates the high stability of our mode-locked lasers. Figure 5.9 (b) shows the linear relationships for two different cavity lengths between the reported of the average output power, with pulse energy, against the laser

pump power. In 103 m cavity length, the pulse energy and average output power were increased from 1.25 nJ to 1.60 nJ and 2.35 mW to 3.02 mW at a pump power of 121.69 mW to 167 mW, respectively. While in 203 m cavity length, the average output power and pulse energy were decreased compared to the previous experiment due to the increase in the cavity length resulting in a high power loss inside the cavity. Hence, the average output power and pulse energy have increased from 0.62 nJ to 0.91 nJ and 0.62 mW to 0.91 mW at the same range of pump power. We believe the damage threshold of our proposed thin-film SA is beyond our operating regime of 185 mW pump power because, when the pump power was increased to maximum and then reduced back to 167 mW, the mode-locking was regained, assuring that the SA was not burnt.

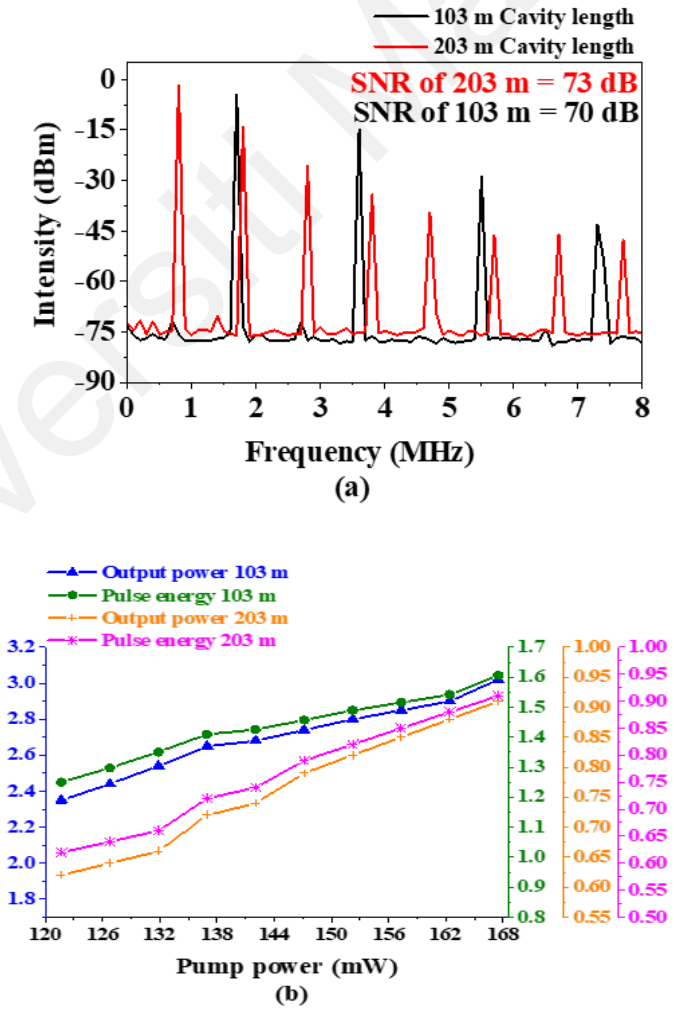

Figure 5.9: The mode-locked performance using two different cavity lengths, (a) RF spectrum, and (b) pulse energy and average output power against various pump power.

Nonlinear polarization evolution (NPE) can also produce passively mode-locked lasers (Hofer et al., 1992; Matsas et al., 1992). In order to validate that only the proposed SA was responsible for the generation of pulsed laser. The proposed SA has removed from the laser cavity, then, cleaned the fiber ferrules and tuned the laser pump power at all the possible ranges. However, there was no pulse formed without the SA in EDFL cavity. Further, by replacing the SA with a pure PVA thin film could also not produce any traces of pulses in the laser cavity. Thus, the cavity of mode-locked laser was produced only by Cr_2AlC-thin film SA in our experimental setup.

Figure 5.10 shows the long-term evaluation of spectra generated by using cavity lengths of 103 m and 203 m. All the wavelength spectrum samples of two mode locked EDFL operations have been taken every 60 minutes within 6 hours. It was observed that all spectrum samples are identical, and this proves the two mode locked EDFL operations were in a stable state for 6 hours. Figure 5.10 (a) shows the long-term evaluation of spectra samples of 103 m cavity length. The first order Kelly sidebands were maintained at the intensities of –8.49 dBm and −10.07 dBm (at 1556.3 nm and 1560 nm). For the second order, the intensities of −29.05 dBm and −30.01 dBm were maintained at 1555 nm and 1561 nm, while the intensity of third-order Kelly side bands were maintained at −34.84 dBm (1554.7 nm) and −37.02 dBm (1561.8 nm). Figure 5.10 (b) shows the long-term evaluation of mode-locked EDFL using cavity length of 203 m that generated output spectra with intensities of –20.96 dBm and –19.43 dBm (at 1557 nm and 1560 nm). In addition, the mode-locked operation worked continuously for three days without any interruptions during that time. Eventually, the new Cr_2AlC thin film has a high resistance for long term illumination.

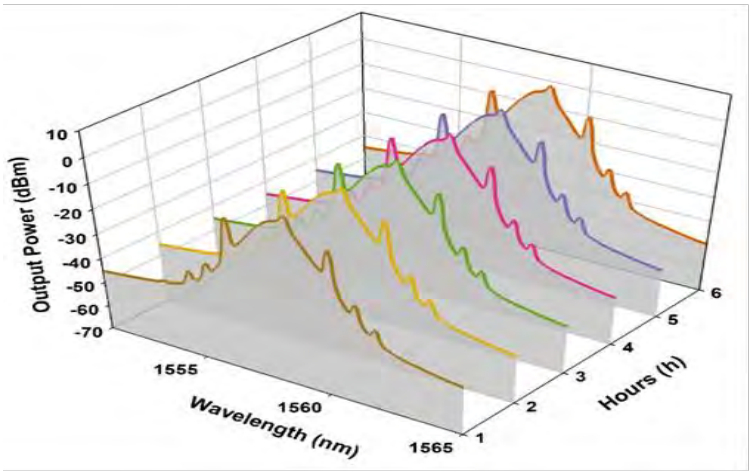

(a)

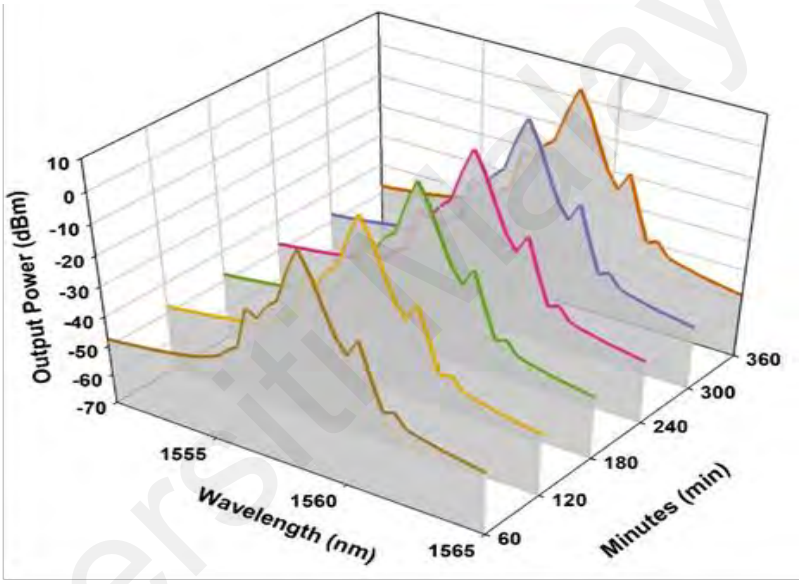

(b)

Figure 5.10: Long-term evaluation of two different mode locked EDFL operations at maximum pump power 167 mW, (a) output spectra based on 103 m cavity length, and (b) output spectra based on 203 m cavity length

Table 5.2 shows the comparison of the proposed Cr_2AlC thin-film performance with other mode-locked using different nanomaterials (Ahmed et al., 2014; Ahmed et al., 2017; Al-Hiti et al., 2020; Al-Hiti et al., 2020; Al-Hiti et al., 2019; Baharom et al., 2019; Hammadi et al., 2018; Mao et al., 2018; Nady et al., 2017; Nady et al., 2018; Salam et al., 2019; Samsamnun et al., 2020; Zulkipli et al., 2020). The repetition rate, pulse width, SNR, and modulation depth of Cr_2AlC thin-film could be compared with other SAs based on outcomes of different laser cavities lengths.

Table 5.2: Performance comparison of proposed SA film with other nanomaterials-based SAs

SAs	Cavity lengths	Mod. Depth	Sat. intensity (MW/cm^2)	Rept. Rate	Pulse Width	SNR	Ref.
Graphene	105 m	6.1 %	21	3.43 MHz	2.24 ps	52 dB	(Hammadi et al., 2018)
Graphene	17.3 m	5.9 %	21	11 MHz	820 fs	45 dB	(Ahmed et al., 2017)
CNT	8.4 m	-	-	15.3 MHz	1.8 ps	-	(Ahmed et al., 2014)
BP	31.8 m	0.3 %	-	5.426 MHz	1.23 ps	50 dB	(Mao et al., 2018)
Flrpic	60 m	12.8 %	5.5	3. 43 MHz	120 ns	38.3 dB	(Salam et al., 2019)
Lu_2O_3	202.5 m	10 %	72	0.97 MHz	2.12 ps	61 dB	(Baharom et al., 2019)
V_2O_3	201 m	7 %	71	1 MHz	3.14 ps	-	(Nady et al., 2018)
Ho_2O_3	11.7 m	45 %	140	17.1 MHz	0.65 ps	75 dB	(Al-Hiti et al., 2019)
NiO	202.5 m	39 %	0.04	0.96 MHz	0.95 ps	-	(Nady et al., 2017)
P_3HT (film)	113.5 m	11 %	80.45	1.838 MHz	2.62 ps	55.23 dB	(Samsamnun et al., 2020)
Eu_2O_3	113.5 m	20%	10	1.8 MHz	3.51 ps	70 dB	(Zulkipli et al., 2020)
WO_3	102.5 m	20 %	0.04	1.85 MHz	2.69 ps	53 dB	(Al-Hiti et al., 2020)
Turmeric	52.5 m	23 %	0.16	3.83 MHz	920 fs	77 dB	(Al-Hiti et al., 2020)

Table 5.2: continued

SAs	Cavity lengths	Mod. Depth	Sat. intensity (MW/cm^2)	Rept. Rate	Pulse Width	SNR	Ref.
8-HQCdCl$_2$H$_2$O	33 m	18 %	0.1	5.6 MHz	950 fs	83 dB	This Work
Cr$_2$AlC	103 m	3.2 %	40	1.88 MHz	2.5 ps	70 dB	This Work
Cr$_2$AlC	203 m	3.2 %	40	1 MHz	4.45 ps	73d B	

5.4 Summary

Ultra-short soliton pulses were successfully generated in EDFL cavity using two types of organic SAs. At first, the thin-film of 8-HQCdCl_2H_2O was experimentally demonstrated to produce different mode locked pulses in three different EDFL cavities. At the maximum input pump power of 167 mW, the 33 m EDFL cavity produced a soliton pulse with the FWHM of 950 fs with a repetition rate of 5.6 MHz, the presence of Kelly sidebands was verified by OSA. However, the 53 m and 103 m of EDFL cavities were recorded FWHM 1.02 ps and 1.53 ps, with a repetition rate of 3.6 MHz and 1.9 MHz, respectively. The passive mode-locked operation EDFL was successfully achieved by utilizing the Cr_2AlC MAX phases as a SA thin film. In 203 cavity length, the output pulses were reported the repetition rate of pulse was 1 MHz, then the 3 dB bandwidth of 0.8 nm, at the center wavelength of 1559 nm. The pulse energy and FWHM were also reported as 0.91 nJ and 4.45 ps, respectively. Then, the length of the cavity decreased to be 103 m and produced 1.88 MHz of pulse of repetition rate, and 2.5 ps of FWHM of the pulse.

CHAPTER 6: CONCLUSION AND FUTURE WORK

6.1 Conclusion

Fiber laser technology became widely available in many applications, from industry, communications, and medicine to material science. The generated pulses from a fiber laser could be designed to have ultra-short pulse width and reasonably high pulse energy. In addition, the fiber lasers are advantageous in terms of low-cost setup, flexibility in design, modular setup, and compactness, thus they are suitable for a wide range of applications. Most of the research works on fiber laser have focused on developing new saturable absorbers (SAs) for generating Q-switched and mode-locked fiber lasers. This thesis describes the applications and fabrications of the new SAs for operations of Q-switching and mode-locking. It aims to develop efficient and low-cost Q-switched and mode-locked fiber lasers operating in the nanosecond and picosecond regime, respectively using two types of SA materials: 8-HQCdCl_2H_2O and Cr_2AlC. Three objectives have been outlined to achieve the aim.

The first objective is to fabricate and characterize new passive SAs based on two different materials: 8-Hydroxyquinolino cadmium chloride hydrate (8-HQCdCl_2H_2O) and chromium aluminum carbide (Cr_2AlC). 8-HQCdCl_2H_2O and Cr_2AlC is belong to the organic and MAX phases family, respectively. In chapter 3, three types of SAs were successfully developed based on both materials as a based material. 8-HQCdCl_2H_2O SA was prepared based on two methods: mechanical exfoliation and thin film while Cr_2AlC was only prepared in form of thin film. The PVA was used as a host polymer in preparing 8-HQCdCl_2H_2O and Cr_2AlC thin films. These SAs were also successfully characterized in terms of physical and chemical characteristics as well as linear and nonlinear absorption properties. Based on twin-detector measuring technique, the modulation depth of the exfoliated 8-HQCdCl_2H_2O on scotch tape, 8-HQCdCl_2H_2O thin film and Cr_2AlC

thin film are obtained at 11 %, 18 % and 3.2 %, respectively. This indicates all the SAs are suitable for use in generating Q-switched and mode-locked pulses in erbium-doped fiber laser (EDFL) cavity.

The second objective is to design and optimize an EDFL cavity to generate Q-switched pulse train in 1.5 μm region with a pulse width in nanosecond regime using the newly developed 8-HQCdCl_2H_2O and Cr_2AlC SAs as a Q-switcher. The generation of Q-switched pulses in the EDFL cavity was successfully validated for all proposed SAs. The exfoliated 8-HQCdCl_2H_2O SA was experimentally demonstrated to produce pulses by a 50/50 output coupler (OC), with the EDFL cavity to generate the high pulse energy of 172 nJ, at the highest output power of 23.4 mW. After changing the 50/50 OC to 95/05 OC, the width of pulses was dropped to 1.66 μs, then the repetition rate pulses rose to 173 kHz. This SA showed good results as a passive Q-switcher, but the lowest pulse width cannot reach nanosecond regime. Nevertheless, the nanosecond pulse generation was successfully realized using the 8-HQCdCl_2H_2O film as SA. The Q-switched laser produced 726 ns pulses with a repetition rate of 150 kHz at pump power of 167 mW. The nanosecond pulses were also successfully generated by using Cr_2AlC thin film as a Q-switcher. The Cr_2AlC based EDFL produced 780 ns pulse with repetition rate of 132 kHz, also the pulse energy was 9 nJ, and the output power was 1.134 mW, at 167 mW of the maximum laser pump power.

The third or final objective is to design and optimize EDFL cavity for generating mode-locked pulse train in 1.5 μm region with a pulse width within picosecond to femtosecond regime using the newly developed 8-HQCdCl_2H_2O and Cr_2AlC SAs. In this work, ultrashort soliton pulses were successfully generated in EDFL cavity using both SAs. The developed 8-HQCdCl_2H_2O thin film was successfully used to demonstrate different mode-locked pulses in three different EDFL cavities. For instance, femtosecond

soliton pulses were obtained in the 33 m EDFL cavity. The laser produced a soliton pulse with the full width at half-maximum (FWHM) of 950 fs at a repetition rate of 5.6 MHz. The passive mode-locked operation of EDFL was successfully achieved by utilizing Cr_2AlC MAX phases as a mode-locker based on 2 different cavities. For instance, in the 203 m cavity, the generated pulses have a 1 MHz of repetition rate of the pulse, and 1559 nm of wavelength at a 3 dB bandwidth of 0.8 nm, where pulse width was 4.45 ps, and 0.91 nJ of the maximum attainable pulse energy. In conclusion, all objectives have been achieved and the Q-switching and mode-locking results are summarized in Tables 6.1 and 6.2, respectively.

Table 6.1: Summary of Q-switching results with the proposed SAs

SA	Max pump power (mW)	Rep rate (kHz)	Pulse width	Energy (nJ)	Output Power (mW)	λ (nm)	SNR (dB)	OC
8-HQCdCl$_2$H$_2$O	167	136	2.076 μs	172	23.4	1530.49	81	50/50
8-HQCdCl$_2$H$_2$O	167	173	1.66 μs	10	1.8	1530.49	75	95/05
8-HQCdCl$_2$H$_2$O PVA	167	150	726 ns	4.5	0.7	1530	72	90/10
Cr_2AlC PVA	167	132	780 ns	9	1.134	1531	67	90/10

Table 6.2: Summary of mode-locking results with the proposed SAs-PVA.

SAs	Cavity lengths	Mod. Dep.	Sat. intensity	Rep Rate	Pulse Widh	E_p (nJ)	Output Power (mW)	λ (nm)
8-HQCdCl$_2$H$_2$O	103 m	18 %	0.1 MW/cm^2	1.9 MHz	1.53 ps	3	5.1	1555
8-HQCdCl$_2$H$_2$O	53 m	18 %	0.1 MW/cm^2	3.6 MHz	1.02 ps	1.6	5.6	1564

Table 6.2: continued

SAs	Cavity lengths	Mod. Dep.	Sat. intensity	Rep. Rate	Pulse Widh	E_p (nJ)	Output Power (mW)	λ (nm)
8-HQCdCl_2H_2O	33 m	18 %	0.1 MW/cm^2	5.6 MHz	950 fs	1.3	7	1562
Cr_2AlC	103 m	3.2%	40 MW/cm^2	1.88 MHz	2.5 ps	1.6	3.02	1558
Cr_2AlC	203 m	3.2%	40 MW/cm^2	1 MHz	4.45 ps	0.91	0.91	1559

6.2 Research Contributions

The main contributions of this research work are:

1. Two SA's thin film were successfully developed using the drop-casting method in conjunction of polyvinyl alcohol (PVA) as a host polymer: 8-HQCdCl_2H_2O and Cr_2AlC thin-film. The 8-HQCdCl_2H_2O SA was also successful realized based on mechanical exfoliation method.
2. The nanosecond pulse generation was successfully demonstrated using the 8-HQCdCl_2H_2O film as SA for the first time via a Q-switching method. At the maximum input pump power of 167 mW, the Q-switched laser produced pulses at a repetition rate of 150 kHz with pulse width of 726 ns.
3. Generation of nanosecond Q-switched pulses was demonstrated for the first time using a Cr_2AlC as a SA. The SA successfully produces shorter pulses, where the pulse width was 780 ns and the repetition rate of the pulse of 132 kHz at the highest input laser power of 167 mW,
4. Ultra-short soliton pulses were successfully generated in EDFL cavity using 8-HQCdCl_2H_2O. By fixing the cavity length at 33 m, the EDFL produced a soliton pulse with the full width at half-maximum (FWHM) of 950 fs with a repetition rate of 5.6 MHz at the pump power of 167 mW.

5. The passive mode-locked operation EDFL has successfully been achieved by utilizing the Cr_2AlC thin film as a SA. At 103 cavity length, the laser produced soliton mode-locked pulse train operating at repetition rate of 1.88 MHz with a pulse duration of 2.5 ps.

6.3 Future Work

This section introduces many interesting future work directions. The future work must find new fabrication methods for thin-film SA of 8-$HQCdCl_2H_2O$ and Cr_2AlC to enhance the absorption properties. Further work also needs to explore the ability of 8-$HQCdCl_2H_2O$ and Cr_2AlC in other wavelength regions such as 1, 2, and 3.5 microns for generating short and ultra-short pulses. The new SAs should also be prepared by depositing 8-$HQCdCl_2H_2O$ or Cr_2AlC onto D-shape fiber to increase the interaction length between materials and oscillating laser. A Q-switching and mode-locking operation with better performance could also be achieved using this technique. The performance of the passive Q-switching and mode-locked operations can also be realized and improved by using other types of materials such as MXenes as thin-film PVA SA. New SAs with a high tolerance threshold and excellent saturation absorption could be continuously explored. Another point for future work is to explore the multi-wavelength pulsed fiber laser by adding some new components such as photonic crystal fiber (PCF) in the setup of the laser cavity. Furthermore, ultrafast fiber lasers will be striving to generate shorter pulse width, higher peak power and pulse energy. The ultra-fast fiber laser era is constantly progressing and preserve an excellent capacity for applications in optoelectronics, optical sensors, communications, etc.

REFERENCES

Addanki, S., Amiri, I. S., & Yupapin, P. (2018). Review of optical fibers-introduction and applications in fiber lasers. *Results in Physics, 10*, 743-750. doi: https://doi.org/10.1016/j.rinp.2018.07.028

Ahmad, H., Albaqawi, H. S. M., Yusoff, N., Chong, W. Y., & Yasin, M. (2019). Q-Switched Fiber Laser at 1.5 μm region using Ti_3AlC_2 MAX phase-based saturable absorber. *IEEE Journal of Quantum Electronics, 56*(2), 1-6. doi: 10.1109/JQE.2019.2949798

Ahmad, H., Ariffin, N. A. M., Aidit, S. N., Ooi, S. I., Yusoff, N., & Zamzuri, A. K. (2021). 1.9 μm mode-locked fiber laser based on evanescent field interaction with metallic vanadium diselenide (VSe_2). *Optik, 230*, 166280. doi: 10.1016/j.ijleo.2021.166280

Ahmad, H., Hassan, H., Safaei, R., Thambiratnam, K., Ismail, M., & Amiri, I. (2017). Molybdenum disulfide side-polished fiber saturable absorber Q-switched fiber laser. *Optics Communications, 400*, 55-60. doi: 10.1016/j.optcom.2017.04.071

Ahmad, H., Salim, M., Thambiratnam, K., Norizan, S., & Harun, S. W. (2016). A black phosphorus-based tunable Q-switched ytterbium fiber laser. *Laser Physics Letters, 13*(9), 1-7. doi: 10.1088/1612-2011/13/9/095103

Ahmed, M., Ali, N., Salleh, Z., Rahman, A., Harun, S., Manaf, M., & Arof, H. (2014). All fiber mode-locked Erbium-doped fiber laser using single-walled carbon nanotubes embedded into polyvinyl alcohol film as saturable absorber. *Optics & Laser Technology, 62*, 40-43. doi: 10.1016/j.optlastec.2014.02.012

Ahmed, M., Ali, N., Salleh, Z., Rahman, A. A., Harun, S. W., Manaf, M., & Arof, H. (2015). Q-switched erbium doped fiber laser based on single and multiple walled carbon nanotubes embedded in polyethylene oxide film as saturable absorber. *Optics & Laser Technology, 65*, 25-28. doi: 10.1016/j.optlastec.2014.07.001

Ahmed, M., Latiff, A., Arof, H., & Harun, S. W. (2016). Ultrafast erbium-doped fiber laser mode-locked with a black phosphorus saturable absorber. *Laser Physics Letters, 13*(9), 095104.

Ahmed, M. H. M., Al-Masoodi, A. H. H., Latiff, A. A., Arof, H., & Harun, S. W. (2017). Mechanically exfoliated 2D nanomaterials as saturable absorber for Q-switched erbium doped fiber laser. *Indian Journal of Physics, 91*(10), 1259-1264.

Ahmed, M. H. M., Al-Masoodi, A. H. H., Yasin, M., Arof, H., & Harun, S. W. (2017). Stretched and soliton femtosecond pulse generation with graphene saturable absorber by manipulating cavity dispersion. *Optik, 138*, 250-255. doi: 10.1016/j.ijleo.2017.03.011

Ahmed, M. H. M., Ali, N. M., Salleh, Z. S., Rahman, A. A., Harun, S. W., Manaf, M., & Arof, H. (2014). All fiber mode-locked Erbium-doped fiber laser using single-walled carbon nanotubes embedded into polyvinyl alcohol film as saturable absorber. *Optics & Laser Technology, 62*, 40-43. doi: 10.1016/j.optlastec.2014.02.012

Ahmed, M. H. M., Latiff, A. A., Arof, H., Ahmad, H., & Harun, S. W. (2016). Soliton mode-locked erbium-doped fibre laser with mechanically exfoliated molybdenum disulphide saturable absorber. *IET Optoelectronics, 10*(5), 169-173. doi: 10.1049/iet-opt.2015.0097

Ahmed, M. H. M., Latiff, A. A., Arof, H., Ahmad, H., & Harun, S. W. (2016). Soliton mode-locked erbium-doped fibre laser with mechanically exfoliated molybdenum disulphide saturable absorber. *IET Optoelectronics, 10*(5), 169-173. doi: 10.1049/iet-opt.2015.0097

Al-Azzawi, A. A., Almukhtar, A. A., Hamida, B., Das, S., Dhar, A., Paul, M. C., Harun, S. (2019). Wideband and flat gain series erbium doped fiber amplifier using hybrid active fiber with backward pumping distribution technique. *Results in Physics, 13*, 102186. doi: 10.1016/j.rinp.2019.102186

Al-Hayali, S. K. M., Mohammed, D. Z., Khaleel, W. A., & Al-Janabi, A. H. (2017). Aluminum oxide nanoparticles as saturable absorber for C-band passively Q-switched fiber laser. *Applied optics, 56*(16), 4720-4726. doi: 10.1364/AO.56.004720

Al-Hiti, A. S., Al-Masoodi, A. H., Harun, S., Yasin, M., & Wong, W. R. (2020). Tungsten trioxide (WO_3) film absorber for generating soliton mode-locked pulses in erbium laser. *Optics & Laser Technology, 131*, 1-9. doi: 10.1016/j.optlastec.2020.106429

Al-Hiti, A. S., Al-Masoodi, A. H. H., Arof, H., Wong, W. R., & Harun, S. W. (2020). Tungsten tri-oxide (WO_3) film absorber for generating Q-switched pulses in erbium laser. *Journal of Modern Optics, 67*(4), 374-382. doi: 10.1080/09500340.2020.1717660

Al-Hiti, A. S., Al-Masoodi, A. H. H., Wong, W. R., & Harun, S. W. (2020). Generation of passively Q-switched ytterbium laser by using tungsten tri-oxide film absorber. *IET Optoelectronics, 14*(5), 278-284. doi: 10.1049/iet-opt.2019.0153

Al-Hiti, A. S., Al-Masoodi, A. H. H., Wong, W. R., Yasin, M., Al-Masoodi, A. H. H., & Harun, S. W. (2021). Nanosecond passively Q-switched fiber laser in the 1.5 μm region using turmeric saturable absorber. *Optics & Laser Technology, 139*, 106971. doi: 10.1016/j.optlastec.2021.106971

Al-Hiti, A. S., Al-Masoodi, A. H. H., Yasin, M., & Harun, S. W. (2020). Femtosecond mode-locked laser at 1.5 μm region using turmeric-based saturable absorber. *Infrared Physics & Technology, 111*, 103548. doi: 10.1016/j.infrared.2020.103548

Al-Hiti, A. S., Rahman, M. F. A., Harun, S. W., Yupapin, P., & Yasin, M. (2019). Holmium oxide thin film as a saturable absorber for generating Q-switched and mode-locked erbium-doped fiber lasers. *Optical Fiber Technology, 52*, 1-7. doi: 10.1016/j.yofte.2019.101996

Al-Khazrajy, K. K., Al-Ghaban, A. M., & Hussain, M. N. A. (2015). The Effect of Aluminum Concentration on The Phase Evolution of The Ternary Ceramics Of (Ti-Al-C) System. *Engineering and Technology Journal, 33*(4), 973-984. doi: https://etj.uotechnology.edu.iq/article_105325.html

Al-Masoodi, A., Ahmed, M., Latiff, A., Arof, H., & Harun, S. W. (2016). Q-switched ytterbium-doped fiber laser using black phosphorus as saturable absorber. *Chinese Physics Letters, 33*(5), 1-4. doi: 10.1088/0256-307X/33/5/054206

Al-Masoodi, A. H., Ahmad, F., Ahmed, M. H., Al-Masoodi, A. H., Alani, I. A., Arof, H., & Harun, S. W. (2018). Q-switched and mode-locked ytterbium-doped fibre lasers with Sb_2Te_3 topological insulator saturable absorber. *IET Optoelectronics, 12*(4), 180-184. doi: 10.1049/iet-opt.2017.0134

Al-Busafi, S. N., Suliman, F. E. O., & Al-Alawi, Z. R. (2014). 8-hydroxyquinoline and its derivatives: Synthesis and applications. *ChemInform, 45*(49), 1-10.

Ali, Z., Cao, C., Li, J., Wang, Y., Cao, T., Tanveer, M., Butt, F. K. (2013). Effect of synthesis technique on electrochemical performance of bismuth selenide. *Journal of Power Sources, 229*, 216-222. doi: 10.1016/j.jpowsour.2012.11.120

Apandi, N. H. M., Zuikafly, S. N. F., Kasim, N., Mohamed, M. A., Harun, S. W., & Ahmad, F. (2019). Observation of dark and bright pulses in Q-switched erbium doped fiber laser using graphene nano-platelets as saturable absorber. *Bulletin of Electrical Engineering and Informatics, 8*(4), 1358–1365. doi: 10.11591/eei.v8i4.1610

Azooz, S., Ahmed, M., Ahmad, F., Hamida, B., Khan, S., Ahmad, H., & Harun, S. (2015). Passively Q-switched fiber lasers using a multi-walled carbon nanotube polymer composite based saturable absorber. *Optik, 126*(21), 2950-2954. doi: 10.1016/j.ijleo.2015.07.065

Baharom, M., Rahman, M., Latiff, A., Wang, P., Arof, H., & Harun, S. (2019). Lutetium oxide film as a passive saturable absorber for generating Q-switched fiber laser at 1570 nm wavelength. *Optical Fiber Technology, 50*, 82-86.

Baharom, M., Rahman, M., Latiff, A., Wang, P., & Harun, S. (2019). Lutetium (III) oxide film as passive mode locker device for erbium-doped fibre laser cavity. *Optics Communications, 446*, 51-55. doi: 10.1016/j.optcom.2019.04.047

Bao, Q., Zhang, H., Wang, Y., Ni, Z., Yan, Y., Shen, Z. X., Tang, D. Y. (2009). Atomic-layer graphene as a saturable absorber for ultrafast pulsed lasers. *Advanced Functional Materials, 19*(19), 3077-3083. doi: 10.1002/adfm.200901007

Baraker, B. M., & Lobo, B. B. (2018). Thermal and electrical transport properties in films of $CdCl_2$ doped PVA-PVP blend. *Recent Advances in Materials Science and Biophysics*, 381-385.

Barsoum, M. (2000). The $M_{N+1} AX_N$ phases: A new class of solids: Thermodynamically stable nanolaminates. *Progress in Solid State Chemistry, 28*(1-4), 201-281. doi: 10.1016/S0079-6786(00)00006-6

Bollig, C., Clarkson, W., & Hanna, D. (1995). Stable high-repetition-rate single-frequency Q-switched operation by feedback suppression of relaxation oscillation. *Optics Letters, 20*(12), 1383-1385. doi: 10.1364/OL.20.001383

Catella, G. C. (2009). *Q-switching technologies: limitations and opportunities: finding the right Q-switch.* Paper presented at the Optical Technologies for Arming, Safing, Fuzing, and Firing V.

Chang, Y. M., Kim, H., Lee, J. H., & Song, Y.-W. (2010). Multilayered graphene efficiently formed by mechanical exfoliation for nonlinear saturable absorbers in fiber mode-locked lasers. *Applied Physics Letters, 97*(21), 211102. doi: 10.1063/1.3521257

Chen, B., Zhang, X., Guo, C., Wu, K., Chen, J., & Wang, J. (2016). Tungsten diselenide Q-switched erbium-doped fiber laser. *Optical Engineering, 55*(8), 081306.

Chen, B., Zhang, X., Wu, K., Wang, H., Wang, J., & Chen, J. (2015). Q-switched fiber laser based on transition metal dichalcogenides MoS_2, $MoSe_2$, WS_2, and WSe_2. *Optics Express, 23*(20), 26723-26737. doi: 10.1364/OE.23.026723

Chen, H., Chen, S.-P., Jiang, Z.-F., & Hou, J. (2015). Versatile long cavity widely tunable pulsed Yb-doped fiber laser with up to 27655th harmonic mode locking order. *Optics Express, 23*(2), 1308-1318. doi: 10.1364/OE.23.001308

Chen, H., Li, L., Ruan, S., Guo, T., & Yan, P. (2016). Fiber-integrated tungsten disulfide saturable absorber (mirror) for pulsed fiber lasers. *Optical Engineering, 55*(8), 081318. doi: 10.1117/1.OE.55.8.081318

Chen, Y., Jiang, G., Chen, S., Guo, Z., Yu, X., Zhao, C., Tang, D. (2015). Mechanically exfoliated black phosphorus as a new saturable absorber for both Q-switching and mode-locking laser operation. *Optics Express, 23*(10), 12823-12833. doi: 10.1364/OE.23.012823

Chen, Y., Jiang, G., Chen, S., Guo, Z., Yu, X., Zhao, C., Fan, D. (2015). Mechanically exfoliated black phosphorus as a new saturable absorber for both Q-switching and Mode-locking laser operation. *Optics Express, 23*(10), 12823-12833. doi: 10.1364/OE.23.012823

Cheng, C.-H., & Lin, G.-R. (2020). Carbon nanomaterials based saturable absorbers for ultrafast passive mode-locking of fiber lasers. *Current Nanoscience, 16*(3), 441-457. doi: 10.2174/1573413715666191114150100

Cheng, K.-N., Lin, Y.-H., & Lin, G.-R. (2013). Single-and double-walled carbon nanotube based saturable absorbers for passive mode-locking of an erbium-doped fiber laser. *Laser Physics, 23*(4), 045105. doi: 10.1088/1054-660X/23/4/045105

Chernysheva, M., Rozhin, A., Fedotov, Y., Mou, C., Arif, R., Kobtsev, S. M., Turitsyn, S. K. (2017). Carbon nanotubes for ultrafast fibre lasers. *Nanophotonics, 6*(1), 1-30. doi: 10.1515/nanoph-2015-0156

Clark, J., & Lanzani, G. (2010). Organic photonics for communications. *Nature Photonics, 4*(7), 438-446.

Clowes, J. (2008). Next generation light sources for biomedical applications: fibre lasers—compact, cost-effective, turnkey solutions. *Optik & Photonik, 3*(1), 36-38. doi: 10.1002/opph.201190174

Coates, J. (2006). Interpretation of infrared spectra, a practical approach. *Encyclopedia of Analytical Chemistry: applications, theory and instrumentation*.

Cole, B., & Goldberg, L. (2017). *Compact and efficient 2µm Tm: YAP lasers with mechanical or passive Q-switching.* Paper presented at the Solid State Lasers

XXVI: Technology and Devices, SPIE LASE, 2017, San Francisco, California, United States.

Cutruneo, M., Torrisi, L., & Scolaro, C. (2012). *Laser Applications in bio-medical field.* Paper presented at the 2nd Workshop-Plasmi, Sorgenti, Biofisica ed Applicazioni.

Dalton, L. R., Sullivan, P. A., Bale, D. H., & Olbricht, B. C. (2007). Theory-inspired nano-engineering of photonic and electronic materials: Noncentrosymmetric charge-transfer electro-optic materials. *Solid-state Electronics, 51*(10), 1263-1277. doi: 10.1016/j.sse.2007.06.022

Degiorgio, V., & Potenza, G. (1967). Energy losses in a passive Q-switched ruby laser. *IEEE Journal of Quantum Electronics, 3*(2), 59-65. doi: 10.1109/jqe.1967.1074448

Degnan, J. J. (1995). Optimization of passively Q-switched lasers. *IEEE Journal of Quantum Electronics, 31*(11), 1890-1901. doi: 10.1109/3.469267

Desurvire, E. (1994). *Erbium-Doped Fiber Amplifiers: Principles and Applications*: Wiley.

Desurvire, E., & Giles, C. R. (1991). Erbium-doped fiber amplifier: Google Patents.

Dong, Z., Li, H., Xia, H., Liu, Y., Wang, Z., & Chen, Y. (2012). *Passively Q-switched erbium-doped fiber laser using a graphene saturable absorber.* Paper presented at the Asia Communications and Photonics Conference.

Drulis, M. K., Drulis, H., Gupta, S., Barsoum, M., & El-Raghy, T. (2006). On the heat capacities of M_2Al C (M= Ti, V, Cr) ternary carbides. *Journal of Applied Physics, 99*(9), 093502. doi: 10.1063/1.2191744

Drulis, M. K., Drulis, H., Gupta, S., Barsoum, M. W., & El-Raghy, T. (2006). On the heat capacities of M_2AlC (M=Ti,V,Cr) ternary carbides. *Journal of Applied Physics, 99*(9), 093502. doi: 10.1063/1.2191744

Dubey, A. K., & Yadava, V. (2008). Laser beam machining - A review. *International Journal of Machine Tools & Manufacture, 48*(6), 609-628. doi: 10.1016/j.ijmachtools.2007.10.017

Ezema, F. (2005). Chemical bath deposition of bismuth chloride oxide (BiClO) thin film and its applications. *Pacific Journal of Science and Technol, 6*(1), 6-15. doi: http://www.akamaiuniversity.us/PJST.htm

Fei, R., Faghaninia, A., Soklaski, R., Yan, J.-A., Lo, C., & Yang, L. (2014). Enhanced thermoelectric efficiency via orthogonal electrical and thermal conductances in phosphorene. *Nano Letters, 14*(11), 6393-6399. doi: 10.1021/nl502865s

Fermann, M., Galvanauskas, A., Sucha, G., & Harter, D. (1997). Fiber-lasers for ultrafast optics. *Applied Physics B: Lasers & Optics, 65*(2), 259–275. doi: 10.1007/s003400050272

Fermann, M., Hofer, M., Haberl, F., & Craig-Ryan, S. (1990). Femtosecond fibre laser. *Electronics Letters, 26*(20), 1737-1738. doi: 10.1049/el:19901109

Fung, M. K., Ng, A. M. C., Djurišić, A. B., Chan, W. K., & Wang, H. (2012). Preparation of 8-hydroxyquinoline wires by decomposition of tris (8-hydroxyquinoline) aluminium. *Journal of Experimental Nanoscience, 7*(5), 578-585. doi: 10.1080/17458080.2010.543992

Gao, J., Ning, T., Liu, Y., Shang, X., Han, X., Guo, Q., Zhang, H. (2019). Generation of high-energy rectangular pulses in a nonlinear polarization rotation mode-locked ring fiber laser. *Applied Optics, 58*(28), 7897-7903. doi: 10.1364/AO.58.007897

Ge, M., Wang, X., Li, G., Lu, C., Zhang, J., & Tu, R. (2019). Synthesis of Cr_2AlC from elemental powders with modified pressureless spark plasma sintering. *Journal of Wuhan University of Technology-Mater. Sci. Ed., 34*(2), 287-292. doi: 10.1007/s11595-019-2048-4

Ge, Y., Zhu, Z., Xu, Y., Chen, Y., Chen, S., Liang, Z., Xu, S. (2018). Broadband nonlinear photoresponse of 2D TiS_2 for ultrashort pulse generation and all-optical thresholding devices. *Advanced Optical Materials, 6*(4), 1701166. doi: 10.1002/adom.201701166

Giles, C. R., & Desurvire, E. (1991). Modeling erbium-doped fiber amplifiers. *Journal of Lightwave Technology, 9*(2), 271-283. doi: 10.1109/50.65886

Go, T., Sohn, Y. J., Mauer, G., Vaßen, R., & Gonzalez-Julian, J. (2019). Cold spray deposition of Cr_2AlC MAX phase for coatings and bond-coat layers. *Journal of the European Ceramic Society, 39*(4), 860-867. doi: 10.1016/j.jeurceramsoc.2018.11.035

Gonzalez-Julian, J., Onrubia, S., Bram, M., & Guillon, O. (2016). Effect of sintering method on the microstructure of pure Cr_2AlC MAX phase ceramics. *Journal of the Ceramic Society of Japan, 124*(4), 415-420. doi: 10.2109/jcersj2.15263

Gonzalez-Julian, J., Go, T., Mack, D. E., & Vaßen, R. (2018). Environmental resistance of Cr_2AlC MAX phase under thermal gradient loading using a burner rig. *Journal of the American Ceramic Society, 101*(5), 1841-1846. doi: 10.1111/jace.15425

Gorshkov, V., Miloserdov, P., Karpov, A., Shchukin, A., & Sytschev, A. (2019). Investigation of the composition and properties of a Cr_2AlC MAX phase-based material prepared by metallothermic SHS. *Physics of Metals and Metallography, 120*(5), 471-475. doi: 10.1134/S0031918X19050041

Gould, R. G. (1959). *The LASER, light amplification by stimulated emission of radiation.* Paper presented at the The Ann Arbor conference on optical pumping, the University of Michigan.

Grabowski, R. C., Droppo, I. G., & Wharton, G. (2011). Erodibility of cohesive sediment: The importance of sediment properties. *Earth-Science Reviews, 105*(3), 101-120. doi: https://doi.org/10.1016/j.earscirev.2011.01.008

Gu, B., Fan, Y.-X., Wang, J., Chen, J., Ding, J., Wang, H.-T., & Guo, B. (2006). Characterization of saturable absorbers using an open-aperture Gaussian-beam Z scan. *Physical Review A, 73*(6), 065803. doi: 10.1103/PhysRevA.73.065803

Guo, B., Xiao, Q. l., Wang, S. h., & Zhang, H. (2019). 2D layered materials: synthesis, nonlinear optical properties, and device applications. *Laser & Photonics Reviews, 13*(12), 1800327. doi: 10.1002/lpor.201800327

Guoyu, H., Song, Y., Li, K., Dou, Z., Tian, J., & Zhang, X. (2015). Mode-locked ytterbium-doped fiber laser based on tungsten disulphide. *Laser Physics Letters, 12*(12), 125102. doi: 10.1088/1612-2011/12/12/125102

Gurnani, V., Singh, A. K., & Venkataramani, B. (2003). Cellulose functionalized with 8-hydroxyquinoline: new method of synthesis and applications as a solid phase extractant in the determination of metal ions by flame atomic absorption spectrometry. *Analytica Chimica Acta, 485*(2), 221-232. doi: 10.1016/S0003-2670(03)00416-1

Hamdalla, T. A., & Hanafy, T. A. (2016). Optical properties studies for PVA/Gd, La, Er or Y chlorides based on structural modification. *Optik, 127*(2), 878-882. doi: 10.1016/j.ijleo.2015.10.187

Hammadi, Y., Mansour, T., Alani, I., Ahmed, M., Al-Masoodi, A., Jusoh, Z., & Harun, S. (2018). Graphene based soliton mode-locked erbium doped fiber laser for supercontinuum generation. *Digest Journal of Nanomaterials and Biostructures, 13*(3), 777-784.

Han, X., Zhang, H., Jiang, S., Zhang, C., Li, D., Guo, Q., Man, B. (2019). Improved laser damage threshold of In_2Se_3 saturable absorber by PVD for high-power mode-locked er-doped fiber laser. *Nanomaterials, 9*(9), 1216. doi: 10.3390/nano9091216

Haris, H., Harun, S., Yupapin, P., Arof, H., & Apsari, R. (2020). Generation of vector soliton pulses with graphene oxide film in mode-locked erbium-doped fiber laser cavity. *Nonlinear Optics, Quantum Optics: Concepts in Modern Optics, 52*(1/2), 111-118.

Harun, S. W., Ismail, M., Ahmad, F., Ismail, M., Nor, R. M., Zulkepely, N., & Ahmad, H. (2012). A Q-switched erbium-doped fiber laser with a carbon nanotube based saturable absorber. *Chinese Physics Letters, 29*(11), 114202. doi: 10.1088/0256-307X/29/11/114202

Hasan, T., Sun, Z., Wang, F., Bonaccorso, F., Tan, P. H., Rozhin, A. G., & Ferrari, A. C. (2009). Nanotube–polymer composites for ultrafast photonics. *Advanced Materials, 21*(38-39), 3874-3899. doi: 10.1002/adma.200901122

Hasegawa, A., & Tappert, F. (1973). Transmission of stationary nonlinear optical pulses in dispersive dielectric fibers. I. Anomalous dispersion. *Applied Physics Letters, 23*(3), 142-144. doi: 10.1063/1.1654836

Hebboul, Z. (2018). Cadmium iodate syntheses and characterization *Heavy Metals* (pp. 15-32): BoD–Books on Demand.

Heiber, M. C., Wagenpfahl, A., & Deibel, C. (2019). Advances in modeling the physics of disordered organic electronic devices *Handbook of Organic Materials for Electronic and Photonic Devices* (pp. 309-347): Elsevier.

Heo, H., Lee, S., & Kim, S. (2019). Broadband absorption enhancement of monolayer graphene by prism coupling in the visible range. *Carbon, 154*, 42-47. doi: 10.1016/j.carbon.2019.07.089

Hettinger, J., Lofland, S., Finkel, P., Meehan, T., Palma, J., Harrell, K., Barsoum, M. (2005). Electrical transport, thermal transport, and elastic properties of M_2AlC (M= Ti, Cr, Nb, and V). *Physical Review B, 72*(11), 115120. doi: 10.1103/PhysRevB.72.115120

Hofer, M., Fermann, M. E., Haberl, F., & Townsend, J. (1990). Active mode locking of a neodymium-doped fiber laser using intracavity pulse compression. *Optics Letters, 15*(24), 1467-1469. doi: 10.1364/OL.15.001467

Hofer, M., Ober, M., Haberl, F., & Fermann, M. (1992). Characterization of ultrashort pulse formation in passively mode-locked fiber lasers. *IEEE Journal of Quantum Electronics, 28*(3), 720-728. doi: 10.1109/3.124997

Huang, X., Yin, Z., Wu, S., Qi, X., He, Q., Zhang, Q., Zhang, H. (2011). Graphene-based materials: synthesis, characterization, properties, and applications. *Small, 7*(14), 1876-1902. doi: 10.1002/smll.201002009

Ismail, E., Kadir, N., Latiff, A., Ahmad, H., & Harun, S. (2016). Black phosphorus crystal as a saturable absorber for both a Q-switched and mode-locked erbium-doped fiber laser. *RSC Advances, 6*(76), 72692-72697. doi: 10.1039/C6RA14008D

Ismail, M. A., Harun, S. W., Ahmad, H., & Paul, M. C. (2016). *Passive Q-switched and Mode-locked Fiber Lasers Using Carbon-based Saturable Absorbers*: IntechOpen.

Isyanto, H., & Chamdareno, P. G. (2017). *The comparison of organic field effect transistor (OFET) structures.* Paper presented at the 2017 2nd International Conference on Frontiers of Sensors Technologies (ICFST).

Jafry, A. A. A., Kasim, N., Nizamani, B., Muhammad, A. R., Harun, S. W., & Yupapin, P. (2020). MAX phase Ti_3AlC_2 embedded in PVA and deposited onto D-shaped fiber as a passive Q-switcher for erbium-doped fiber laser. *Optik, 224*, 165682. doi: 10.1016/j.ijleo.2020.165682

Jafry, A. A. A., Kasim, N., Rusdi, M. F. M., Rosol, A. H. A., Yusoff, R. A. M., Muhammad, A. R., Harun, S. W. (2020). MAX phase based saturable absorber for mode-locked erbium-doped fiber laser. *Optics & Laser Technology, 127*, 106186. doi: 10.1016/j.optlastec.2020.106186

Jafry, A. A. A., Muhammad, A. R., Kasim, N., Rosol, A. H. A., Rusdi, M. F. M., Ab Alim, N. N. N., Yupapin, P. (2021). Ultrashort pulse generation with MXene Ti3C2Tx embedded in PVA and deposited onto D-shaped fiber. *Optics & Laser Technology, 136*, 106780. doi: 10.1016/j.optlastec.2020.106780

Ji, D., Li, T., & Fuchs, H. (2020). Patterning and applications of nanoporous structures in organic electronics. *Nano Today, 31*, 100843. doi: 10.1016/j.nantod.2020.100843

Jiang, M., Ma, H., Ren, Z., Chen, X., Long, J., Qi, M., Bai, J. (2013). A graphene Q-switched nanosecond Tm-doped fiber laser at 2 μm. *Laser Physics Letters, 10*(5), 055103. doi: 10.1088/1612-2011/10/5/055103

Jiang, T., Yin, K., Wang, C., You, J., Ouyang, H., Miao, R., Chen, H. (2020). Ultrafast fiber lasers mode-locked by two-dimensional materials: review and prospect. *Photonics Research, 8*(1), 78-90. doi: 10.1364/PRJ.8.000078

Jomaa, I., Noureddine, O., Gatfaoui, S., Issaoui, N., Roisnel, T., & Marouani, H. (2020). Experimental, computational, and in silico analysis of $(C_8H_{14}N_2)_2[CdCl_6]$ compound. *Journal of Molecular Structure, 1213*, 128186. doi: 10.1016/j.molstruc.2020.128186

Jung, M., Koo, J., Chang, Y., Debnath, P., Song, Y., & Lee, J. (2012). An all fiberized, 1.89-μm Q-switched laser employing carbon nanotube evanescent field interaction. *Laser Physics Letters, 9*(9), 669.

Kang, X., Wang, J., Wu, H., Liu, J., Aksay, I. A., & Lin, Y. (2010). A graphene-based electrochemical sensor for sensitive detection of paracetamol. *Talanta, 81*(3), 754-759. doi: 10.1016/j.talanta.2010.01.009

Kataura, H., Kumazawa, Y., Maniwa, Y., Umezu, I., Suzuki, S., Ohtsuka, Y., & Achiba, Y. J. S. m. (1999). Optical properties of single-wall carbon nanotubes. *Synthetic Metals, 103*(1-3), 2555-2558. doi: 10.1016/S0379-6779(98)00278-1

Keller, U. (2003). Recent developments in compact ultrafast lasers. *Nature, 424*(6950), 831-838. doi: 10.1038/nature01938

Keller, U., Miller, D., Boyd, G., Chiu, T., Ferguson, J., & Asom, M. J. O. l. (1992). Solid-state low-loss intracavity saturable absorber for Nd: YLF lasers: an antiresonant semiconductor Fabry–Perot saturable absorber. *Optics Letters, 17*(7), 505-507. doi: 10.1364/OL.17.000505

Keller, U., Weingarten, K. J., Kartner, F. X., Kopf, D., Braun, B., Jung, I. D., Der Au, J. A. (1996). Semiconductor saturable absorber mirrors (SESAM's) for femtosecond to nanosecond pulse generation in solid-state lasers. *IEEE Journal of Selected Topics in Quantum Electronics, 2*(3), 435-453. doi: 10.1109/2944.571743

Kindeel, A. S., Dawood, I. J., & Aziz, M. R. (2013). Synthesis and characterization of some mixed ligand complexes containing (8-hydroxyquinoline) and (2-picoline) with some metal ions. *Baghdad Science Journal, 10*(2), 396-404. doi: 10.21123/bsj.2013.10.2.396-404

Kwon, S., Lee, J., & Lee, J. H. (2021). A Q-switched fiber laser using a Ti_2AlN-based saturable absorber. *Laser Physics, 31*(2), 025103. doi: 10.1088/1555-6611/abd938

Latiff, A., Kadir, N., Ismail, E., Shamsuddin, H., Ahmad, H., & Harun, S. (2017). All-fiber dual-wavelength Q-switched and mode-locked EDFL by SMF-THDF-SMF structure as a saturable absorber. *Optics Communications, 389*, 29-34. doi: 10.1016/j.optcom.2016.12.011

Lau, K., Ker, P. J., Abas, A., Alresheedi, M., & Mahdi, M. (2019). Long-term stability and sustainability evaluation for mode-locked fiber laser with graphene/PMMA saturable absorbers. *Optics Communications, 435*, 251-254. doi: 10.1016/j.optcom.2018.11.051

Lau, K., Muhammad, F., Latif, A., Bakar, M. A., Yusoff, Z., & Mahdi, M. (2017). Passively mode-locked soliton femtosecond pulses employing graphene saturable absorber. *Optics & Laser Technology, 94*, 221-227. doi: 10.1016/j.optlastec.2017.03.035

Lee, D., Nguyen, T. D., Han, J., & Park, S. (2007). Oxidation of Cr_2AlC at 1300 C in air. *Corrosion Science, 49*(10), 3926-3934. doi: 10.1016/j.corsci.2007.03.044

Lee, J., Jung, M., Koo, J., Chi, C., & Lee, J. H. (2014). Passively Q-Switched 1.89-μm fiber laser using a bulk-structured Bi_2Te_3 topological insulator. *IEEE Journal of Selected Topics in Quantum Electronics, 21*(1), 31-36. doi: 10.1109/JSTQE.2014.2329934

Lee, J., Kwon, S., & Lee, J. H. (2019). Ti_2AlC-based saturable absorber for passive Q-switching of a fiber laser. *Optical Materials Express, 9*(5), 2057-2066. doi: 10.1364/OME.9.002057

Lei, K., Li, F., Mu, C., Wang, J., Zhao, Q., Chen, C., & Chen, J. (2017). High K-storage performance based on the synergy of dipotassium terephthalate and ether-based electrolytes. *Energy & Environmental Science, 10*(2), 552-557. doi: 10.1039/C6EE03185D

Li, D., Castillo, A. E. D. R., Jussila, H., Ye, G., Ren, Z., Bai, J., Bonaccorso, F. (2016). Black phosphorus polycarbonate polymer composite for pulsed fibre lasers. *Applied Materials Today, 4*, 17-23. doi: 10.1016/J.APMT.2016.05.001

Li, D., Zhao, S., Li, G., & Yang, K. (2005). Optimization of passively Q-switched lasers by taking into account intracavity laser spatial distribution. *Optical and Quantum Electronics, 37*(10), 927-942. doi: 10.1007/S11082-005-2113-4

Li, H., Huang, Z., Xie, Y., Chen, X., Wang, J., Zhang, L., & Zhang, C. (2019). Ultrafast nonlinear optical response of molybdenum nano-film in wide wavelength range. *Optical Materials, 95*, 109244. doi: 10.1016/j.optmat.2019.109244

Li, L., Pang, L., Wang, Y., & Liu, W. (2021). W x Nb (1− x) Se 2 nanosheets for ultrafast photonics. *Nanoscale, 13*(4), 2511-2518.

Li, L., Pang, L., Zhao, Q., Wang, Y., & Liu, W. (2020). Niobium disulfide as a new saturable absorber for an ultrafast fiber laser. *Nanoscale, 12*(7), 4537-4543. doi: 10.1039/C9NR10873D

Li, S., Yu, W., Zhai, H., Song, G., Sloof, W., & Van der Zwaag, S. (2011). Mechanical properties of low temperature synthesized dense and fine-grained Cr_2AlC ceramics. *Journal of the European Ceramic Society, 31*(1-2), 217-224. doi: 10.1016/j.jeurceramsoc.2010.08.014

Li, X., Wang, Y., Wang, Y., Zhao, W., Yu, X., Sun, Z., Wang, Q. J. (2014). Nonlinear absorption of SWNT film and its effects to the operation state of pulsed fiber laser. *Optics Express, 22*(14), 17227-17235. doi: 10.1364/OE.22.017227

Li, Z., Pang, C., Li, R., & Chen, F. (2020). Low-dimensional materials as saturable absorbers for pulsed waveguide lasers. *Journal of Physics: Photonics, 2*(3), 031001. doi: 10.1088/2515-7647/ab8a5a

Liu, G., Lyu, Y., Li, Z., Wu, T., Yuan, J., Yue, X., Fu, S. (2020). Q-switched erbium-doped fiber laser based on silicon nanosheets as saturable absorber. *Optik, 202*, 163692. doi: 10.1016/j.ijleo.2019.163692

Liu, H. H., Chow, K. K., Yamashita, S., & Set, S. Y. (2013). Carbon-nanotube-based passively Q-switched fiber laser for high energy pulse generation. *Optics & Laser Technology, 45*, 713-716. doi: https://doi.org/10.1016/j.optlastec.2012.05.005

Liu, J., Zuo, X., Wang, Z., Wang, L., Wu, X., Ke, P., & Wang, A. (2018). Fabrication and mechanical properties of high purity of Cr_2AlC coatings by adjustable Al contents. *Journal of Alloys and Compounds, 753*, 11-17. doi: 10.1016/j.jallcom.2018.04.100

Liu, M., Ouyang, Y., Hou, H., Liu, W., & Wei, Z. (2019). Q-switched fiber laser operating at 1.5 μm based on WTe 2. *Chinese Optics Letters, 17*(2), 020006.

Liu, W., Liu, M., OuYang, Y., Hou, H., Lei, M., & Wei, Z. (2018). CVD-grown $MoSe_2$ with high modulation depth for ultrafast mode-locked erbium-doped fiber laser. *Nanotechnology, 29*(39), 394002. doi: 10.1088/1361-6528/aad0b3

Liu, W., Zhu, H.-l., & Duan, Y. (2020). Effective chemicals against novel coronavirus (COVID-19) in china. *Current Topics in Medicinal Chemistry, 20*(8), 603-605. doi: 10.2174/1568026620999200305145032

Liu, X., Guo, Q., & Qiu, J. (2017). Emerging low-dimensional materials for nonlinear optics and ultrafast photonics. *Advanced Materials, 29*(14), 1605886. doi: 10.1002/adma.201605886

Luo, Z., Wu, D., Xu, B., Xu, H., Cai, Z., Peng, J., Wang, F. (2016). Two-dimensional material-based saturable absorbers: towards compact visible-wavelength all-fiber pulsed lasers. *Nanoscale, 8*(2), 1066-1072. doi: 10.1039/C5NR06981E

Luo, Z., Zhou, M., Weng, J., Huang, G., Xu, H., Ye, C., & Cai, Z. (2010). Graphene-based passively Q-switched dual-wavelength erbium-doped fiber laser. *Optics Letters, 35*(21), 3709-3711.

Ma, C., Wang, C., Gao, B., Adams, J., Wu, G., & Zhang, H. (2019). Recent progress in ultrafast lasers based on 2D materials as a saturable absorber. *Applied Physics Reviews, 6*(4), 041304. doi: 10.1063/1.5099188

Ma, Z., Yang, L., Liu, L., Wang, S., & Peng, L.-M. (2020). Silicon-waveguide-integrated carbon nanotube optoelectronic system on a single chip. *ACS Nano, 14*(6), 7191–7199. doi: 10.1021/acsnano.0c02139

Mak, K. F., Lee, C., Hone, J., Shan, J., & Heinz, T. F. (2010). Atomically thin MoS_2: a new direct-gap semiconductor. *Physical Review Letters, 105*(13), 136805. doi: 10.1103/PhysRevLett.105.136805

Malic, E., & Knorr, A. (2013). *Graphene and carbon nanotubes: ultrafast optics and relaxation dynamics*: John Wiley & Sons.

Mao, D., Cui, X., Gan, X., Li, M., Zhang, W., Lu, H., & Zhao, J. (2017). Passively Q-switched and mode-locked fiber laser based on an ReS2 saturable absorber. *IEEE*

Journal of Selected Topics in Quantum Electronics, 24(3), 1-6. doi: 10.1109/JSTQE.2017.2713641

Mao, D., Li, M., Cui, X., Zhang, W., Lu, H., Song, K., & Zhao, J. (2018). Stable high-power saturable absorber based on polymer-black-phosphorus films. *Optics Communications, 406*, 254-259. doi: 10.1016/j.optcom.2016.11.027

Mao, D., Zhang, S., Wang, Y., Gan, X., Zhang, W., Mei, T., Zhao, J. (2015). WS_2 saturable absorber for dissipative soliton mode locking at 1.06 and 1.55 μm. *Optics Express, 23*(21), 27509-27519. doi: 10.1364/OE.23.027509

Margulis, V. A., & Sizikova, T. (1998). Theoretical study of third-order nonlinear optical response of semiconductor carbon nanotubes. *Physica B: Condensed Matter, 245*(2), 173-189. doi: 10.1016/S0921-4526(97)00676-5

Markom, A. M., Sen-Winson, M. W., Paul, M. C., & Harun, S. W. (2017). *Ultrafast soliton mode-locked Zirconia-based Erbium-doped fiber laser with carbon nanotubes saturable absorber.* Paper presented at the IOP Conference Series: Materials Science and Engineering.

Mary, R., Choudhury, D., & Kar, A. K. (2014). Applications of fiber lasers for the development of compact photonic devices. *IEEE Journal of Selected Topics in Quantum Electronics, 20*(5), 72-84. doi: 10.1109/JSTQE.2014.2301136

Matsas, V., Newson, T., Richardson, D., & Payne, D. N. (1992). Self-starting, passively mode-locked fibre ring soliton laser exploiting non-linear polarisation rotation. *Electronics Letters, 28*(15), 1391-1393. doi: 10.1049/el:19920885

Mayer, B., Regler, A., Sterzl, S., Stettner, T., Koblmüller, G., Kaniber, M., Finley, J. (2017). Long-term mutual phase locking of picosecond pulse pairs generated by a semiconductor nanowire laser. *Nature Communications, 8*(1), 1-6. doi: 10.1038/ncomms15521

Mears, R. J., Reekie, L., Jauncey, I., & Payne, D. N. (1987). Low-noise erbium-doped fibre amplifier operating at 1.54 μm. *Electronics Letters, 23*(19), 1026-1028. doi: 10.1049/el:19870719

Meftah, S., Benhaliliba, M., Kaleli, M., Benouis, C., Yavru, C., & Bayram, A. (2020). Optical and electrical characterization of thin film MSP heterojunction based on organic material Al/p-Si/P3HT/Ag. *Physica B: Condensed Matter, 593*, 412238. doi: 10.1016/j.physb.2020.412238

Mocker, H. W., & Collins, R. J. A. P. L. (1965). Mode competition and self-locking effects in a Q-switched ruby laser. *Applied Physics Letters, 7*(10), 270-273. doi: 10.1063/1.1754253

Mohammed, D., & Al-Janabi, A. (2016). Passively Q-switched erbium doped fiber laser based on double walled carbon nanotubes-polyvinyl alcohol saturable absorber. *Laser Physics, 26*(11), 115108. doi: 10.1088/1054-660X/26/11/115108

Mollenauer, L. F., Stolen, R. H., & Gordon, J. P. (1980). Experimental observation of picosecond pulse narrowing and solitons in optical fibers. *Physical Review Letters, 45*(13), 1095. doi: 10.1103/PhysRevLett.45.1095

Nady, A., Ahmed, M. H. M., Latiff, A. A., Ooi, C. R., & Harun, S. W. (2017). Femtoseconds soliton mode-locked erbium-doped fiber laser based on nickel oxide nanoparticle saturable absorber. *Chinese Optics Letters, 15*(10), 100602. doi: 10.3788/COL201715.100602

Nady, A., Baharom, M. F., Latiff, A. A., & Harun, S. W. (2018). Mode-locked erbium-doped fiber laser using vanadium oxide as saturable absorber. *Chinese Physics Letters, 35*(4), 044204. doi: 10.1088/0256-307X/35/4/044204

Nady, A., Mathkoor, F., & Harun, S. W. (2019). Theoretical Study on Passively Mode-Locked Fiber Lasers with Saturable Absorber. *Fiber and Integrated Optics, 38*(1), 76-89. doi: 10.1080/01468030.2018.1527417

Nandiyanto, A. B. D., Oktiani, R., & Ragadhita, R. (2019). How to read and interpret FTIR spectroscope of organic material. *Indonesian Journal of Science and Technology, 4*(1), 97-118. doi: 10.17509/ijost.v4i1.15806

Ngo, N. Q. (2010). *Ultra-fast fiber lasers: principles and applications with MATLAB® models*: CRC Press.

Nishizawa, N. (2014). Ultrashort pulse fiber lasers and their applications. *Japanese Journal of Applied Physics, 53*(9), 090101. doi: 10.7567/JJAP.53.090101

Niu, K., Sun, R., Chen, Q., Man, B., & Zhang, H. (2018). Passively mode-locked Er-doped fiber laser based on SnS 2 nanosheets as a saturable absorber. *Photonics Research, 6*(2), 72-76. doi: 10.1364/PRJ.6.000072

Nizamani, B., Khudus, M. A., Salam, S., Najm, M. M., Jafry, A., Hanafi, E., Harun, S. (2021). Q-switched and mode-locked laser based on aluminium zinc oxide deposited onto D-shape fiber as a saturable absorber. *Results in Optics*, 100057. doi: 10.1016/j.rio.2021.100057

O'Mahony, M. J., Simeonidou, D., Hunter, D. K., & Tzanakaki, A. (2001). The application of optical packet switching in future communication networks. *IEEE Communications Magazine, 39*(3), 128-135. doi: 10.1109/35.910600

Okhotnikov, O., Grudinin, A., & Pessa, M. (2004). Ultra-fast fibre laser systems based on SESAM technology: new horizons and applications. *New journal of physics, 6*(1), 177. doi: 10.1088/1367-2630/6/1/177

Pan, H., Chu, H., Pan, Z., Zhao, S., Yang, M., Chai, J., Li, D. (2020). Large-scale monolayer molybdenum disulfide (MoS2) for mid-infrared photonics. *Nanophotonics, 9*(16), 4703-4710. doi: 10.1515/nanoph-2020-0331

Pan, H., Lin, H., Shen, Q., & Zhu, J. J. (2008). Cadmium (II)(8-Hydroxyquinoline) Chloride Nanowires: Synthesis, Characterization and Glucose-Sensing Application. *Advanced Functional Materials, 18*(22), 3692-3698. doi: 10.1002/adfm.200800492

Park, M., Kim, H. J., Jeong, I., Lee, J., Lee, H., Son, H. J., Ko, M. J. (2015). Mechanically recoverable and highly efficient perovskite solar cells: investigation of intrinsic flexibility of organic–inorganic perovskite. *Advanced Energy Materials, 5*(22), 1501406. doi: 10.1002/aenm.201501406

Pile, D. (2013). Fibre laser directions. *Nature Photonics, 7*(11), 846-847. doi: 10.1038/nphoton.2013.306

Pirzio, F., Negri, J. R., Pizzurro, S., Piccinini, E., & Agnesi, A. (2020). Assessment of broad usability of a simple analytic model for passively Q-switched lasers with Cr: YAG saturable absorbers. *Journal of the Optical Society of America B, 37*(6), 1659-1663. doi: 10.1364/JOSAB.392097

Prakash, N., Manjunath, A., & Somashekar, R. (2013). Studies on AC electrical conductivity of $CdCl_2$ doped PVA polymer electrolyte. *Advances in Condensed Matter Physics, 2013*, 690629 doi: 10.1155/2013/690629

Prakash, N., Manjunath, A., & Somashekar, R. (2013). Studies on AC electrical conductivity of CdCl2 doped PVA polymer electrolyte. *Advances in Condensed Matter Physics, 2013*.

Prasad, V., Semwogerere, D., & Weeks, E. R. (2007). Confocal microscopy of colloids. *Journal of Physics: Condensed Matter, 19*(11), 113102. doi: 10.1088/0953-8984/19/11/113102

Puniredd, S., Pisula, W., & en, K. (2013). Influence of film morphology on optical and electronic properties of organic materials *Woodhead Publishing Limited* (Vol. 39, pp. 83-101): Materials Science.

Qin, Z., Xie, G., Zhang, H., Zhao, C., Yuan, P., Wen, S., & Qian, L. (2015). Black phosphorus as saturable absorber for the Q-switched Er: ZBLAN fiber laser at 2.8 μm. *Optics Express, 23*(19), 24713-24718. doi: 10.1364/OE.23.024713

Quimby, R. S. (2006). *Photonics and lasers: an introduction*: John Wiley & Sons.

R. Rosdin, A. A. A. Jafry, & S. W. Harun. (2019). Nanosecond pulsed laser generation with bismuth (III) tellurite saturable absorber. *Chalcogenide Letters,, 16*(5), 209-214.

Rahman, M., Rusdi, M., Latiff, A., Hisyam, M., Dimyati, K., & Harun, S. (2019). *Passively Q-switched Erbium doped fiber laser by incorporating a segment of Thulium doped fiber saturable absorber.* Paper presented at the Journal of Physics: Conference Series.

Razak, N. N., Latiff, A. A., Zakaria, Z., & Harun, S. W. (2017). Q-switched erbium-doped fiber laser with a black phosphorus saturable absorber. *Photonics Letters of Poland, 9*(2), 72-74. doi: 10.4302/plp.v9i2.737

Razak, N. N., Yasin, M., Zakaria, Z., Latiff, A. A., & Harun, S. W. (2017). Q-switched fiber laser with tungsten disulfide saturable absorber prepared by drop casting method. *Photonics Letters of Poland, 9*(3), 103-105. doi: 10.4302/plp.v9i3.752

Reich, S., Thomsen, C., & Maultzsch, J. (2008). *Carbon nanotubes: basic concepts and physical properties*: John Wiley & Sons.

Ren, Q., Xu, Q., Xia, H., Luo, X., Zhao, F., Sun, L., Peng, Y. (2017). High performance photoresponsive field-effect transistors based on MoS_2/pentacene heterojunction. *Organic Electronics, 51*, 142-148. doi: 10.1016/j.orgel.2017.07.022

Ren, Y., Feng, M., Ren, A., Zhang, K., Yang, J., Sun, G., Liu, Z. (2019). Dynamics of the passive synchronisation of erbium-and ytterbium-doped fibre Q-switched lasers with a common graphene saturable absorber. *Laser Physics, 29*(8), 085101. doi: 10.1088/1555-6611/ab23ec

Saglamyurek, E., Jin, J., Verma, V. B., Shaw, M. D., Marsili, F., Nam, S. W., Tittel, W. (2015). Quantum storage of entangled telecom-wavelength photons in an erbium-doped optical fibre. *Nature Photonics, 9*(2), 83-87. doi: 10.1038/nphoton.2014.311

Salam, S., Al-Masoodi, A., Al-Hiti, A. S., Al-Masoodi, A. H., Wang, P., Wong, W. R., & Harun, S. (2019). FIrpic thin film as saturable absorber for passively Q-switched and mode-locked erbium-doped fiber laser. *Optical Fiber Technology, 50*, 256-262. doi: 10.1016/j.yofte.2019.04.005

Salam, S., Al-Masoodi, A. H. H., Yasin, M., & Harun, S. W. (2020). Soliton mode-locked Er-doped fiber laser by using Alq3 saturable absorber. *Optics & Laser Technology, 123*, 105893. doi: 10.1016/j.optlastec.2019.105893

Salam, S., Harun, S. W., Al-Masoodi, A. H., Ahmed, M. H., Al-Masoodi, A. H., Alani, I. A., Yasin, M. (2019). Tris-(8-hydroxyquinoline) aluminium thin film as saturable absorber for passively Q-switched erbium-doped fibre laser. *IET Optoelectronics, 13*(5), 247-253. doi: 10.1049/iet-opt.2018.5149

Salam, S., Sulaiman, S., Al-Masoodi, A., Al-Azzawi, A. A., & Harun, S. (2019). Q-switched ytterbium-doped fiber laser by using FIrpic as a saturable absorber. *OSA Continuum, 2*(7), 2145-2152. doi: 10.1364/OSAC.2.002145

Salam, S., Wong, W. R., Al-Masoodi, A., & Harun, S. W. (2019). High-energy Q-switched ytterbium-doped all-fiber laser with tris-(8-hydroxyquinoline) aluminum as saturable absorber. *Optical Materials Express, 9*(8), 3215-3225.

Salam, S., Wong, W. R., Al-Masoodi, A. H. H., & Harun, S. W. (2019). High-energy Q-switched ytterbium-doped all-fiber laser with tris-(8-hydroxyquinoline) aluminum as saturable absorber. *Optical Materials Express, 9*(8), 3215. doi: 10.1364/ome.9.003215

Salyulev, A. B., & Potapov, A. M. (2016). Electrical Conductivity of Molten $CdCl_2$ at Temperatures as High as 1474 K. *Zeitschrift für Naturforschung A, 71*(7), 673-675. doi: 10.1515/zna-2016-0075

Samsamnun, F., & Zulkipli, N. (2020). Poly (3-hexylthiophene-2, 5-diyl) regioregular (P_3HT) thin film as saturable absorber for passively Q-switched and mode-locked erbium-doped fiber laser. *Optical Fiber Technology, 54*, 102073. doi: 10.1016/j.yofte.2019.102073

Samsamnun, F. S. M., Zulkipli, N. F., Khudus, M., Bakar, A. S. A., Majid, W. H. A., & Harun, S. W. (2019). Nanosecond pulse generation with a gallium nitride saturable absorber. *OSA Continuum, 2*(1), 134-141. doi: 10.1364/OSAC.2.000134

Samsamnun, F. S. M., Zulkipli, N. F., Majid, W., Khudus, M., Shuhaimi, A., Rosol, A. H. A., Harun, S. W. (2020). MEH-PPV organic material as saturable absorber for Q-switching and mode-locking applications. *Journal of Modern Optics, 67*(8), 746-753. doi: 10.1080/09500340.2020.1769762

Samsamnun, F. S. M., Zulkipli, N. F., Sarjidan, M. A. M., Harun, S. W., Majid, W., Khudus, M., Jafry, A. A. A. J. O. F. T. (2020). Poly (3-hexylthiophene-2, 5-diyl) regioregular (P_3HT) thin film as saturable absorber for passively Q-switched and mode-locked erbium-doped fiber laser. *Optical Fiber Technology, 54*, 102073. doi: 10.1016/j.yofte.2019.102073

Scardaci, V., Rozhin, A., Tan, P., Wang, F., White, I., Milne, W., & Ferrari, A. (2007). Carbon nanotubes for ultrafast photonics. *Physica Status Solidi (b), 244*(11), 4303-4307. doi: 10.1002/pssb.200776194

Schneider, J. M., Sun, Z., Mertens, R., Uestel, F., & Ahuja, R. (2004). Ab initio calculations and experimental determination of the structure of Cr_2AlC. *Solid State Communications, 130*(7), 445-449. doi: 10.1016/j.ssc.2004.02.047

Sennaroglu, A. (2017). *Solid-state lasers and applications*: CRC press.

Set, S. Y., Yaguchi, H., Tanaka, Y., & Jablonski, M. (2004). Ultrafast fiber pulsed lasers incorporating carbon nanotubes. *IEEE Journal of Selected Topics in Quantum Electronics, 10*(1), 137-146. doi: 10.1109/JSTQE.2003.822912

Shabat, A., & Zakharov, V. (1972). Exact theory of two-dimensional self-focusing and one-dimensional self-modulation of waves in nonlinear media. *Soviet Journal of Experimental and Theoretical Physics, 34*(1), 62.

Shahedi, Z., Jafari, M. R., & Zolanvari, A. A. (2017). Synthesis of ZnQ_2, CaQ_2, and CdQ_2 for application in OLED: optical, thermal, and electrical characterizations. *Journal of Materials Science: Materials in Electronics, 28*(10), 7313-7319. doi: 10.1007/s10854-017-6417-5

Sheberla, D., Sun, L., Blood-Forsythe, M. A., Er, S. l., Wade, C. R., Brozek, C. K., Dinc , M. (2014). High electrical conductivity in Ni3 (2, 3, 6, 7, 10, 11-hexaiminotriphenylene) 2, a semiconducting metal–organic graphene analogue. *Journal of the American Chemical Society, 136*(25), 8859-8862. doi: 10.1021/ja502765n

Shi, W., Fang, Q., Zhu, X., Norwood, R. A., & Peyghambarian, N. (2014). Fiber lasers and their applications. *Applied Optics, 53*(28), 6554-6568. doi: 10.1364/AO.53.006554

Shukla, N., Liu, C., Jones, P. M., & Weller, D. (2003). FTIR study of surfactant bonding to FePt nanoparticles. *Journal of Magnetism and Magnetic materials, 266*(1-2), 178-184.

Siegman, A. E. (1986). Lasers university science books. *Mill Valley, CA, 37*(208), 169.

Snitzer, E. (1966). Glass lasers. *Proceedings of the IEEE, 54*(10), 1249-1261. doi: 10.1109/PROC.1969.7231

Soboh, R. S., Al-Masoodi, A. H. H., Erman, F. N., Al-Masoodi, A. H., Arof, H., Yasin, M., & Harun, S. W. (2020). Zinc phthalocyanine thin film as saturable absorber for Q-switched pulse generation. *Optical Fiber Technology, 57*, 102235. doi: 10.1016/j.yofte.2020.102235

Sokol, M., Yang, J., Keshavan, H., & Barsoum, M. W. (2019). Bonding and oxidation protection of Ti_2AlC and Cr_2AlC for a Ni-based superalloy. *Journal of the European Ceramic Society, 39*(4), 878-882. doi: 10.1016/j.jeurceramsoc.2018.10.019

Solodyankin, M. A., Obraztsova, E. D., Lobach, A. S., Chernov, A. I., Tausenev, A. V., Konov, V. I., & Dianov, E. M. (2008). Mode-locked 1.93 μm thulium fiber laser with a carbon nanotube absorber. *Optics Letters, 33*(12), 1336-1338. doi: 10.1364/OL.33.001336

Sotor, J., Sobon, G., Kowalczyk, M., Macherzynski, W., Paletko, P., & Abramski, K. M. (2015). Ultrafast thulium-doped fiber laser mode locked with black phosphorus. *Optics Letters, 40*(16), 3885-3888. doi: 10.1364/OL.40.003885

Sotor, J., Sobon, G., Macherzynski, W., Paletko, P., Grodecki, K., & Abramski, K. M. (2014). Mode-locking in Er-doped fiber laser based on mechanically exfoliated Sb_2Te_3 saturable absorber. *Optical Materials Express, 4*(1), 1-6. doi: 10.1364/OME.4.000001

Spalatu, N., Krunks, M., & Hiie, J. (2017). Structural and optoelectronic properties of $CdCl_2$ activated CdTe thin films modified by multiple thermal annealing. *Thin Solid Films, 633*, 106-111. doi: 10.1016/j.tsf.2016.09.042

Spühler, G., Paschotta, R., Fluck, R., Braun, B., Moser, M., Zhang, G., Keller, U. (1999). Experimentally confirmed design guidelines for passively Q-switched microchip lasers using semiconductor saturable absorbers. *Journal of the Optical Society of America B, 16*(3), 376-388. doi: 10.1364/JOSAB.16.000376

Stetser, D., & DeMaria, A. (1966). Optical spectra of ultrashort optical pulses generated by mode-locked glass: Nd lasers. *Applied Physics Letters, 9*(3), 118-120. doi: 10.1063/1.1754670

Su, X., Wang, Y., Zhang, B., Zhao, R., Yang, K., He, J., Tao, X. (2016). Femtosecond solid-state laser based on a few-layered black phosphorus saturable absorber. *Optics Letters, 41*(9), 1945-1948. doi: 10.1364/OL.41.001945

Sun, B., Zhu, C.-H., Liu, Y., Wang, C., Wan, L.-J., & Wang, D. (2017). Oriented covalent organic framework film on graphene for robust ambipolar vertical organic field-effect transistor. *Chemistry of Materials, 29*(10), 4367-4374. doi: 10.1021/acs.chemmater.7b00800

Sun, G., Zhou, J., Yu, F., Zhang, Y., Pang, J. H. L., & Zheng, L. (2012). Electrochemical capacitive properties of CNT fibers spun from vertically aligned CNT arrays. *Journal of Solid State Electrochemistry, 16*(5), 1775-1780. doi: 10.1007/s10008-011-1606-2

Ta, Q. T. H., Tran, N. M., & Noh, J.-S. (2021). Pressureless manufacturing of Cr_2AlC compound and the temperature effect. *Materials and Manufacturing Processes, 36*(2), 200-208. doi: 10.1080/10426914.2020.1819547

Tallman, D. J., Anasori, B., & Barsoum, M. W. (2013). A critical review of the oxidation of Ti_2AlC, Ti_3AlC_2 and Cr_2AlC in air. *Materials Research Letters, 1*(3), 115-125. doi: 10.1080/21663831.2013.806364

Tang, D., Zhang, H., Zhao, L., & Wu, X. (2008). Observation of high-order polarization-locked vector solitons in a fiber laser. *Physical Review Letters, 101*(15), 153904. doi: 10.1103/PhysRevLett.101.153904

Tian, W.-B., Wang, P.-L., Kan, Y.-M., Zhang, G.-J., Li, Y.-X., & Yan, D.-S. (2007). Phase formation sequence of Cr_2AlC ceramics starting from Cr–Al–C powders. *Materials Science and Engineering: A, 443*(1-2), 229-234. doi: 10.1016/j.msea.2006.08.064

Tian, W., Wang, P., Zhang, G., Kan, Y., Li, Y., & Yan, D. (2006). Synthesis and thermal and electrical properties of bulk Cr_2AlC. *Scripta Materialia, 54*(5), 841-846. doi: 10.1016/j.scriptamat.2005.11.009

Tian, W. b., Wang, P. l., Zhang, G. j., Kan, Y. m., & Li, Y. x. (2007). Mechanical properties of Cr_2AlC ceramics. *Journal of the American Ceramic Society, 90*(5), 1663-1666. doi: 10.1111/j.1551-2916.2007.01634.x

Voiry, D., Salehi, M., Silva, R., Fujita, T., Chen, M., Asefa, T., Chhowalla, M. (2013). Conducting MoS_2 nanosheets as catalysts for hydrogen evolution reaction. *Nano Letters, 13*(12), 6222-6227. doi: 10.1021/nl403661s

Walmsley, I., Waxer, L., & Dorrer, C. (2001). The role of dispersion in ultrafast optics. *Review of Scientific Instruments, 72*(1), 1-29. doi: 10.1063/1.1330575

Wang, C. (1963). Optical giant pulses from a Q-switched laser. *Proceedings of the IEEE, 51*(12), 1767-1767. doi: 10.1109/PROC.1963.2690

Wang, F. (2017). Two-dimensional materials for ultrafast lasers. *Chinese Physics B, 26*(3), 034202. doi: 10.1088/1674-1056/26/3/034202

Wang, G. (2017). Wavelength-switchable passively mode-locked fiber laser with mechanically exfoliated molybdenum ditelluride on side-polished fiber. *Optics & Laser Technology, 96*, 307-312. doi: 10.1016/j.optlastec.2017.05.030

Wang, J., Cai, Z., Xu, P., Du, G., Wang, F., Ruan, S., Hasan, T. (2015). Pulse dynamics in carbon nanotube mode-locked fiber lasers near zero cavity dispersion. *Optics Express, 23*(8), 9947-9958. doi: 10.1364/OE.23.009947

Wang, K., Szydłowska, B. M., Wang, G., Zhang, X., Wang, J. J., Magan, J. J., Blau, W. J. (2016). Ultrafast nonlinear excitation dynamics of black phosphorus nanosheets from visible to mid-infrared. *ACS Nano, 10*(7), 6923-6932. doi: 10.1021/acsnano.6b02770

Wang, N., Lu, B.-L., Qi, X.-Y., Jiao, Y., Wen, Z.-R., Chen, H.-W., & Bai, J.-T. (2019). Passively Q-switched ytterbium-doped fiber laser with $ReSe_2$ saturable absorber. *Optics & Laser Technology, 116*, 300-304. doi: 10.1016/j.optlastec.2019.03.043

Wang, Y., Huang, G., Mu, H., Lin, S., Chen, J., Xiao, S., He, J. (2015). Ultrafast recovery time and broadband saturable absorption properties of black phosphorus suspension. *Applied Physics Letters, 107*(9), 091905. doi: 10.1063/1.4930077

Weiner, A. (2011). *Ultrafast optics* (Vol. 72): John Wiley & Sons.

Wen, M., Xu, J., Liu, L., Lai, P.-T., & Tang, W.-M. (2017). Improved electrical performance of multilayer MoS_2 transistor with NH_3-annealed ALD HfTiO gate dielectric. *IEEE Transactions on Electron Devices, 64*(3), 1020-1025. doi: 10.1109/TED.2017.2650920

Wise, F., Chong, A., & Renninger, W. H. (2008). High-energy femtosecond fiber lasers based on pulse propagation at normal dispersion. *Laser & Photonics Reviews, 2*(1-2), 58-73. doi: 10.1002/lpor.200710041

Woodward, R. I., & Kelleher, E. J. (2015). 2D saturable absorbers for fibre lasers. *Applied Sciences, 5*(4), 1440-1456. doi: 10.3390/app5041440

Woodward, R. I., & Kelleher, E. J. J. A. S. (2015). 2D saturable absorbers for fibre lasers. *5*(4), 1440-1456. doi: 10.3390/app5041440

Wu, K., Zhang, X., Wang, J., Li, X., & Chen, J. (2015). WS_2 as a saturable absorber for ultrafast photonic applications of mode-locked and Q-switched lasers. *Optics Express, 23*(9), 11453-11461. doi: 10.1364/OE.23.011453

Xiao, L.-O., Li, S.-B., Song, G., & Sloof, W. G. (2011). Synthesis and thermal stability of Cr_2AlC. *Journal of the European Ceramic Society, 31*(8), 1497-1502. doi: 10.1016/j.jeurceramsoc.2011.01.009

Xing, G., Guo, H., Zhang, X., Sum, T. C., & Huan, C. H. A. (2010). The physics of ultrafast saturable absorption in graphene. *Optics Express, 18*(5), 4564-4573. doi: 10.1364/OE.18.004564

Xu, H., Chen, W., Zhan, P., & Liu, X. (2015). 8-Hydroxyquinoline: a privileged structure with a broad-ranging pharmacological potential. *MedChemComm, 6*(1), 61-74. doi: 10.1039/C4MD00284A

Xu, X., Zhai, J., Wang, J., Chen, Y., Yu, Y., Zhang, M., Tang, Z. (2014). Passively Q-switching induced by the smallest single-walled carbon nanotubes. *Applied Physics Letters, 104*(17), 171107. doi: 10.1063/1.4874649

Xue, M., Zhang, X., Tang, H., & Li, C. (2014). Synthesis of high purity Cr_2AlC nanolamellas with improved tribological properties for oil-based additives. *RSC Advances, 4*(74), 39280-39286. doi: 10.1039/C4RA06719C

Yamashita, S. (2011). A tutorial on nonlinear photonic applications of carbon nanotube and graphene. *Journal of Lightwave Technology, 30*(4), 427-447. doi: 10.1109/JLT.2011.2172574

Yan, P., Chen, H., Yin, J., Xu, Z., Li, J., Jiang, Z., Sun, Z. (2017). Large-area tungsten disulfide for ultrafast photonics. *Nanoscale, 9*(5), 1871-1877. doi: 10.1039/C6NR09183K

Yang, Y., Da Costa, R. C., Fuchter, M. J., & Campbell, A. J. (2013). Circularly polarized light detection by a chiral organic semiconductor transistor. *Nature Photonics, 7*(8), 634-638. doi: 10.1038/nphoton.2013.176

Yang, Y., Yang, S., Li, C., & Lin, X. (2019). Passively Q-switched and mode-locked Tm-Ho co-doped fiber laser using a WS2 saturable absorber fabricated by chemical vapor deposition. *Optics & Laser Technology, 111*, 571-574.

Yefet, S., & Pe'er, A. (2013). A review of cavity design for Kerr lens mode-locked solid-state lasers. *Applied Sciences, 3*(4), 694-724. doi: 10.3390/app3040694

Yu, Z., Song, Y., Tian, J., Dou, Z., Guoyu, H., Li, K., Zhang, X. (2014). High-repetition-rate Q-switched fiber laser with high quality topological insulator Bi_2Se_3 film. *Optics Express, 22*(10), 11508-11515. doi: 10.1364/OE.22.011508

Yusoff, R., Jafry, A., Kasim, N., Munajat, Y., Harun, S., & Halim, N. (2019). *Q-switched ytterbium-doped fiber laser using graphene oxide as passive saturable absorber.* Paper presented at the Journal of Physics: Conference Series.

Zhang, H., Bao, Q., Tang, D., Zhao, L., & Loh, K. (2009). Large energy soliton erbium-doped fiber laser with a graphene-polymer composite mode locker. *Applied Physics Letters, 95*(14), 141103. doi: 10.1063/1.3244206

Zhang, H., Lu, S., Zheng, J., Du, J., Wen, S., Tang, D., & Loh, K. J. O. e. (2014). Molybdenum disulfide (MoS_2) as a broadband saturable absorber for ultra-fast photonics. *Optics Express, 22*(6), 7249-7260. doi: 10.1364/OE.22.007249

Zhang, H., Tang, D., Wu, X., & Zhao, L. (2009). Multi-wavelength dissipative soliton operation of an erbium-doped fiber laser. *Optics Express, 17*(15), 12692-12697. doi: 10.1364/OE.17.012692

Zhang, H., Tang, D., Zhao, L., Bao, Q., & Loh, K. (2009). Large energy mode locking of an erbium-doped fiber laser with atomic layer graphene. *Optics Express, 17*(20), 17630-17635. doi: 10.1364/OE.17.017630

Zhang, K., Feng, M., Ren, Y., Liu, F., Chen, X., Yang, J., Tian, J. (2018). Q-switched and mode-locked Er-doped fiber laser using $PtSe_2$ as a saturable absorber. *Photonics Research, 6*(9), 893-899. doi: 10.1364/PRJ.6.000893

Zhang, L., Guo, L., Xiong, B., Yan, X., Sun, L., Hou, W., Li, J. (2010). LD side-pumped high beam quality passive Q-switched and mode-locked Nd: YAG laser based on SESAM. *Laser Physics, 20*(9), 1798-1801. doi: 10.1134/S1054660X10170196

Zhang, L., Wang, Y., Yu, H., Sun, L., Hou, W., Lin, X., & Li, J. (2011). Passive mode-locked Nd: YVO 4 laser using a multi-walled carbon nanotube saturable absorber. *Laser Physics, 21*(8), 1382-1386. doi: 10.1134/S1054660X11150333

Zhang, M., Wu, Q., Zhang, F., Chen, L., Jin, X., Hu, Y., Zhang, H. (2019). 2D black phosphorus saturable absorbers for ultrafast photonics. *Advanced Optical Materials, 7*(1), 1800224. doi: 10.1002/adom.201800224

Zhao, L., Li, S. B., Wen, G. A., Peng, B., & Huang, W. (2006). Imidazole derivatives: Thermally stable organic luminescence materials. *Materials Chemistry and Physics, 100*(2-3), 460-463. doi: 10.1016/j.matchemphys.2006.01.025

Zhao, W., Chen, G., Li, W., Wang, G., & Zeng, C. (2019). All-fiber saturable absorbers for ultrafast fiber lasers. *IEEE Photonics Journal, 11*(5), 1-19. doi: 10.1109/JPHOT.2019.2941580

Zhou, W., Mei, B., & Zhu, J. (2009). On the synthesis and properties of bulk ternary Cr_2AlC ceramics. *Materials Science, 27*(4/1), 973-980.

Zuikafly, S. N. F., Khalifa, A., Ahmad, F., Shafie, S., & Harun, S. (2018). Conductive graphene as passive saturable absorber with high instantaneous peak power and pulse energy in Q-switched regime. *Results in Physics, 9*, 371-375.

Zulkipli, N. F., & Jafry, A. A. A. (2020). Generation of Q-switched and mode-locked pulses with Eu_2O_3 saturable absorber. *Optics & Laser Technology, 127*, 106163. doi: 10.1016/j.optlastec.2020.106163

Zulkipli, N. F., Samsamnun, F. S. M., Rosol, a. H. a., Altuncu, a., Rusdi, M. F. M., Mahyuddin, M. B. H., Harun, S. W. (2020). Sc_2O_3 PVA film for switching and mode-locking application in erbium-doped fiber laser cavity. *Fiber and Integrated Optics, 39*(3), 137-148. doi: 10.1080/01468030.2020.1805529